

WARSAW UNIVERSITY OF TECHNOLOGY

DISCIPLINE OF SCIENCE – PHYSICAL SCIENCES
FIELD OF SCIENCE – NATURAL SCIENCES

Ph.D. THESIS

Abeer Sami, M.Sc.

**POLYMER ELECTROLYTES COMPRISING OLIGOMERIC
LITHIUM BORATE SALTS AND POLY(ETHYLENE OXIDE)**

Supervisor
Professor Michał Marzantowicz, Ph.D., D.Sc.

WARSAW 2024

Acknowledgements

I would like to express my heartfelt gratitude to all the people who made this work possible.

*To my supervisor, **Prof. PhD, DSc, Eng. Michał Marzantowicz**, for the pleasant atmosphere conducive to scientific work, his immense patience and time, as well as his invaluable help and valuable comments at every stage of the work,*

*To **Prof. PhD, DSc, Eng. Franciszek Krok**, for organizing meetings, helpful comments, and advice on research results and scientific work, and creative discussions full of valuable tips,*

*To the memory of **Prof. PhD, DSc, Eng. Józef Dygas**, for his help in developing some of the results of the research.*

(بِسْمِ اللَّهِ الرَّحْمَنِ الرَّحِيمِ)

(نَرْفَعُ دَرَجَاتٍ مِّنْ نَّشَأٍ وَفَوْقَ كُلِّ ذِي عِلْمٍ عَلِيمٌ)
(صدق الله العظيم)

*This thesis I dedicated to **my parents**, who have provided me with unwavering support throughout my life; to **my beloved husband Abdelwahab**, kids **Lilian ,Faisal and Ilyas**, who have tolerated my hectic schedule and offered me moral and psychological support; and to **my siblings**, who have always been there for me.*

Abstract

Ionically conductive polymers are promising materials for application as an electrolyte in rechargeable batteries. In this thesis, the main object of study is the correlation between electrolyte composition and ionic conductivity, as well as its dielectric and thermal properties. Polymer electrolytes comprising lithium borate salts and high molecular weight poly(ethylene oxide) PEO are prepared by casting from solution. The branched structure of borate salts, obtained in a two-step synthesis process, includes three oligomeric oxyethylene segments of various length n and a butyl group. The weight proportions of polymer and oligomeric salts are chosen so that they represent certain molar proportions of EO units (coming both from anion and from polymer matrix) to lithium: 50:1, 32:1, 16:1, and 10:1. Samples of the electrolytes are investigated by differential scanning calorimetry (DSC) and impedance spectroscopy in a wide range of temperature. For each electrolyte, characteristic parameters such as glass transition temperature T_g and the ideal glass transition T_0 are calculated. It is found, that some systems – for example, electrolytes composed of borate salt with average length $n=7.5$ and molar ratio EO:Li of 32:1 and 50:1, exhibit values of the glass transition temperature lower than the values obtained for pure PEO and pure borate salt. The low T_g partially compensates decrease of conductivity caused by crystallization. Interestingly, mixed PEO-borate salt systems also exhibit transference numbers higher than those of pure borate salt.

Keywords: Lithium borate, Oligomer, Poly(ethylene oxide), Glass transition temperature, Ionic conductivity

Streszczenie

Rozprawa doktorska o proponowanym tytule „Elektrolity polimerowe składające się z oligomerycznych soli boranów litu i poli(tlenku etylenu)” zawiera opis badań materiałów przewodzących jony litu. Materiały tego typu znajdują zastosowanie m.in. w ogniwach litowo-jonowych. Zastosowanie soli oligomerycznych o rozbudowanej strukturze anionu daje nadzieję na ograniczenie transportu ładunku poprzez aniony, a zwiększenie udziału w przewodzeniu jonów litu. Praca ma charakter eksperymentalny, a na podstawie otrzymanych wyników badań formułowane są hipotezy dotyczące wpływu matrycy polimerowej z poli(tlenku etylenu) o strukturze liniowej na właściwości układu i mechanizmu transportu jonów w badanych materiałach. Rozgałęziona struktura soli boranowych, otrzymana w dwuetapowym procesie syntezy, zawiera trzy oligomeryczne segmenty oksyetylenowe o różnej długości n oraz grupę butylową. Elektrolity polimerowe zawierające sole boranu litu i poli(tlenek etylenu) PEO o dużej masie cząsteczkowej wytwarzano metodą odlewania z roztworu.. Proporcje wagowe soli polimerowych i oligomerycznych dobrano tak, aby reprezentowały określone proporcje molowe jednostek EO (pochodzących zarówno z anionu, jak i z matrycy polimerowej) do litu: 50:1, 32:1, 16:1 i 10:1 .

Próbki elektrolitów badano metodą różnicowej kalorymetrii skaningowej (DSC) i spektroskopii impedancyjnej w szerokim zakresie temperatur. Dla każdego elektrolitu obliczono na podstawie pomiarów kalorymetrycznych temperaturę zeszklenia T_g , i temperaturę topnienia, a z wyników otrzymanych metodami elektrycznymi temperaturę idealnego zeszklenia T_0 . Stwierdzono, że niektóre układy – np. elektrolity złożone z soli boranowej o średniej długości ramion $n=7,5$ jednostek EO i stosunku molowym EO:Li wynoszącym 32:1 i 50:1, wykazują wartość temperatury zeszklenia niższą od wartości otrzymanych dla czystego PEO i czystej soli boranowej. W porównaniu do czystej soli boranowej, niska temperatura zeszklenia częściowo kompensuje spadek przewodności spowodowany krystalizacją. Co ciekawe, mieszane układy soli boranowych i PEO wykazują również współczynnik przenoszenia jonów litu wyższy niż czysta sól boranowa. ot ejaD .ainawosotsaz ogenzcytkarp hci od hcycązdaworp nadab hcyzslad od ęwytkepsrep

Słowa kluczowe: boran litu, oligomer, poli(tlenek etylenu), temperatura zeszklenia, przewodnictwo jonowe

Contents

Abstract	7
Streszczenie	8
1. Introduction	15
2. Polymer electrolytes – general review	17
2.1 Lithium-ion batteries	17
2.2 Electrolyte	18
-Organic Liquid Electrolytes:	20
-Liquid Electrolytes (Non-organic):	20
-Polymeric Electrolytes:	21
2.3 Ionic Conduction Mechanism in Solid Polymer Electrolytes	22
2.4 Types of polymer electrolytes	26
2.4.1 Liquid electrolyte systems	26
2.4.2 Solid polymer electrolytes	27
• Solid conductive polymer based on linear polyethers:	27
• Polymer electrolyte comprising organic plasticizers:	27
• Polymer gel electrolyte:	28
2.5 Poly(ethylene oxide) – PEO	30
2.6 Lithium salts	31
2.7 Lithium alkyltrialkoxoborates $\text{Li}[\text{Bu}(\text{RO})_3\text{B}]$	33
2.8 Transference numbers	33
2.9 Conductivity of semicrystalline polymer PEO-based electrolyte.....	35
1. Degree of Crystallinity	35
2. Dopant Salt	35
3. Temperature.....	36
2.10 Dielectric properties of polymer electrolytes	38
3. Experimental Techniques	41
3.1 Differential Scanning Calorimetry (DSC).....	41
3.2 AC Impedance Spectroscopy	42
3.3 Transference Number Estimation.....	53
3.3.1. Bruce-Vincent method	53
3.3.2. Watanabe method.....	54
4. Experimental: preparation of materials and characterization methods.	55

4.1 Materials.....	55
4.2 Synthesis and characterization of lithium alkyltrialkoxoborates Li[Bu(RO) ₃ B].....	55
4.3 Preparation and characterization of polymer electrolytes	56
4.4 Impedance spectroscopy measurements.....	58
4.5 Differential scanning calorimetry measurements	62
4.6 Measurements of lithium transference number	63
5. Results and discussion.....	65
5.1 Thermal properties of the studied system.....	65
5.2 Electrical properties of the studied system.....	75
5.2.1. Ionic conductivity.....	75
5.2.1.1 Conductivity of borate salts with different length n of oligomeric groups:	77
5.2.1.2 Conductivity of electrolytes representing the same molar ratio EO:Li and different length n of oligomeric groups:	78
5.2.2 Ideal Glass Transition Temperature T_0	87
5.2.3 Dielectric properties	93
5.3 Transference numbers	103
6. Conclusions	106
References:	108

List of Figures

Fig. 2.1. Schematic draw of Li-ion battery .	17
Fig. 2.2. Cation motion in a polymer electrolyte assisted by polymer chains .	23
Fig. 2.3. Contributions to ion mobility .	25
Fig. 2.4. Concept structure of gel electrolyte. The polymer chains remain unchanged.	29
Fig. 2.5. Polyelectrolyte conceptual structure. The polymer chains have opposite charges to the counter ion.	29
Fig. 2.6. The helical structure of PEO .	30
Fig. 2.7. A Scheme structure of Li[Bu(RO) ₃ B].	33
Fig. 2.8. Values of the lithium transport number and cation transference number for the PEO:LITFSI system by several research groups .	35
Fig. 2.9. Temperature dependence of the ionic conductivity for PEO:LiTFSI electrolyte with molar ratio 10:1 EO:Li .	37
Fig. 2.10. Debye dielectric dispersion curve.	39
Fig. 3.1. A DSC scan with common features.	42
Fig. 3.2. Current-voltage characteristics and impedances of basic circuit elements.	43
Fig. 3.3. Plots of the sinusoidal voltage and current at a specific frequency related to a cell. V = voltage, I = current, and θ = phase difference .	43
Fig. 3.4. Vector representation of cell resistance Z . Z' and Z'' are the real and imaginary components of a complex resistance .	44
Fig. 3.5. A blocking electrode cell and the model circuit .	46
Fig. 3.6. An ideal AC impedance trace for a polymer electrolyte .	48
Fig. 3.7. Simulations of the real spectrum of dielectric function ϵ for selected values of parameters a and b , with constant values of relaxation strength $H = 10$, relaxation time $\tau = 10^{-3}$ S and high frequency limit of dielectric constant $\epsilon_{\infty} = 1$	52
Fig. 3.8. Simulations of the imaginary spectrum of dielectric function ϵ for selected values of parameters a and b , with constant values of relaxation strength $H = 10$, relaxation time $\tau = 10^{-3}$ S and high-frequency limit of dielectric constant $\epsilon_{\infty} = 1$	52
Fig. 4.1. Glovebox system.	58
Fig. 4.2. Schematic presentation of cross-section of gas-tight sample holder with adjustable spring loading of upper electrode .	59
Fig. 4.3. Measuring holder (No.2) with gas-tight screwed lid (No.1) and electrode in Teflon cover (No.3).	59
Fig. 4.4. Diagram of the knob for adjusting the distance (top view).	60
Fig. 4.5. The measuring system for impedance spectroscopy.	62

Fig. 4.6. Differential Scanning Calorimeter (DSC) Q2000 series of TA Instruments	63
Fig. 5.1. DSC traces recorded during first heating at a rate of 20 °C /min, for pure borate salts with different length of oligomeric chains.	66
Fig. 5.2. DSC traces of polymer electrolytes composed of high M_W PEO and [(RO) ₃ BBu]Li ($n=1$) with different EO:Li. All data collected during second heating cycle.	68
Fig. 5.3. DSC traces of polymer electrolytes composed of linear PEO and borate salts, length of oligomeric arms ($n=2$), measured during second heating. The samples vary by molar ratio EO:Li.	69
Fig. 5.4. DSC traces of polymer electrolytes composed of linear PEO and borate salts, length of oligomeric arms ($n=3$), measured during second heating. The samples vary by molar ratio EO:Li.	70
Fig. 5.5. DSC traces of polymer electrolytes composed of linear PEO and borate salts, length of oligomeric arms ($n=7.5$), measured during second heating. The samples vary by molar ratio EO:Li.	71
Fig. 5.6. Values of the melting point of studied polymer electrolytes. Melting points of pure borate salts and pure PEO were plotted as references.	73
Fig. 5.7. Integrated heat of fusion of studied electrolytes.	74
Fig. 5.8. Values of glass transition temperature T_g of studied electrolytes.	75
Fig. 5.9. Equivalent circuit used for fitting of impedance spectra (a) and complex plane plots of impedance spectra of selected samples: amorphous lithium borate salt with ($n=7.5$) measured at 25 °C (b), semicrystalline electrolyte EO:Li molar ratio of 32:1 comprising salt with ($n=7.5$) and linear PEO measured at 25 °C (c) and the same electrolyte measured in amorphous state at 70 °C (d). Solid lines represent impedance of the fitted equivalent circuit model.	76
Fig. 5.10. Temperature dependence of ionic conductivity during first cooling run, plotted for salt with different length n of oligomeric groups.	78
Fig. 5.11. Temperature dependence of ionic conductivity during first cooling run, plotted for electrolytes with the same EO:Li ratio of 10:1, and different length n of oligomeric groups.	80
Fig. 5.12. Temperature dependence of ionic conductivity during first cooling run, plotted for electrolytes with the same EO:Li ratio of 16:1, and different length n of oligomeric groups.	80
Fig. 5.13. Temperature dependence of ionic conductivity during first cooling run, plotted for electrolytes with the same EO:Li ratio of 32:1, and different length n of oligomeric groups.	81
Fig. 5.14. Temperature dependence of ionic conductivity during first cooling run, plotted for electrolytes with the same EO:Li ratio of 50:1, and different length n of oligomeric groups.	81
Fig. 5.15. Ionic conductivity of studied electrolytes at 25 °C (a) and at 70 °C (b) as a function of EO:Li. Figure (c) shows conductivity at selected temperatures as a function of borate salt weight fraction in the electrolyte W_S . The conductivity of pure PEO and borate salts are shown as references.	83

Fig. 5.16. Temperature dependence of ionic conductivity plotted for electrolyte with EO:Li of 50:1, and length of oligomeric arms ($n=7.5$). Solid lines represent fit with VTF function.	88
Fig. 5.17. Values of ideal glass transition temperature T_0 of studied electrolytes.	90
Fig. 5.18. Temperature dependence of ionic conductivity plotted for electrolyte with EO:Li of 50:1, and length of oligomeric arms ($n=7.5$). Solid lines represent fit with VTF function.	92
Fig. 5.19. Temperature dependence of ionic conductivity plotted for electrolyte with EO:Li of 50:1, and length of oligomeric arms ($n=1$). Solid lines represent fit with VTF function.	92
Fig. 5.20. Real (a) and imaginary (b) part of dielectric function ϵ for electrolytes prepared using oligomeric salt with ($n=7.5$) at the low temperature limit of investigated range. Data for pure PEO and oligomeric salt are presented as reference. Solid lines represent equivalent circuit fit. Dotted and dashed lines represent dielectric relaxations. Plot for pure PEO is plotted according to Y scale, other plots were shifted by 1.5 in respect to each other.	95
Fig. 5.21. Real (a) and imaginary (b) part of dielectric function ϵ and real part of conductivity σ (c) for electrolytes prepared using oligomeric salt with ($n=7.5$). Data for pure PEO and oligomeric salt are presented as reference. Solid lines represent equivalent circuit fit. Dotted and dashed lines in (a) and (b) represent dielectric relaxations, and dashed lines in (c) represent local conductivity. Plot for pure PEO is plotted according to Y scale, other plots were shifted by 1.5 in respect to each other.	97
Fig. 5.22 a-d: Complex plane plots of plots of impedance spectra measured at room temperature: oligomeric salt with ($n=7.5$) (a), electrolyte comprising oligomeric salt, ($n=7.5$) and PEO, EO:Li molar ratio of 32:1 (b), electrolyte comprising oligomeric salt, ($n=7.5$) and PEO, EO:Li of 50:1 (c), pure PEO (d). e-f: Spectral plots of real part of dielectric permittivity (e) and real part of conductivity (f). Solid lines represent equivalent circuit fit. Dashed lines in (f) represent local conductivity. Data for pure PEO are plotted according to Y scale, other plots are shifted by 1.5 in respect to each other.	99
Fig. 5.23 a-d: Complex plane plots of impedance spectra measured at 70°C: oligomeric salt with $n=7.5$ (a), electrolyte comprising oligomeric salt, ($n=7.5$) and PEO, EO:Li molar ratio of 32:1 (b), electrolyte comprising oligomeric salt, ($n=7.5$) and PEO, EO:Li of 50:1 (c), pure PEO (d). e-f: Spectral plots of real part of dielectric permittivity (e) and the real part of conductivity (f). Solid lines represent equivalent circuit fit. Dashed lines in (f) represent local conductivity. Data for pure PEO are plotted according to the Y scale, other plots are shifted by 1.5 in respect to each other.	102
Fig. 5.24. The chronoamperometric and the impedance data, used for calculation of the apparent lithium transference numbers (t^+) of electrolytes based on the borate salt with oligomeric arm length of ($n=7.5$): the electrolyte with a ratio of ethylene monomer to lithium (EO:Li) of 50:1 comprising the salt and PEO (a), the electrolyte EO:Li=32:1 comprising salt and PEO (b), the neat salt EO:Li=22.5:1 (c). All measurement were performed at 80 °C ..	103

List of Tables

Table 2.1. Different types of electrolytes for lithium secondary batteries.	19
Table 2.2. Structures and characteristics of frequently used lithium salts in polymer electrolytes	32
Table 2.3. The ionic conductivity at room temperature for rapidly cooled amorphous PEO:LiTFSI electrolytes	37
Table 4.1. Materials used in the study.....	55
Table 4.2. Weight proportions (PEO to salt) and molar proportions EO:Li of electrolytes comprising oligomeric borate salts with various length of and PEO. The last row presents intrinsic EO:Li molar proportions of borate salts.....	57
Table 5.1. The values of T_g, T_0, T_m and Q_F for Lithium alkyltrialkoxylborate salts system with different length of oligomeric groups.....	67
Table 5.2. Melting point and heat of fusion, obtained from analysis of DSC data for electrolytes comprising oligomeric borate salts (Lithium alkyltrialkoxylborates) with various length of oligomeric groups and PEO.	72
Table 5.3. Values of the glass transition temperature T_g (midpoint) obtained for electrolytes comprising oligomeric borate salts (Lithium alkyltrialkoxylborates) with various length of oligomeric unit and PEO.....	72
Table 5.4. Ionic conductivity of electrolytes samples in case of cooling run at 25 °C and 70 °C	87
Table 5.5. Values of the ideal glass transition temperature T_0 obtained from fit of VTF function to conductivity data for electrolytes comprising oligomeric borate salts with various length of oligomeric and PEO, and $(T_g - T_0)$	89
Table 5.6. Logarithm of Decoupling Indexes ($LogR_t$) of electrolytes comprising oligomeric borate salts with various length of and PEO	93
Table 5.7. The apparent transference numbers (t^+) of electrolytes based on the borate salt with oligomeric arm length of ($n=7.5$) (neat salt or with PEO) measured at 80 °C.....	105

1. Introduction

The majority of research and development efforts put into lithium-ion batteries are directed toward the improvement of electrodes, rather than the electrolyte, which has seen little change in composition over the past few decades. This is due to the fact that the electrodes are that what determine the energy density of the battery. However, the electrolyte is an essential component of the battery because it plays a role in the overall power capability of the battery. This is because of the internal resistance of the bulk electrolyte as well as the interfaces between the electrodes and the electrolyte.

The primary purpose of the development of rechargeable lithium batteries is the production of energy storage units that have a long cycle life together with a high energy and power density as well as good charge retention. When selecting an electrolyte for a rechargeable lithium battery, the following properties are essential [10]:

1. Good ionic conductivity ($>10^{-3}$ S/cm at room temperature) to reduce internal resistance.
2. Lithium ion transference number close to unity (to limit concentration polarization).
3. Broad electrochemical voltage window (0 to 5V).
4. Thermal stability in typical working conditions – usually from -20 °C up to 70 °C.
5. Compatibility with other cell parts.

The rechargeable lithium ion battery that utilizes a solid type of polymer electrolyte (SPE) is considered to have a safety advantage over the organic liquid electrolyte as a result of their lower reactivity with lithium and the absence of a volatile, flammable organic solvent. This is due to the fact that SPEs do not contain a volatile organic solvent. Another potential advantage of the solid polymer battery is its capability to be easily fabricated in a variety of shapes and forms. Extremely thin batteries for cell phones, personal digital assistants (PDAs), and similar applications can be manufactured. In addition, large thin plates can be manufactured and assembled in a multiplate prismatic structure to create batteries with a very high energy density [1].

The overall goal of this study is to achieve high ionic conductivity in a polymeric system and, at the same time, limit anion mobility. The first requirement can be achieved by developing new lithium salts aimed at delocalization of anion charge, which lowers the melting temperature of the salt and promotes dissociation. The second goal may be reached by development of salts with large, oligomeric anions, which are expected to have low mobility and thus increase lithium transference number. In this work, we compare the electrical and thermal properties of electrolytes obtained by mixing oligomeric borate salts with long

molecular weight poly(ethylene oxide). Four different lengths of oligomeric arms are studied, as well as several concentrations of lithium ions in the electrolyte. Selection of best candidates for solid polymer electrolyte is made based on analysis of the obtained data.

2. Polymer electrolytes – general review

2.1 Lithium-ion batteries

Although some electronic devices still use primary lithium cells, most modern Li-ion batteries are rechargeable. During the discharge process, the lithium ions migrate from the negative electrode to the positive electrode. Charging by an external power source reverses this process. To enable efficient ion exchange between the electrodes, in a typical rechargeable lithium-ion battery a semi-liquid electrolyte is used as the medium. In such a case, a porous separator is used to create electrical separation between the anode and cathode, preventing an internal short circuit while enabling ions to move through the electrolyte. In general, a battery will use an electrochemical oxidation-reduction process to transform the chemical energy that is stored in the electrodes into electric energy [11]. As shown in Fig. 2.1, in most designs the positive electrode is made of lithiated metal oxides (in the presented example LiCoO_2). Carbon (graphite) is typically used as the material for the negative electrode. An external DC power supply is used to recharge the battery. During the charging process, the lithium ions migrate through the electrolyte from the positive electrode to the negative electrode, where they are intercalated in the carbon. Throughout the process of discharging, an external load is connected to the battery, and the lithium ions stored in the carbon move back to the cathode.

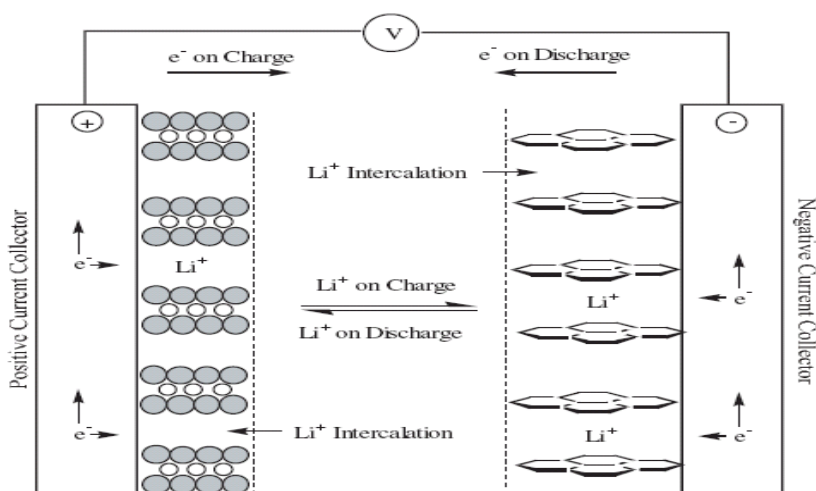


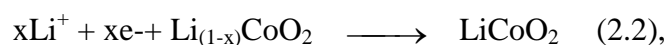
Fig. 2.1. Schematic draw of Li-ion battery [12].

The following are the electrochemical reactions:

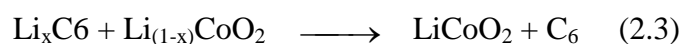
half-reaction at the negative electrode:



half-reaction at the positive electrode:



overall reaction:



Depending on the electrolytes used, lithium-ion batteries can be classified into one of four types:

- The macroporous separator is filled with a liquid electrolyte, often a solution of lithium salt in a mixture of organic solvents.
- Polymer gel electrolyte: composed of a dense polymer matrices soaked with lithium salts and organic solvents.
- Solvent-free polymer electrolyte, in which the polymer matrix plays the role of a solvent for Li salts
- Ceramic “all solid state” electrolyte

Since 1978, when Michel Armand first suggested polyether–alkali–metal salt complexes as possible materials for electrochemical devices, a lot of research has been done on these systems, especially high molecular weight poly(ethylene oxide)–lithium salt, to learn more about their basic properties and use this knowledge to create new generations of polymer electrochemical devices [13].

2.2 Electrolyte

The electrolyte physically separates the electrodes but also acts as a transport medium for Li^+ ions between them. There are primarily two types of systems that may be distinguished: liquid and solid electrolytes. The first one needs an extra layer (e.g. porous membrane) to keep the electrodes apart, but the second one can work on its own. For use in batteries, lithium ions need to have conductivities of around 10^{-3} S/cm [14]. In addition to the conductivity requirements, electrolytes must be electrochemically stable over the whole potential range employed in lithium-ion battery (LIB), which ranges from 0 V to 4.8 V. Organic carbonates such as ethylene carbonate / dimethyl carbonate (EC/DMC) combined with lithium

salts are among the most commonly used electrolytes. EC/DMC with the common LiPF_6 has a thermodynamical stability from 0.8 V to 4.5 V [15]. Because of its kinetic stability, it may still be employed with graphite anodes at 0.3 V. Ionic liquids are frequently used for high-potential applications since some are stable up to 5.0 V [16].

When metallic lithium is used as the anode, dendrites often form. Their growth can eventually lead to a short-circuit of the cell. This problem may be addressed by using solid electrolytes [17]. However, such electrolytes have either lower conductivity than liquid systems or are difficult to produce on an industrial scale. Table 2.1 gives a brief overview of the properties of some electrolytes that are often used in LIBs. Polymer electrolytes have attracted the attention of the scientific community for many years [18] and achieving ionic conductivity sufficient for practical applications still remains one of the main research goals in this field.

Table 2.1. Different types of electrolytes for lithium secondary batteries.

Properties	Organic liquid electrolytes	Ionic liquid electrolytes	Solid polymer electrolytes	Gel polymer electrolytes
Composition	Organic solvents +lithium salts	RT ionic liquids +lithium salts	Polymer +lithium salts	Organic solvents + polymer + lithium salts
Ion conductivity	High	High	Low	Relatively high
Low-temp. performance	Relatively good	Poor	Poor	Relatively good
Thermal stability	Poor	good	Excellent	Relatively good

The electrolyte of lithium-ion batteries typically consists of a LiX salt and a solvent. Some of the electrolytes used in Li-ion batteries, such as organic liquid electrolytes, non-organic liquid electrolytes and polymeric electrolytes, have a number of advantages and disadvantages compared to the aqueous electrolytes typically used in other electrochemical systems.

-Organic Liquid Electrolytes:

Advantages:

- High ionic conductivity: Organic solvents can dissolve a wide range of salts, leading to high conductivity.
- Wide electrochemical stability window: Many organic solvents have a broad potential range, allowing for a wider range of electrochemical applications.
- Flexibility: Organic solvents can be easily tailored by selecting different solvent-salt combinations to optimize performance for specific applications.

Disadvantages:

- Safety concerns: Some organic solvents can be volatile and flammable, posing safety risks, especially in high-temperature environments.
- Limited stability: Organic solvents can degrade over time due to chemical reactions or electrolyte decomposition, affecting long-term stability and reliability.
- Environmental impact: Some organic solvents may have negative environmental consequences if they leak or are improperly disposed of.

-Liquid Electrolytes (Non-organic):

Advantages:

- High Ionic Conductivity: Similar to organic liquid electrolytes, non-organic liquid electrolytes can also offer high ionic conductivity, enabling efficient ion transport.
- Compatibility: They can be compatible with a wide range of electrode materials and electrolyte systems, making them versatile for various electrochemical applications.
- Cost-effectiveness: Non-organic liquid electrolytes can often be more cost-effective compared to some alternative electrolyte types, contributing to their widespread use in commercial applications.

Disadvantages:

- Safety Concerns: Similar to organic liquid electrolytes, non-organic liquid electrolytes can pose safety risks due to flammability and volatility.
- Limited Electrochemical Stability: Non-organic liquid electrolytes may have a narrower electrochemical stability window compared to some other electrolyte types, limiting their use in high-voltage applications.
- Environmental Impact: Some non-organic liquid electrolytes may contain toxic or environmentally harmful components, necessitating proper disposal and recycling measures.

-Polymeric Electrolytes:

Advantages:

- Flexibility: Polymeric electrolytes can be engineered to have specific mechanical properties, making them suitable for flexible and conformal device designs.
- Improved safety: Some polymer electrolytes exhibit lower flammability and higher thermal stability compared to organic liquid electrolytes.
- Ease of processing: Polymeric electrolytes can be processed using relatively simple techniques such as solution casting or electrode position.

Disadvantages:

- Lower ionic conductivity: Polymeric electrolytes often have lower conductivity compared to liquid electrolytes, although recent advancements have improved this aspect.
- Swelling and mechanical issues: Polymeric electrolytes may swell in the presence of liquid electrolytes or solvents, leading to mechanical instability or decreased performance.
- Compatibility issues: Compatibility between polymers and electrode materials can be challenging, and interface stability may pose a problem, affecting device performance and longevity [1,2,3-5].

Throughout the 20th century, the majority of synthetic polymers were put to use either as structural materials or as insulators. But, in the past thirty years, they have been modified to function as conductors of electrons or ions.

When combined with appropriate salts, many polymers may perform as solid solvents, and form an electrolyte with the ability to transport ions. Polymer electrolytes are one of the most essential parts of all-solid-state electrochemical devices. These devices include rechargeable batteries and supercapacitors. Polymer electrolytes have two important functions in supercapacitors and batteries: (1) they transport cations (mostly lithium ions), and (2) they perform the function of a separator or an electrode spacer [6-7].

When considering the capacity of a polymer electrolyte to solvate ions, it is necessary to mention the acceptor-donor numbers (AN and DN) associated with the formation of coordination bonds between the solvent and solute in the system. Polymers with a strong DN, such as polyethers, polyamines, or polythiols, are promising candidates for use as the

electrolyte. This is due to the fact that electron lone pairs located at oxygen, nitrogen, or sulfur in such polymers have the ability to solvate the lithium cation [8]. Poly(ethylene oxide) (PEO)-based compounds have been studied among those with high DN because they form more stable complexes with inorganic salts and have a greater solvating capacity for salt than any other polymers [9].

2.3 Ionic Conduction Mechanism in Solid Polymer Electrolytes

After P.V. Wright found that polyethene oxide (PEO) conducts lithium ions, M. B. Armand was the first to suggest using a solvent-free(dry) polymer electrolyte in a battery [19-20]. A polymer host and alkali metal salts comprise the dry polymer electrolyte. Polymer hosts, like the etheric oxygen in an oxy-ethylene or oxy-propylene unit, include polar groups (repeated functional groups) that can interact with cations. A polymer host must provide high solubility of the salt, facile ion dissociation, and efficient ion diffusion. In polymer structures, ion dissociation units like ethylene-oxide and ethylene-imine speed up the dissociation of electrolyte salts into ions.

At first, most researchers thought that ion transport was mostly caused by the crystalline domains of a polymer, with the ions moving along the PEO helices thought to be the main mechanism. Nevertheless, it was quickly determined that the amorphous phase is mainly responsible for ion transport, with the exception of certain crystalline PEO:salt stoichiometric complexes [21]. The mobility of lithium ions is enhanced by the segmental relaxation of the polymer, and in general, lithium ions tend to travel through the amorphous domains of the polymer by establishing and breaking coordination bonds with the ether oxygen atoms. The objective to increase conductivity has mostly focused on enhancing polymer mobility in the amorphous phase [22]. The general expression which describes conductivity can be written as:

$$\sigma = ne\mu, \quad (2.4),$$

n : the concentration of mobile ions

e : the elementary electric charge

μ : the ion mobility.

Because the fraction of "free" ions is such an essential parameter, an increased degree of salt dissociation in the polymer might result in an increase in the conductivity [23]. According to simulations based on molecular dynamics, the Li^+ ions appear to be complexed to the PEO matrix through about five ether oxygens of a PEO chain. As a result, the mobility

of the cations appears to be significantly restricted as a result of this complexation [24]. As a consequence of this, the mobility of the cations is related to the movements of the complex segments of the PEO chain. Cation transport may therefore be seen as the movement of lithium ions between complexation sites. This movement is made possible by the segmental mobility of the PEO matrix. Cations are able to "hop" between the coordination sites of nearby chains. This phenomenon, known as interchain and intrachain hopping, is supported by the mobility of polymer chains.

It is believed that the segmental movements of the polymer improve ion mobility by forming and breaking the coordination bonds between the cation and the polymer, as well as by giving free volume for the ion to diffuse through (see Fig. 2.2).

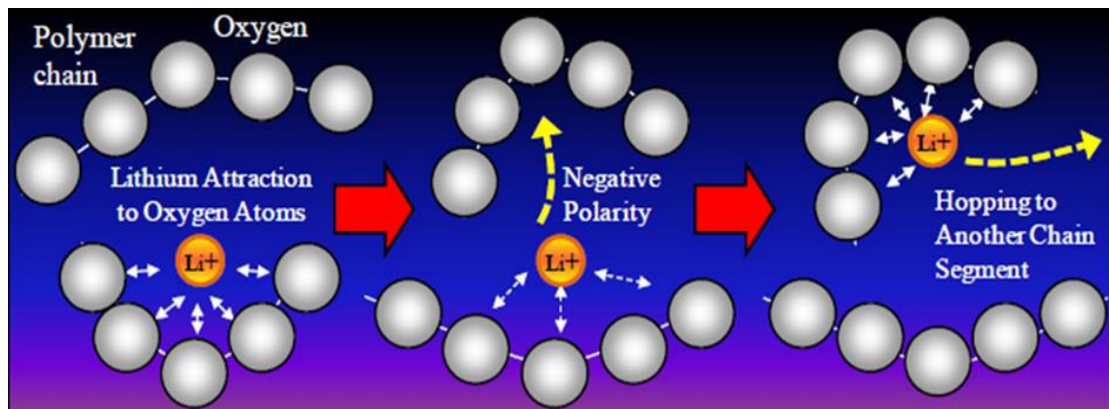


Fig. 2.2. Cation motion in a polymer electrolyte assisted by polymer chains [25].

The ion transport phenomenon is greatly affected by temperature. Since polymer relaxation and segmental motion exhibit a strong dependence on the temperature, the ionic conductivity of the polymer electrolyte is also strongly affected by changes in temperature [26]. When the temperature rises, the combination of redistribution of free volume and material expansion allows polymer segments, ionic species, or solvated molecules to move across the electrolyte [27].

Therefore, amorphous and semi-crystalline solid polymer electrolytes require local relaxation and segmental motion of the polymer (PEO) chains in order to enable the transport of ions (Li^+). This can happen faster if the polymer is above its crystallization and melting temperatures, which for PEO is above 60 °C [28]. In liquid, ions move with their solvent sheaths intact, and ion transport is related to the macroscopic viscosity of the solvent. However, in solid polymer, where the polymer chains get more tangled and can't move over long distances, ion transport is related to the microscopic viscosity of the segments of the

polymer chains. Ion transport through polymer chains must overcome two activation barriers, which are illustrated in Fig. 2.3. One is the solvation of the ions by the EO units. This Arrhenius-dependent process involves the formation and breaking of coordination bonds and conductivity is provided by:

$$\sigma = A \exp\left(\frac{-E_a}{KT}\right) \quad (2.5),$$

where σ is the conductivity, A is a constant, and E_a is the activation energy associated with the bonds. If the bonds are too strong, the cations become immobile, as ions in the solid polymer must dissociate from coordination sites in order to move. To ensure that salt can be dissolved, the cation-polymer bonds must be sufficiently strong; nevertheless, they must also be sufficiently weak to permit cation mobility. Ions are transported from one coordination site to another as part of the cation transport. This process is related to the segmental motion of the polymer and the thermal dependence of conductivity is described by Vogel-Tammann-Fulcher (VTF) formula [29-31].

$$\sigma = \sigma_0 \exp\left(-\frac{B}{T - T_0}\right) \quad (2.6),$$

where σ_0 is the preexponential conductivity, B is the pseudoactivation energy for conduction, and T_0 is the ideal glass transition temperature, usually about 50 K below T_g . At this temperature, the segmental motions of the matrix are considered completely frozen and there is no redistribution of free volume. This equation suggests also that at a given temperature above T_g faster segmental motion is expected for polymer with low T_g .

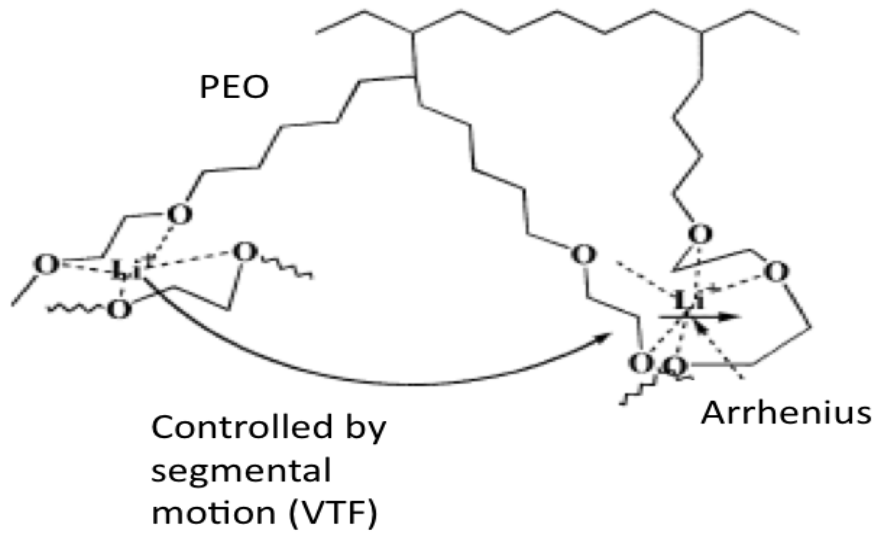


Fig. 2.3. Contributions to ion mobility [32].

The VTF mechanism of conductivity is related to the T_g , limiting the rate at low temperatures. When the temperature is high enough, the movement of the segments is easy enough that the Arrhenius process becomes rate limiting. The conductivity at constant pressure and temperature may also be linked to the ion concentration via:

$$\sigma(T, P) = qc(\mu_+ + \mu_-) \quad (2.7),$$

where q is the charge, c is the concentration, and μ is the mobility for the cations and anions. The mobility is related to the diffusion coefficient D through the Nernst-Einstein relation:

$$\mu = \frac{qD}{KT} \quad (2.8)$$

When it comes to ion diffusion, the effect of a high number of ions is similar to the effect of a high temperature. Since anion does not form strong bonds with polymer hosts, anion transport mostly depends on free segmental motion, or aVTF-type dependence, at all temperatures and concentrations.

2.4 Types of polymer electrolytes

2.4.1 Liquid electrolyte systems

Electrolytes described as “liquid” include a lithium salt that has been dissolved in a suitable solvent or a combination of solvents, as well as a membrane that is electronically separated from the rest of the solution (also known as a "separator") to prevent a short circuit from occurring between the electrodes. They have desirable characteristics such as high ionic conductivity, thermal stability within the circumstances of the environment, a reasonably broad electrochemical stability window, and the simplicity of acquiring and manipulating the material [33-39].

The choice of solvents is restricted to those that can solvate and conduct ions, as well as those that have a low melting point, a high boiling point, and relatively low vapor pressure in order to give a wide operating temperature range. The most frequently used organic solvents in liquid electrolyte systems are ethylene carbonate (EC), propylene carbonate (PC), and diethylene carbonate (DEC). As a single solvent cannot meet all of these requirements, a combination of solvents with different chemical and physical characteristics is frequently utilized instead. As a result, most liquid electrolyte systems consist of a lithium salt dissolved in a combination of two or more solvents [40-41].

Various lithium salts are employed in these liquid electrolytes, which has a direct impact on the performance of the battery in terms of capacity and cycle life. The lithium salts LiClO_4 , LiBOB, LiPF_6 , LiBF_4 , and LiTFSI are among the most widely used. Even though LiClO_4 has high ionic conductivity and easily dissociates in organic solvents, its application in lithium-ion batteries is restricted because it is an extremely powerful oxidizer, which raises a number of safety issues [39]. LiPF_6 is another lithium salt that is often used and has a high ionic conductivity. This salt is also very cheap, naturally flame-retardant, and very stable in both oxidation and reduction [42].

The lithium salt is dissociated into mobile ions by the liquid electrolyte, which makes it possible for electrochemical processes to proceed in the presence of a potential difference, with the main potential gradient occurring at the electrode interfaces [43]. In galvanic cells, they have a wide range of applications and exhibit high ionic conductivity. On the other hand, they have a number of deficiencies, including corrosiveness, leakage, and the absence of a solid barrier between the electrodes. Therefore, they are usually used in combination with an inert polymer membrane or a sponge-like polymeric separator. In this case, the polymer only

provides mechanical support of the electrolyte and does not play an active role in the conduction process.

2.4.2 Solid polymer electrolytes

When a solid polymer electrolyte is utilized in the battery, an extra separator is not required, and the electrolyte medium may be produced as an ultrathin film. This makes it possible to create a solid state battery that has a high energy density [44]. The ion conductive polymers can be divided into the following categories [45]:

- ***Solid conductive polymer based on linear polyethers:***

In the initial studies, polymer electrolytes were obtained mainly by dissolving a small amount of lithium salt in the polymer matrix; this type of electrolyte system is referred to as a "salt-in-polymer" system. Polyethers are frequently employed in this context due to the presence of oxygen atoms with free electron pairs that can act as electron donors to coordinate cations. Since Wright's discovery in 1973 that poly (ethylene oxide) (PEO) complexes with alkali metal salts exhibit ionic conductivity, poly (ethylene oxide) (PEO) has been the subject of the greatest amount of research [46]. PEO is very well compatible with the majority of the salts of the alkali metals, and it has a good adhesion to the electrodes when it is in the form of a thin layer.

It is well known that the transport of ions depends primarily on the relaxation rate of polymer segments therefore, unrestricted segmental movements result in high ion conductivity. At ambient temperature, PEO molecules tend to crystallize, forming ordered structures (lamellae). This decreases the freedom of movement of polymer segments and consequently the ionic conductivity. Even though these materials have excellent mechanical properties, their conductivity at room temperature is typically less than 10^{-4} S/cm, which is lower than the acceptable ionic conductivity of 10^{-3} S/cm required for practical applications.

- ***Polymer electrolyte comprising organic plasticizers:***

The second generation of conductive polymers concentrated on the use of low T_g polymers (such as polydimethylsiloxane (PDMS)) that incorporated plasticizers (such as propylene carbonate or ethylene carbonate) to make the polymer chains flexible. This was done in order to improve the ionic conductivity of the material when it was exposed to ambient conditions [47-48]. Plasticizer reduces the glass transition temperature (T_g) of the solid conductive polymer by generating an isothermal rise in the configurational entropy of the system, which in turn enhances the chain mobility. The insertion of a large amount of low

(T_g) additives, on the other hand, typically results in the loss of the material's mechanical properties (often a semi-liquid consistency is obtained) and makes it impractical as electrode separator [49-51]. Using a crosslinked polymer network is another way to stop crystallization and keep the right mechanical properties. With this method, the electrolyte matrix is obtained by adding a crosslinking agent to the linear polymer chains. It's easy to process such network into thin films and membranes that can be used as separators.

• ***Polymer gel electrolyte:***

Gel polymer electrolytes were first suggested by Feuillade who received a patent for concept of thin batteries in 1973 [45]. Ionically conductive polymer gels are a non-aqueous ion conductive material that has been the subject of extensive research since the 1990s. This research has been conducted in electrochemical applications such as batteries and electric double-layer capacitors, as well as electromechanical applications such as actuators. On the basis of the network structure of the polymer, these materials can be divided into two categories: gel electrolytes and polyelectrolyte gels (see Fig. 2.4 and Fig. 2.5). Gel electrolytes are typically polymer-electrolyte liquid combined systems in which ion conduction occurs predominantly in the liquid electrolyte medium [45]. The polymer chain does not include an ionic group, and the cations and anions are both mobile and contribute to ion conduction. Such materials have several advantages, like relatively mild temperature dependence of conductivity, which is a result of low activation energy for ion hopping in the liquid. Polyelectrolyte gel, on the other hand, is made up of covalently bound ionic groups (either cationic or anionic) in the polymer chains, and the only mobile ions are the counter ions. Depending on the chemical composition of polymer chains and the structure of the polymer network, the polymer matrix can interact with mobile ions strongly or weakly [52-53]. When the interaction is weak, the gel system acts more like a liquid electrolyte because most of the ions move through the solvent medium, and the polymer matrix keeps the structure of the system intact. In systems with strong interaction between ions and polymer matrix, the gel functions more like a solid polymer electrolyte because ion diffusion is accompanied by strong ion-polymer-segment coupling.

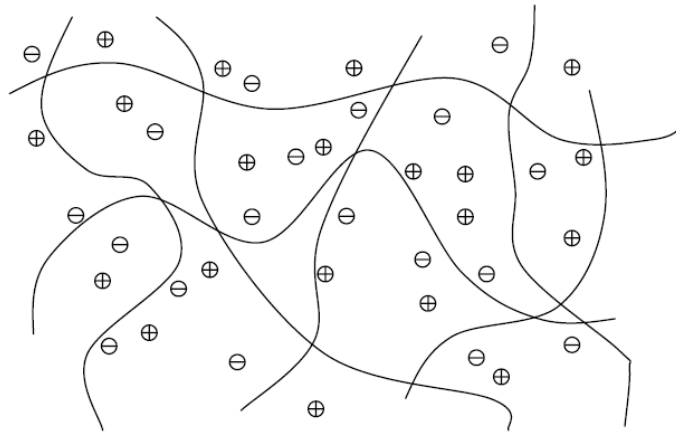


Fig. 2.4. Concept structure of gel electrolyte. The polymer chains remain unchanged.

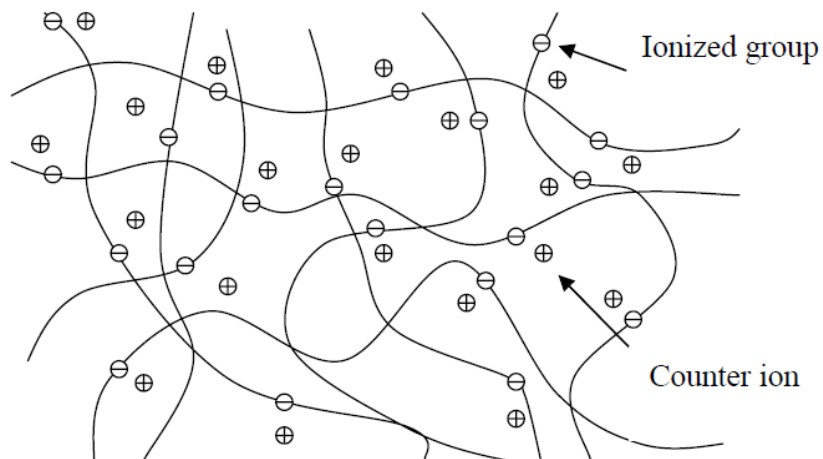


Fig. 2.5. Polyelectrolyte conceptual structure. The polymer chains have opposite charges to the counter ion.

Gel electrolyte typically consists of a polymer, a solvent, and a salt. At a low to moderate crosslink density, the polymer matrix can swell significantly with the solvent-salt solution [54]. Maintaining appropriate mechanical strength under constant pressures throughout a temperature range that may be experienced in rechargeable cells is crucial [55]. For use in electric vehicles, this temperature range is -20 to 60 °C [54]. Gel electrolytes have a greater conductivity than “all-solid” ionically conductive polymers at ambient temperature (around 10^{-3} S/cm).

2.5 Poly(ethylene oxide) – PEO

The most common polymer host to build the electrolyte is reported to be high molecular weight poly(ethylene oxide) PEO. The main chain molecule $-\text{CH}_2-\text{CH}_2-\text{O}-$ dissolves the lithium salts quite effectively in comparison to other polymers. This is because it has a considerable ability to donate electrons. The interaction between polymer chains and lithium ion provides a right balance of solubility versus freedom of ion movement along the molecule. PEO is characterized by a low glass transition temperature (T_g), strong film-forming ability, outstanding solubility for lithium salts, good electrochemical stability against lithium metal, and good chain flexibility at a relatively cheap cost. The degree of crystallinity for a polymer-based electrolyte (PEO-LiX complex) is related to the ratio of EO/Li, which indicates the number of ether oxygens per Li-ion [56].

Without lithium salts, PEO is a semi-crystalline polymer with 60–80% crystallinity below its melting point, which is around 60 °C. The crystallinity and melting point exhibit a mild dependence on the length of the macromolecular chains— chains of high molecular weight may exhibit more entanglements and less crystallinity. Various additives or structural modifications can suppress the crystallization process of the polymer matrix or stoichiometric PEO:salt crystalline phases. Bolloré126 (manufacturer of electric vehicles), effectively demonstrated the potential of polyethers for solid state battery application in electric vehicles by introducing so-called Lithium Metal Polymer (LMP) battery technology in 2011. As a result, more than 8000 vehicles are currently operating on the LMP technology, demonstrating that PEO and its variants are both of contemporary interest and practically extremely relevant [57-58].

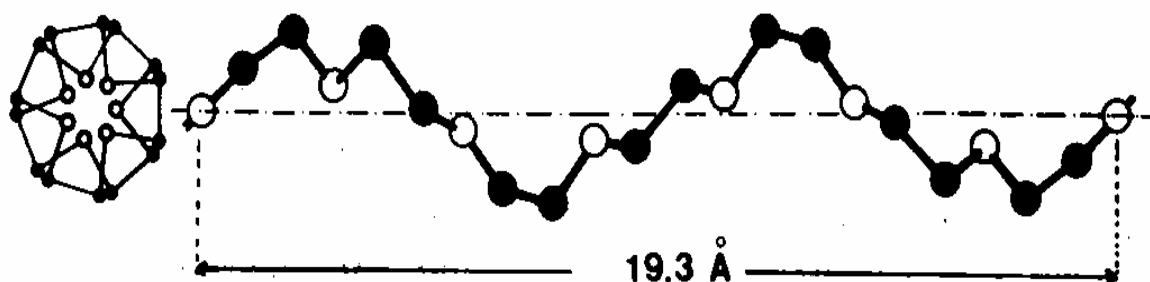
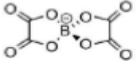

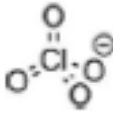

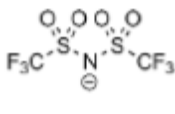
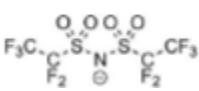
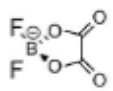


Fig. 2.6. The helical structure of PEO [59-60].

2.6 Lithium salts

Polymer electrolyte performance depends not only on kind of the macromolecular matrix but also on the lithium salt. One method for making polymer electrolytes more conductive is increasing the number of charge carriers by using a salt that easily dissociates into ions. It is important to provide adequate salt concentration, which ensures a balance between the concentration of free ions and formation of ion pairs and aggregation of salt. Ion migration can be affected by aggregates because they can hinder cation-polymer chain coordination. Salts that are suitable for use should have an anion of possibly large size and delocalized negative charge, and a low basicity, which will result in excellent salt dissociation, fewer ion pairings, and high conductivity in the PEO matrix. Many salts which meet these criteria have been developed, which are briefly presented in Table 2.2

Table 2.2. Structures and characteristics of frequently used lithium salts in polymer electrolytes [61]

Lithium salts	Anions	Main characteristics
LiBOB		<p>😊 High electrochemical stability and long term stability</p> <p>😞 Form highly resistive SEI-film (low conductivity in comparison to LiPF6 and LiTFSI)</p>
LiPF₆		<p>😊 High conductivity, favor SEI formation</p> <p>😞 Decomposes in the presence of moisture and with electrolytes at high temperature resulting in the formation of HF</p>
LiClO₄		<p>😊 Broad electrochemical stability window</p> <p>😞 Low solubility in carbonate type solvent</p>
LiBF₄		<p>😊 Broad electrochemical stability window</p> <p>😞 Low solubility in carbonate type solvent</p>
LiTFSI		<p>😊 High solubility, conductivity, electrochemical stability</p> <p>😞 Unable to form passivation layer on Al current collectors (Al-degradation and corrosion)</p>
LiBETI		<p>😊 High solubility, conductivity, electrochemical stability</p> <p>😞 Unable to form passivation layer on Al current collectors</p>
LiDFOB		<p>😊 High electrochemical stability and cycling behavior, Able to form passivation layer on Al current collectors</p> <p>😞 Lower solubility in carbonate type solvent compared to LiTFSI and LiPF6 but higher than LiBOB</p>

2.7 Lithium alkyltrialkoxyborates Li[Bu(RO)₃B]

To meet the requirements and meet the overarching objective of this research, which is to produce high ionic conductivity of a polymeric system while simultaneously limiting the mobility of anions, new electrolytes needed to be created. A combination of the concepts of novel salts and polyelectrolytes has resulted in the synthesis of lithium salts that include anions of molecular weights that are typical for oligomers. New lithium borate salts were produced by the research team of E. Zygadło-Monikowska et al. [62] at the Warsaw University of Technology using a straight forward reaction involving trialkoxyborates and butyllithium. The resulting materials have a general formula of Li[CH₃(OCH₂CH₂)_nO]₃BC₄H₉ with oxyethylene substituents (EO) of (*n* = 1, 2, 3, and about 7.5). The main aim of the synthesis of the new salts was to combine the benefits of ionic liquids and polyelectrolytes, while also compensating for the drawbacks of each of those systems. The expansion of the anion structure has been accomplished via the addition of oligomers, which are short chains of polymer molecules. These groups have a comparatively low molecular weight in relation to their size, and as a result, they are designed to reduce anion mobility without sacrificing the energy density of the whole system.

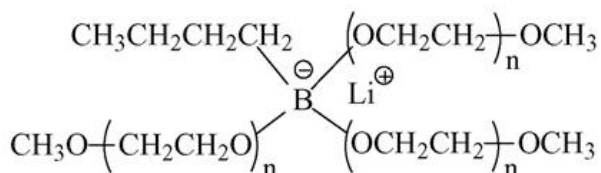


Fig. 2.7. A Scheme structure of Li[Bu(RO)₃B].

2.8 Transference numbers

Determination of ion cation transference numbers (also known as T_+) is required for a comprehensive electrochemical characterization of battery electrolytes. In the polymer electrolyte system, two ionic species are present the cation (Li^+) and the anion (A^-). The following equation provides a definition for ionic conductivity;

$$\sigma = \sigma_{\text{Li}^+} + \sigma_{\text{A}^-} \quad (2.9)$$

The parameter that represents the proportion of the current density that is carried by one of the ions to the overall density is called the transference number. The following relationship shows how it relates to conductivity [63-64]:

$$T_+ = \frac{\sigma_{Li^+}}{\sigma_{Li^+} + \sigma_{A^-}} \quad (2.10)$$

During the operation of the cell, lithium cations migrate to an electrode (anode on charging, cathode on discharging) and anions move in the opposite way. However, only cations enter intercalation electrodes, and anions accumulate on the electrode surface. This can result in a concentration gradient in the system, which in turn restricts the amount of power that the cell is able to produce. As a result, there is a great concern about growth in concentration polarization and resulting decrease of cell performance, and efforts are being made to prevent this phenomena by creating salt with a high cationic transference number.

Only lithium cations are important for the process of charging and discharging, but ionic conductivity measurements include the transport of both Li^+ and its counter ion. The transference number has a value between 0 and 1 because it describes a fraction of the current carried by a given ionic species. This value is important when considering how a battery cell will work in the long run. Low T_+ electrolytes cause lithium salt concentration gradients to form over time. This leads to poor high-rate performance and limits on how much power a cell can deliver. Studies have suggested that electrolytes exhibiting high T_+ (close to unity) are far superior in applications that require a high discharge rate than electrolytes with low T_+ , even when the conductivity of the materials is reduced by more than an order of magnitude. Li-ion T_+ values that are closest to 1 are therefore very desirable. Investigation of the cationic transference number in the electrolyte can be performed using different techniques, for example the potentiostatic polarization (PP) method, the galvanostatic polarization (GP) method [65], the electromotive force (emf) method [66], the Pulse Field Gradient (PFG)-NMR [67] and the impedance measurement [68].

As an example, in Fig. 2.8 electrolyte lithium ion transference number Li^+ are shown for PEO:LiTFSI electrolytes representing different concentration of lithium salt. These values are generally low, and for dilute systems much lower than 0.5. The differences arise from the fact, that some methods are designed to detect all positively charged mobile species, whereas others follow lithium, but regardless of its charge.

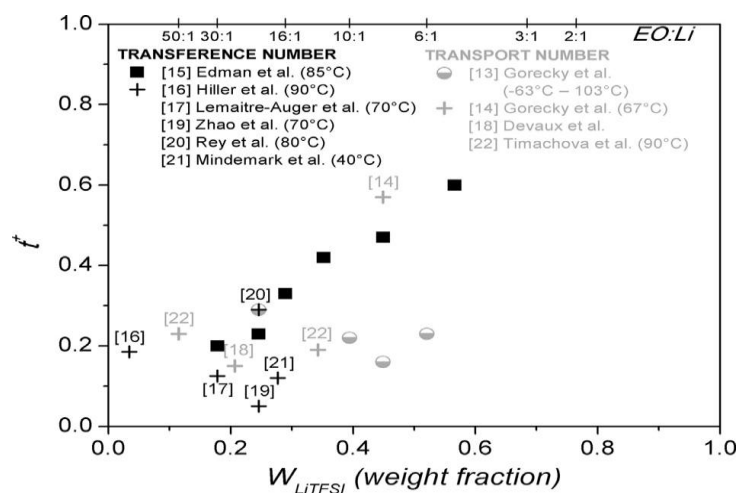


Fig. 2.8. Values of the lithium transport number and cation transference number for the PEO:LITFSI system by several research groups [69].

2.9 Conductivity of semicrystalline polymer PEO-based electrolyte

Temperature, the type and concentration of the dopant salt, and the degree of crystallinity all affect the conductivity of semicrystalline polymer Poly(ethylene oxide) (PEO)-based electrolytes [89-90]. As in any complex thermodynamical system, the conductivity of semicrystalline electrolyte may depend on its thermal history, and therefore different ionic conductivity values may be obtained at the same temperature. In semicrystalline electrolytes based on PEO, the crystalline fraction may be pure polymer (low salt concentrations), pure salt (high salt concentrations) as well as stoichiometric crystalline complexes of polymer and salt (middle salt concentration range).

1. Degree of Crystallinity

Crystalline areas: The crystalline areas of PEO-based electrolytes are usually less conductive due to the closely packed polymer chains, which restrict ion mobility. Most polymer-salt crystalline complexes are also poorly conductive or lack continuity of conduction channels.

Amorphous areas: The amorphous areas improve conductivity by allowing ions to move more freely. Therefore, better conductivity is often associated with a larger percentage of amorphous phase.

2. Dopant Salt

Type of Salt: Lithium salts like LiClO_4 , LiBF_4 , and LiTFSI are frequently utilized in PEO-based electrolytes. The mobility and dissociation of ions are influenced by the salt selection. Some salts introduce disorder in the polymer structure, decreasing crystallinity.

Salt Concentration: The quantity of charge carriers is maximized at the ideal salt concentration. Ion pairing and aggregation caused by an excessive concentration can lower conductivity.

3. Temperature

Thermal Activation: The greater segmental mobility of the polymer chains in the amorphous areas, which promotes ion transport, causes conductivity in PEO-based electrolytes to rise with temperature.

Melting of Crystalline Domains: For pure PEO, the crystalline domains melt at temperatures higher than PEO melting point, which is around 65 °C. This increases the amorphous content and improves conductivity. As stated above, the addition of lithium salts may decrease melting temperatures by introduction of structural disorder. However, with increasing amount of salt stoichiometric crystalline complexes may form, that have melting point higher than that of pure polymer. Therefore, for most lithium salts the practical approach to this problem is to find eutectic polymer/salt ratio with a low melting point. For PEO:LiTFSI, such a ratio occurs around 10:1 EO:Li.

As an example, Fig. 2.9 depicts the temperature-dependent conductivity of a PEO:LiTFSI semicrystalline electrolyte with a molar ratio of 10:1 EO:Li. The system can be obtained in three different states: molten amorphous, semicrystalline above glass transition temperature, and glassy state (semicrystalline or undercooled glassy melt). Above melting temperature of crystalline phases (Pure PEO or PEO:LiTFSI complexes), the conductivity is independent of the sample's thermal history.

The conductivity decreases gradually as the molten sample gradually cools. Crystallization can influence the temperature dependence of conductivity below the melting temperature as the crystalline lamellae are poorly conductive and block transport in amorphous phase. In the vicinity of the glass transition, crystallization is impossible because the chain cannot organize into lamellae [81].

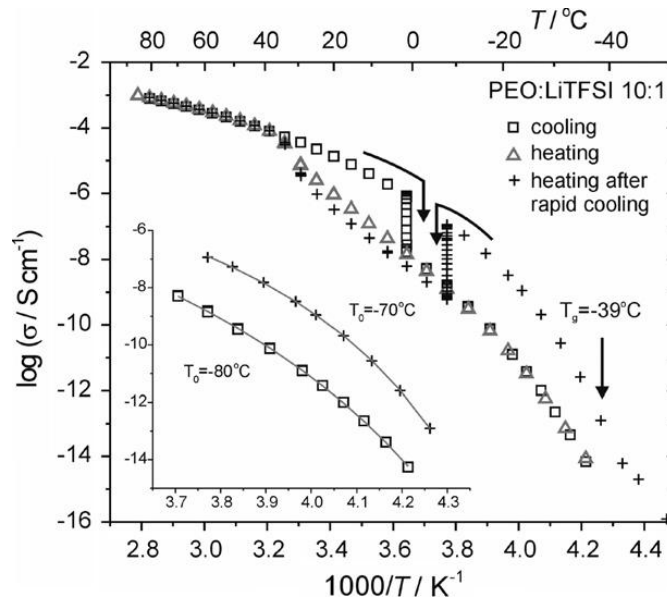


Fig. 2.9. Temperature dependence of the ionic conductivity for PEO:LiTFSI electrolyte with molar ratio 10:1 EO:Li [81].

Lascaud et al. [87] state that the formation of PEO complexes with salt determines the characteristics of the system as the quantity of salt in the electrolyte increases. Complexation may occur in both the crystalline and amorphous phases [88]. The impact of the creation of stoichiometric polymer:salt complexes on the characteristics of an electrolyte is insignificant when the concentration of salt in the polymer matrix is low. The LiTFSI salt essentially functions as a plasticizer in this type of electrolyte. A system like this is the PEO:LiTFSI electrolyte, which has a 50:1 molar ratio.

At room temperature, according to M. Marzantowicz et al. [91], the results obtained for PEO:LiTFSI electrolytes of various content of salt are summarized in table 2.3. All these values are in comparable with the present work.

Table 2.3. The ionic conductivity at room temperature for rapidly cooled amorphous PEO:LiTFSI electrolytes

$\sigma_{20\text{ }^\circ\text{C}}$ S/cm ⁻¹	50:1	16:1	10:1	8:1	6:1	3:1
	-6.9	-5.9	-5.6	-5.4	-8.7	-8.4

However, most of PEO – based systems exhibit obvious sharp drops on conductivity in the temperature of 65 °C due to the crystallization of PEO.

2.10 Dielectric properties of polymer electrolytes

The study of dielectric relaxation in solid polymer electrolytes is a great way to learn about how ions and molecules interact. The dielectric parameters related to relaxation processes are especially important in ion-conducting polymers, where the dielectric constant is a key indicator of how well a polymer material can dissolve salts. The dielectric relaxation and the frequency-dependent conductivity are both particularly sensitive to the movement of charged species and dipoles inside the polymer electrolytes. The low-frequency dielectric parameters of polyethylene oxide (PEO) and polypropylene oxide based polymer electrolytes have been investigated by Wintersgill and Fontanella [70]. It has been demonstrated that the composition of the additives and the temperature have a significant impact on the dielectric parameters. Polymers can be polar or non-polar. This feature affects significantly the dielectric properties.

Examples of polar polymers include PMMA, PVC, PA (Nylon), PC while non-polar polymers include PTFE (and many other fluoropolymers), PE, PP and PS. Under alternating electric field, polar polymers require some time to align the dipoles. At very low frequencies the dipoles have sufficient time to align with the field before it changes direction. At very high frequencies the dipoles do not have time to align before the field changes direction. At intermediate frequencies the dipoles move but have not completed their movement before the field changes direction and they must realign with the changed field. Polar polymers at low frequencies (e.g. 10 mHz) generally have dielectric constants of between 3 and 9 and at high frequencies (e.g. 10 MHz) generally have dielectric constants of between 3 and 5. For non-polar polymer the dielectric constant is independent of the alternating current frequency because the electron polarization is effectively instantaneous hence they always have dielectric constants of less than 3 [71].

The delayed response of the polymer dipoles against the applied electrical field is called dielectric relaxation. The earliest model of relaxation behavior is originally derived from Debye relaxation model [72]. In this model, real and imaginary part of dielectric constant can be represented as in Fig. 2.10

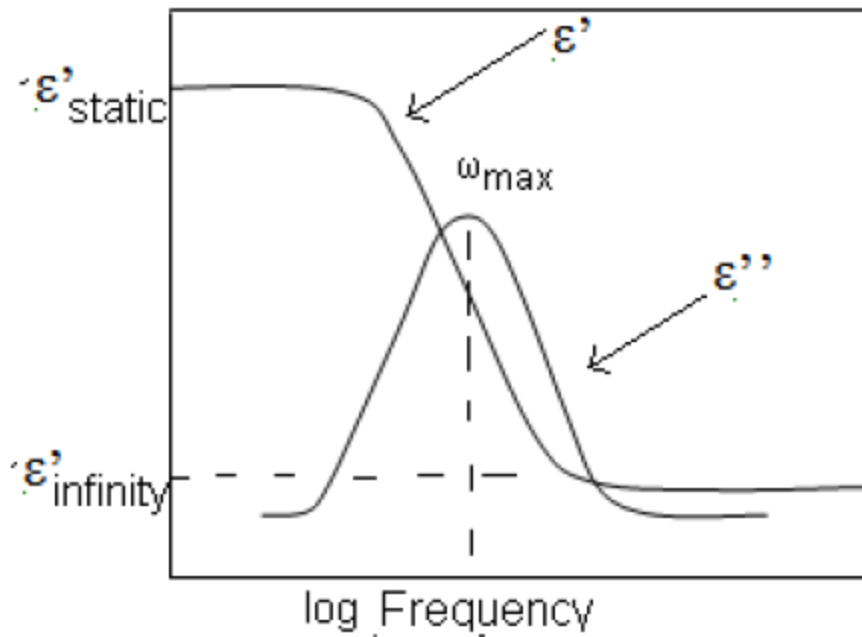


Fig. 2.10. Debye dielectric dispersion curve.

The complex dielectric behavior of a polymer electrolyte is expressed as:

$$\epsilon^* = \epsilon' + i\epsilon'' \quad (2.11),$$

where ϵ' representing the real part of the dielectric constant so-called relative permittivity constant or dielectric constant and ϵ'' representing imaginary part of the dielectric constant called relative loss permittivity or dielectric loss in the polymer electrolyte system. These dielectric properties can be expressed as:

$$\epsilon' = \frac{C_p d}{\epsilon_0 A} \quad (2.12),$$

$$\epsilon'' = \frac{\sigma}{\omega \epsilon_0} \quad (2.13),$$

where C_p = parallel equivalent static capacitance

d = thickness of sample

ϵ_0 = permittivity of free space ($8.856 \times 10^{-14} \text{ Fcm}^{-1}$)

A = surface Area of sample

σ = Ionic Conductivity of sample

ω = angular frequency ($2\pi f$)

Temperature affects dielectric properties. At lower temperature, the segmental motion of the chain is practically frozen. This effect reduces the dielectric constant in respect to the room temperature. As the temperature is increased the intermolecular forces between polymer chains are weakened which enhances thermal agitation. The polar group will be more free to orient allowing it to keep up with the changing electric field. At sufficiently higher temperatures, the dielectric constant is again reduced due to strong thermal motion, which disturbs the orientation of the dipoles. At this latter stage, the polarization effectively brings a minimal contribution to the dielectric constant.

Significant chain and segmental motions occur in polymers, e.g. $\text{CH}_2\text{CH}_2\text{O}$, CH_2Cl and $-\text{COOC}_2\text{H}_5$ and they are identified as follows [73]:

- i. α relaxation: micro-Brownian motion of the whole chain. Formally this motion is designated as glass transition.
- ii. β relaxation: rotation of polar groups around C-C bond and conformational flip of the cyclic unit.
- iii. γ relaxation: liberation of phenyl ring and limited C-H segmental chain movement.

3. Experimental Techniques

The relationship between the electrical and structural properties was studied using two methods: differential scanning calorimetry (DSC), which was used to study thermal properties, especially the T_g , and the melting point, and electrochemical impedance spectroscopy (EIS), which was used to study electrical properties, especially ionic conductivity and dielectric properties. Because these are used frequently throughout the thesis, particularly EIS, this section covers the basic background information on both methods. In addition, the technique that was used to determine the share of lithium ions in the charge transport has been described. It is generally known that both types of ions (cations and anions) may be mobile in polymer electrolytes. As a result, it is essential to determine what proportion of the current is carried by which mobile species. This is what is known as the measurement of the 'transport or transference' number.

3.1 Differential Scanning Calorimetry (DSC)

Differential scanning calorimeter (DSC) records the amount of heat that is needed to raise the temperatures of the sample and the reference (inert across the temperature range, which is commonly an empty aluminum pan) at a consistent rate (as a function of temperature and time). The heat flow is equivalent to the change in enthalpy since the measurement chamber is at constant pressure:

$$\left(\frac{dq}{dt}\right)_p = \frac{dH}{dt} \quad (3.1),$$

where:

dH/dt represents the rate of change of enthalpy (H) with respect to time (t).

The quantity of heat that flows to the sample during the phase transition might be larger or less than the reference in order to keep the sample at the same temperature. In endothermic processes, such as melting, the heat transfer to the sample is positive relative to the reference. As compared to the reference, the amount of heat that flows to the sample during an exothermic process, such as crystallization, is negative. The heat flow and the rate scan of the temperature can be used to figure out the heat capacity:

$$C_p = \left(\frac{dq}{dT}\right)_p = \left(\frac{dH}{dT}\right)_p = \frac{dH}{dt} \frac{dt}{dT} \quad (3.2),$$

where:

dT/dt represents the rate of change of temperature (T) with respect to time (t) [92].

During glass transition, upon heating the amorphous polymer sample changes from a brittle glass to a flexible rubber. This transition considerably impacts polymer segmental motion. The polymer's specific heat, coefficient of thermal expansion, and dielectric constant change significantly. The glass transition temperature T_g shows up on the DSC curve as a shift of the baseline in the endothermic direction (Fig. 3.1). The heat capacity varies on a second-order transition (T_g), but there is no heat transmission to the surroundings, and the volume changes smoothly to accommodate the increased segmental motion. At first order transitions (T_c and T_m), there is a sudden change in volume, as well as heat exchange between a system and its surroundings. The values of the read temperatures may change depending on the speed of the heating or cooling cycle and the mass of the tested material, the greater the mass and the rate of temperature change, the greater the shift in relation to the actual values.

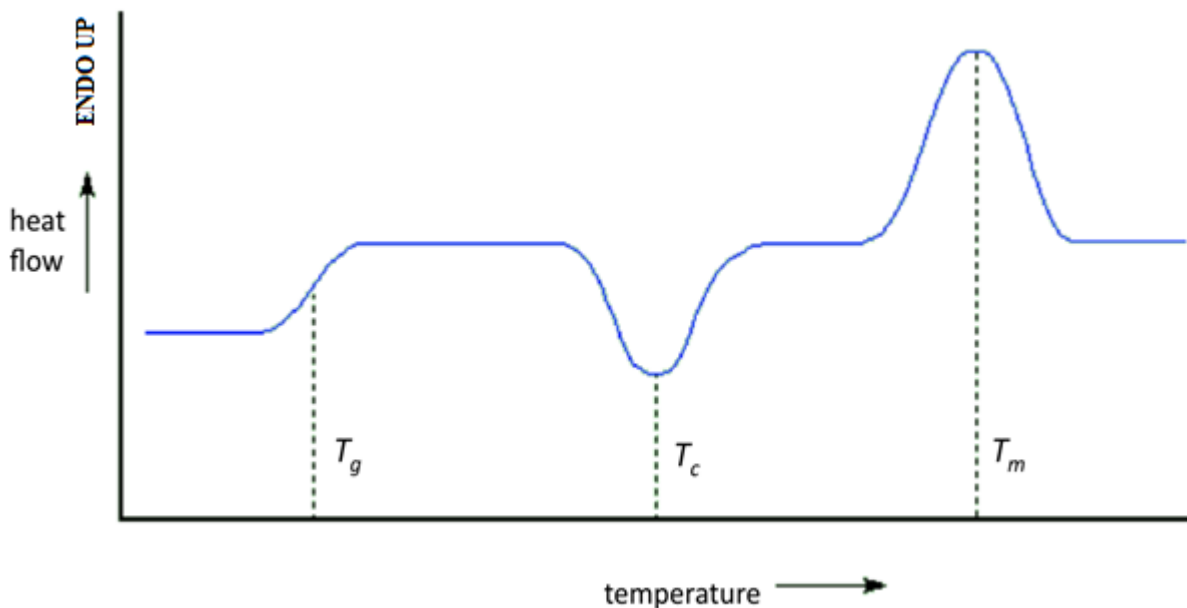


Fig. 3.1. A DSC scan with common features.

3.2 AC Impedance Spectroscopy

The EIS is a powerful technique used in many fields, including material science, electrochemistry, and electronics that takes in a frequency-dependent, small-amplitude

sinusoidal voltage perturbation and assesses the current response. Due to the fact that the entire electrochemical system can be usually modeled using simple circuit elements such as resistors, capacitors, and inductors, and that their current-voltage characteristics have different frequency dependencies, changing the frequency can separate the different processes and determine how much each one contributed to the impedance spectrum. The basic elements that can be used to model the system, as well as their impedances and current-voltage characteristics, are shown in Fig. 3.2.




Resistor		$V = I \times R$	$Z_R = R$
Capacitor		$I = C \frac{dV}{dt}$	$Z_C = \frac{1}{j\omega C} = -\frac{j}{\omega C}$
Inductor		$V = L \frac{dI}{dt}$	$Z_L = j\omega L$

Fig. 3.2. Current-voltage characteristics and impedances of basic circuit elements

Alternating current methods have certain benefits over direct current methods; for example, a simple cell with inert blocking electrodes may be utilized to provide information not only on ion migration but also on polarization phenomena.

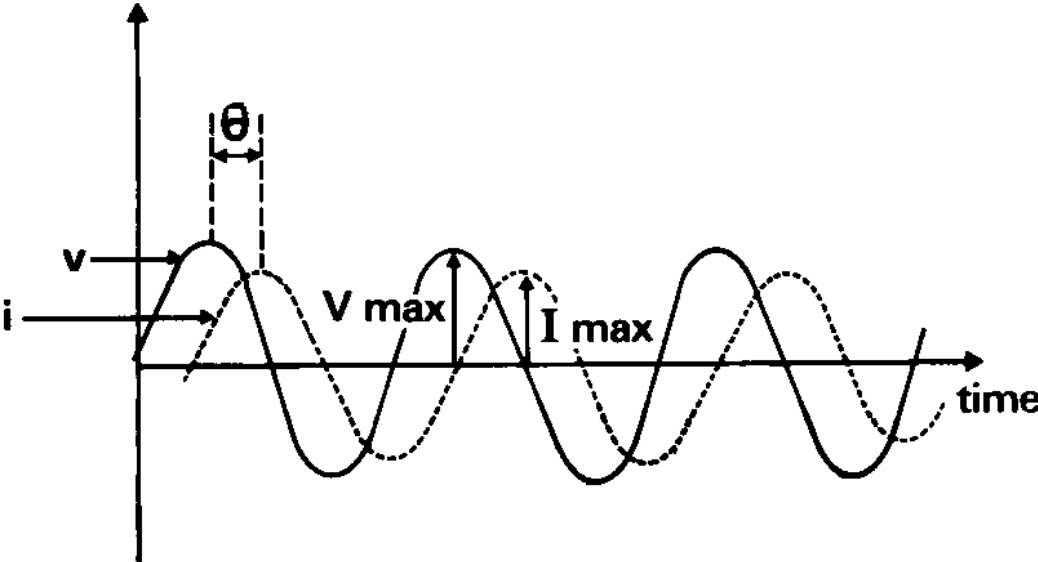


Fig. 3.3. Plots of the sinusoidal voltage and current at a specific frequency related to a cell. $V =$ voltage, $I =$ current, and $\theta =$ phase difference [60].

The basic idea behind the experiment is to apply a sinusoidal voltage to the sample and observe the resulting current oscillation (Fig. 3.3). Voltage and current are only related by Ohm's Law ($V=IR$) in a direct current experiment. An alternating current measurement needs two factors to establish a relationship between voltage and current: impedance modulus and phase. The modulus is calculated by dividing the maximum voltage by the maximum current (V_{max}/I_{max}). The second criterion to take into consideration is the phase difference θ between the sinusoidal current and voltage signals. The combination of these two parameters represents the cell impedance, Z . The frequency of the applied voltage through an electrochemical cell affects not only the amplitude but also the phase angle of the impedance of the studied object. In a typical impedance measurement the frequency is varied in a broad frequency range (usually from mHz to MHz).

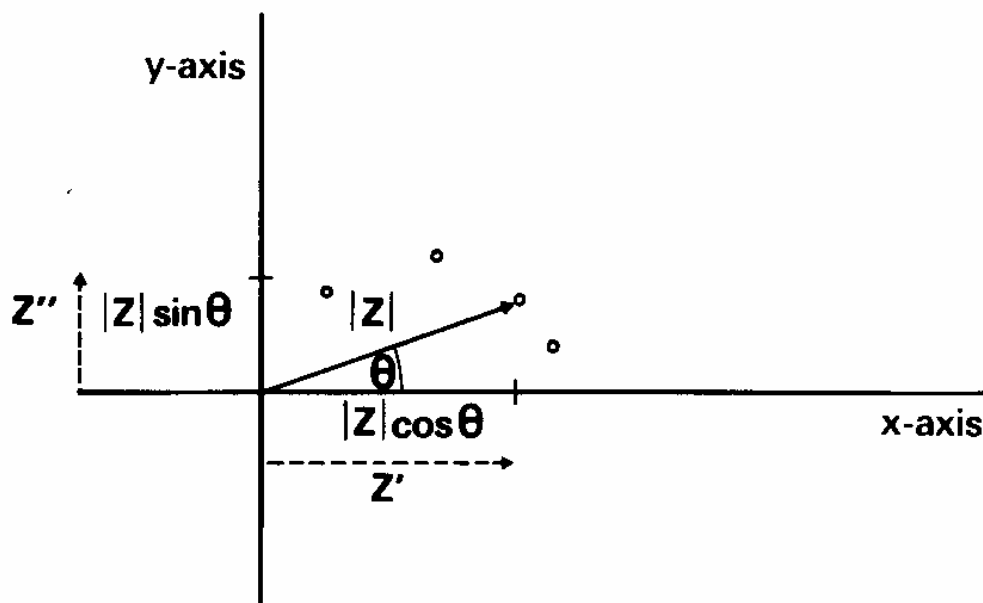


Fig. 3.4. Vector representation of cell resistance Z . Z' and Z'' are the real and imaginary components of a complex resistance [60].

Impedance is considered to be a vector quantity since it has both a length and a direction and can be represented by complex numbers. The impedance of a circuit may be calculated from the impedances of its components by treating the impedance as complex numbers and applying the laws of complex algebra. Hence an impedance, Z , can thus be expressed as $Z=Z'-jZ''$. This is what's referred to as a complex number's standard form, and it may be represented on a vector diagram (Fig. 3.4) with the y-axis representing the imaginary dimension and the x-axis representing the real dimension. A "model" circuit diagram might be used for the interpretation of the response of measured sample when an impedance measurement is made.

A circuit with a response similar to the experimental one is called an equivalent circuit. When there is only one resistor present, the current and voltage oscillations will be in phase with one another, $\theta=0$. Hence, there will not be any imaginary components in the impedance, and as a consequence, its modulus will simply equal the resistance, $|Z|=R$. In the vector diagram, this is depicted as a line with a length of R along the real axis. Moreover, this value is frequency-independent. For a single capacitor, the voltage is 90 degrees behind the current, so the phase angle is written as $-\pi/2$. In this case, the impedance has no real components and depends on the capacitance size as well as the frequency, $|Z|=1/\omega C$. This is depicted as a line or spike along the imaginary axis in a vector diagram.

When these components are linked in series, the sum of their impedances gives the total impedance of the circuit. Therefore, $Z^*=R-j/\omega C$ for a single resistor and capacitor in series. In the vector diagram, the value of resistor R shifts the capacitance “spike” along the real axis. When the components are linked in parallel, it is required to sum the admittances (the reciprocal of the impedance) in order to compute the overall impedance of the circuit.

$$Y^* = 1/Z^* \quad (3.3),$$

and

$$Y^* = Y_1^* + Y_2^* + Y_3^* + \dots \quad (3.4),$$

also

$$Y^* = Y' + jY'' = \frac{1}{(Z' - jZ'')} \quad (3.5),$$

thus

$$Y' = \frac{Z'}{(Z'^2 - Z''^2)}, Y'' = \frac{Z''}{(Z'^2 - Z''^2)} \quad (3.6) \quad (3.7),$$

because the admittance of a resistor is equal to $1/R$ and the admittance of a capacitor is equal to $j\omega C$, the equation for a resistor and a capacitor that are linked in parallel is as follows:

$$Y_{total} = 1/R + j\omega c \quad (3.8),$$

thus the impedance is simply the inverted of this;

$$Z^*_{total} = \frac{1}{1/R + j\omega c} \quad (3.9),$$

$$Z^* = R \left[\frac{1}{1 + (\omega RC)^2} \right] - jR \left[\frac{(\omega RC)}{1 + (\omega RC)^2} \right] \quad (3.10),$$

in the complex plane, a semicircle of diameter R is defined by the last equation in the complex plane. The impedance of the capacitor and the resistor are both identical at the frequency that corresponds to the maximum of the semicircle.

$$R = \frac{1}{\omega_{max} C} \quad (3.11),$$

$$\therefore \omega_{max} RC = 1 \quad (3.12),$$

giving

$$Z^* = R \left[\frac{1}{2} \right] - jR \left[\frac{1}{2} \right] \quad (3.13)$$

A resistor and capacitor connected in parallel but in series with another capacitor is the simplest model circuit that explains the usual behavior of the cell with ionic conductor (Fig. 3.5).

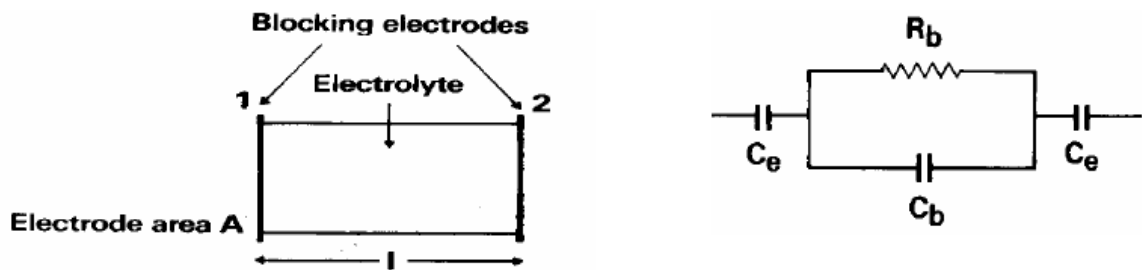


Fig. 3.5. A blocking electrode cell and the model circuit [60].

This illustrates a polymer electrolyte sample placed between two blocking electrodes. As the electrodes become alternately positively and negatively charged due to the alternating current, mobile ions in the electrolyte move in the applied electric field. The movement of the ions is obstructed by a resistance R_b . In an electric field, the polymer matrix of the electrolyte will not move over long distances but will polarize; the capacitance C_b in the circuit indicates this phenomenon. A double layer is created when ions reach the blocking electrode, and this double layer is associated with the capacitance C_e . The model circuit design includes two such capacitors since the effect happens at both electrodes.

Because R_b and C_b occur naturally in parallel to one another, they are represented in the model circuit in the same manner.

The relationship between the polymer dielectric constant and the polymer polarization capacitance, C_b , is as follows:

$$C_b = \frac{A\epsilon\epsilon_0}{l} \quad (3.14),$$

where A is the electrode area, l is the electrode separation distance, ϵ is the dielectric constant of the polymer and ϵ_0 is the permittivity of free space ($8.85 \times 10^{-14} \text{ Fcm}^{-1}$). As C_e is added to the bulk capacitance and resistance in series, the total circuit impedance may be calculated by adding the impedance due to C_e to the impedance due to the RC part of the model circuit:

$$Z^*_{total} = R_b \left[\frac{1}{1 + (\omega R_b C_b)^2} \right] - j \left(R_b \left[\frac{\omega R_b C_b}{1 + (\omega R_b C_b)^2} \right] + \frac{1}{\omega C_e} \right) \quad (3.15).$$

This equation explains the shape below (Fig. 3.6). When doing an AC impedance test on a polymer electrolyte, this is the shape that is seen the majority of the time.

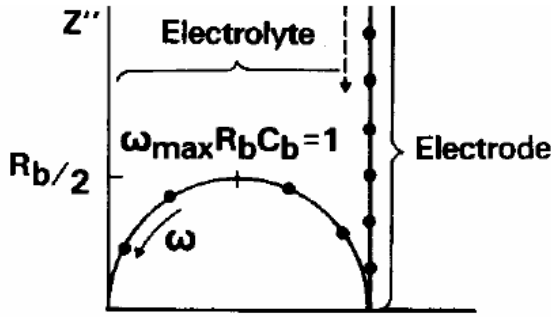


Fig. 3.6. An ideal AC impedance trace for a polymer electrolyte [60].

This curve may provide several different pieces of information, one of which is the bulk resistance. Because of this, it is possible to determine the specific conductivity of the sample, which is expressed in Scm^{-1} :

$$\sigma = \frac{1}{R_b} \left(\frac{l}{A} \right) \quad (3.16),$$

where l/cm is the electrode separation distance and A/cm^2 is the contact area of one of the electrodes. Since the impedance of a capacitor changes with frequency, simplifications can be made at the extremes of frequency. At high frequencies, the resistance that is connected with the capacitor ($1/\omega C_b$) has an order that is comparable to that of R_b . This means that the electrode capacitance has a very small effect (See Eqn. 3.15). Hence, the equivalent circuit may be reduced to a combination of a resistor and a capacitor that is connected in parallel. A simple semicircle will represent the AC impedance trace. For low frequencies, a comparable simplification is possible. Here, the bulk resistance is much lower than the impedance of the capacitor. So, the bulk capacitance has a small effect on the charge flow. The equivalent circuit is simplified to a series combination of the bulk resistance and electrode capacitance. The trace will take the form of a vertical line that is shifted horizontally by an amount equal to the bulk resistance.

A constant phase element (CPE) models the frequency dispersion or the power-law frequency dependence. This element can be used to depict various physical processes, like the transport of charge through a non-uniform energy barrier landscape, transport in two-phase or multi-phase structures with extended geometry (for example fractal structures), and low-loss dielectric phenomena. This element can also model cases in which the characteristic time of

the charge transport process has a certain distribution— that in many real systems is found more practical than assuming a single value.

$$Z = \frac{1}{(j\omega)^\alpha Q} = \frac{1}{(j\omega\tau_0)^\alpha} \quad (3.17),$$

where, Q is the CPE “strength” (usually expressed in Farads), which is proportional to the active area, and τ_0 is the characteristic time constant. The exponent α is dimensionless. When $\alpha=1$, the CPE behaves as a capacitor; when $\alpha=0$, the CPE behaves as a resistor; when $\alpha=-1$, the CPE behaves as an inductor; and when $\alpha=1/2$, the CPE behaves as the Warburg impedance, which describes a semi-infinite linear diffusion through a large planar electrode. In all cases, both α and Q do not depend on the frequency. This description is suitable for the impedance experiments in this thesis. The electrical response of the interfacial layer between electrolyte and electrode in real systems is not purely capacitive. The contact between the electrode and the sample might occasionally affect the results of the measurements. The insufficient contact between the layers may result from the fact that the two surfaces at the interface are not flat. This may be fixed by either polishing the electrodes or heating the sample to stimulate plastic deformation around the electrode surface imperfections. The contact area between electrodes can also be increased by applying pressure to the electrodes. In the complex plane plots, the electrode “tail” is not vertical, and the response of the interfacial layer is usually fitted by a constant phase element rather than a capacitor. The semicircle region of the figure can also be distorted due to dielectric relaxation, ion-ion interactions, and inhomogeneities in the polymer electrolyte [60]. Such distortion, often seen as a downward shift of the semicircle center along the imaginary axis, may be described by CPE element.

One of the effects that have a significant impact on the electrical properties of polymeric electrolytes are dielectric relaxations. Relaxation can be understood as the response of polar fragments of the polymer chain to external stimulation. Under the influence of a changing electric field, the material is oriented towards polar groups according to its direction. The time after which the segments return to the state before the change of orientation is called relaxation time τ . This can apply to both large-scale segmental movements and short-range (local) movements of the polymer chain.

In the impedance spectrum, in the imaginary part of the electric permeability near the frequency corresponding to the relaxation frequency, the maximum dielectric losses will be observed [84]. Analysis of the shape and position of this maximum allows the study of the

dynamics of the polymer matrix movements. The simplest model describing the effect of relaxation on the electrical response is the Debye model:

$$f(t) = \exp\left(\frac{-t}{\tau_p}\right) \quad (3.18),$$

where :

$f(t)$ —dielectric response function,

t —time,

τ —Debye relaxation time.

This function describes the disappearance of dielectric polarization as a function of time, and one of its physical models is the behavior of a spherical particle in a viscous medium [85].

With the dielectric response function, the dielectric permittivity can be linked in imaginary form as follows:

$$\frac{\varepsilon^*(\omega) - \varepsilon_\infty}{\varepsilon_s - \varepsilon_\infty} = \int_0^\infty \left| \frac{df(t)}{dt} \right| \cdot \varepsilon^{-i\omega t} dt = \frac{1}{1 + i \cdot \omega \cdot \tau_p} \quad (3.19),$$

where:

$f(t)$ —dielectric response function,

t —time,

τ_p — Debye relaxation time,

$\varepsilon^*(\omega)$ —imaginary part of dielectric permittivity as a function of frequency,

ε_s —static permittivity,

ε_∞ —high-frequency limit of the dielectric constant.

In the case of solid bodies, there may be several positions of equilibrium states, and with each one there is a potential barrier, which significantly complicates the phenomena of relaxation in these materials. It assumes then that the model will include more Debye relaxation with a

certain distribution of relaxation times. This is mainly due to the widening of the maximum dielectric losses visible on the impedance spectrum for amorphous substances.

$$f(t) = \int_0^{\infty} g(\tau) \cdot \exp\left(\frac{-t}{\tau}\right) d(\ln \tau) \quad (3.20),$$

$f(t)$ —dielectric response function,

t —time,

τ —relaxation time.

Considering this relaxation time distribution as a function of the dielectric response $f(t)$ (formula 3.20) and in the related (3.21) imaginary dielectric permeability, a better convergence of the curve matching the impedance data can be obtained. The following function then takes the form of Havriliak-Negami [84]:

$$\varepsilon^*(\omega) - \varepsilon_{\infty} = \frac{H}{\left(1 + (i \cdot \omega \cdot \tau_p)^a\right)^b} \quad (3.21),$$

H —relaxation strength

a —constant that describes the peak width

b —constant that describes the peak asymmetry

τ_p —Debye relaxation time,

$\varepsilon^*(\omega)$ —imaginary part of dielectric permittivity as a function of frequency,

ε_s —static permittivity,

ε_{∞} —high-frequency limit of the dielectric constant.

The relaxation strength H , is taken to be the difference between the low-frequency and high-frequency limits of the dielectric constant ie. $H = \Delta\varepsilon = \varepsilon_s - \varepsilon_{\infty}$. Whereas parameters a and b are responsible for the shape of the relaxation time distribution curve, where the maximum of the function is visible for τ . The parameter a is related to the width of the maximum curve, and the parameter b is responsible for the asymmetry of the edges. For the case in which the parameters $a, b = 1$, we get the Debye equation, which corresponds to one time τ . The

influence of the values of a and b parameters on the shape of the spectrum of the real and imaginary part of the dielectric function is presented on the Figs. 3.7 and 3.8 respectively.

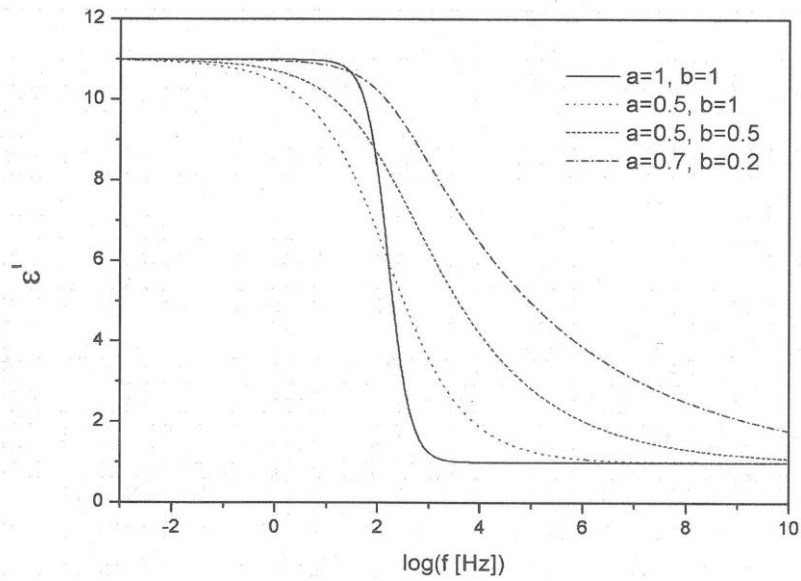


Fig. 3.7. Simulations of the real spectrum of dielectric function ϵ for selected values of parameters a and b , with constant values of relaxation strength $H = 10$, relaxation time $\tau = 10^{-3}$ S and high frequency limit of dielectric constant $\epsilon_{\infty} = 1$.

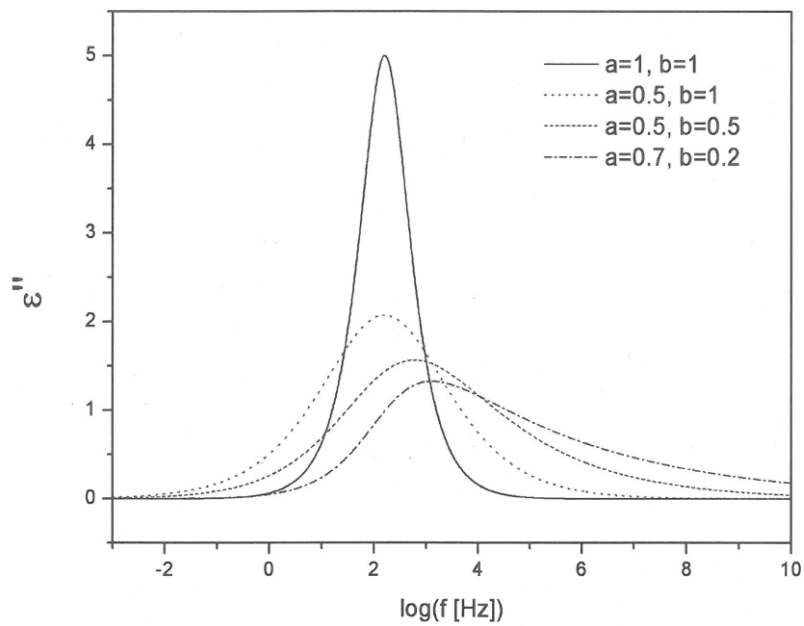


Fig. 3.8. Simulations of the imaginary spectrum of dielectric function ϵ for selected values of parameters a and b , with constant values of relaxation strength $H = 10$, relaxation time $\tau = 10^{-3}$ S and high-frequency limit of dielectric constant $\epsilon_{\infty} = 1$.

3.3 Transference Number Estimation

As it was mentioned before lithium transference numbers are a more specific property that is defined as the amount of total ionic conductivity that comes from lithium cations alone. There are a few methods that can be used to accurately measure T_+ , in the current work we focused on the two below methods:

3.3.1. Bruce-Vincent method

The T_+ measurement technique, which used a combination of EIS and chronoamperometry, was first disclosed in the year 1989 [74]. The EIS was utilized in order to deconvolute the contributions of high rate processes, such as those that take place at the interface between the electrolyte and the electrode. The technique of chronoamperometry was utilized so that the more slow processes, like diffusion, could be characterized. Also provided was the formula for computing T_+ , which is as follows:

$$T_+ = \frac{I_s (\Delta V - I_0 R_{i0})}{I_0 (\Delta V - I_s R_{is})} \quad (3.22),$$

ΔV – a potential disturbance that is imposed on the measuring cell while a chronoamperometric measurement is being carried out.

I_0 – “initial” electric current. It is a current that is measured at the start of the salt concentration gradient that builds up in the bulk of an electrolyte. In order to evaluate this instant, the EIS data were analyzed.

I_s – “steady-state” or “stationary” electric current. It is an electric current that remains constant throughout time and is measured after a little potential difference has been introduced into the system. It takes a considerable amount of time for the transient effects to fade away and for the system to converge to the steady state for a typical polymer electrolyte.

R_{i0} and R_{is} are the interface resistances (similarly to subscripts in I_0 and I_s , characters “0” and “S” mean “initial” and “steady state” respectively).

It is much harder to interpret the results of EIS measurements when the circuit is not open (i.e. when there is a bias/offset potential, as in the HF EIS). Moreover, this type of biased EIS will cause the steady state to be distorted, particularly when it is applied at low frequencies. This,

in turn, may have an effect on the validity of the I_s estimation or significantly lengthen the time required to complete the measurement process. In the present research, the procedure implemented a modification of Bruce-Vincent method.

3.3.2. Watanabe method

An approach that combines impedance measurements and potentiostatic polarization for the estimation of cationic transport number was also established by Watanabe and co-workers [75]. In this method, the transport number is described by the formula:

$$T_+ = \frac{R_{bs}}{\frac{\Delta V}{I_s} - R_{is}} \quad (3.23),$$

where R_{bs} is the bulk resistance after d.c. polarization, and the other values have the same significance as those given in eq. (3.22)

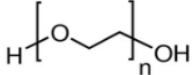
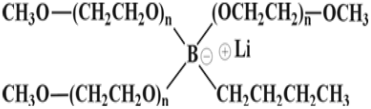
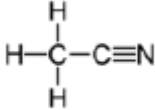
In general, the interface resistance should be determined based on the EIS measured at an open-circuit potential and after the potentiostatic polarization from which the I_s was taken. This is because the properties of a system can change over time. It is also very important to precondition the measuring cell with a new sample to speed up the process of achieving a thermodynamic state that is relatively stable.

4. Experimental: preparation of materials and characterization methods.

4.1 Materials

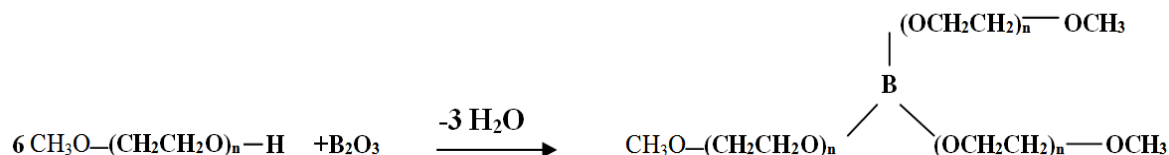
The molecular formula, weight, and structure, chemical name, and source of materials used in the experiments in this thesis are listed in Table 4.1. Studied systems comprised high molecular weight PEO as the polymer matrix and the lithium oligomeric salt with general formula $\{\text{Li}[\text{CH}_3(\text{OCH}_2\text{CH}_2)_n\text{O}]_3\text{BC}_4\text{H}_9\}$. The electrolytes were obtained by solvent-casting method, using acetonitrile as the solvent.

Table 4.1. Materials used in the study.

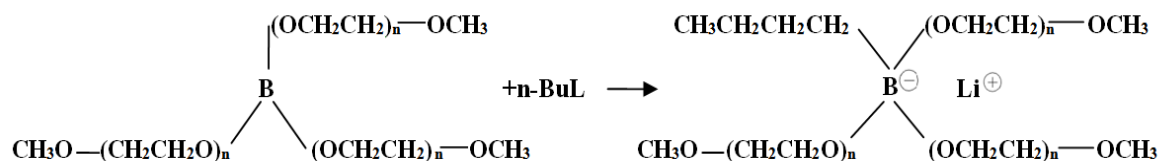
Name	Molecular Formula	Molecular Structure	Molecular Weight g/mol	Source
Polyethylene Oxide	$\text{H}-(\text{O}-\text{CH}_2-\text{CH}_2)_n-\text{OH}$		5×10^6	Aldrich
Lithium alkyltrialkoxy borates	$\text{Li}[\text{Bu}(\text{RO})_3\text{B}]$		$n1=300$ $n2=431.75$ $n3=563.75$ $n7.5=1097.8$	Faculty of Chemistry/ Warsaw university of technology
Acetonitrile	$\text{C}_2\text{H}_3\text{N}$		41.05	Aldrich

4.2 Synthesis and characterization of lithium alkyltrialkoxyborates $\text{Li}[\text{Bu}(\text{RO})_3\text{B}]$

Lithium borate salts were prepared at the Faculty of Chemistry, Warsaw University of Technology by a two-step synthesis process, described below. In the first step of the salt synthesis, trialkoxyborates were obtained from B_2O_3 and respective oxyethylene glycol monomethyl ethers with the removal of the produced water in the form of an azeotrope with toluene [76], according to the reaction scheme:



The obtained trialkoxy derivatives of boron were converted into the form of lithium salts in the reaction with *n*-butyllithium (Aldrich), according to the following scheme:



($n = 1, 2, 3, 7.5$).

The reactions were performed by gradually dropping the butyllithium solution in hexane to the trialkoxyborane solution in hexane during vigorous stirring and cooling of the reaction mixture due to the strong exothermal effect. After completion of the reaction, the product was washed several times with hexane and dried under reduced pressure. In the resulting structure of the anion, four groups are bonded to the central boron atom: one butyl group and three oligomeric ethylene oxide segments. Four different types of anions were obtained, varying in length of these oligomeric segments. Such a structure has been confirmed by NMR basing on ^1H (Varian 400 MHz) and ^{11}B referenced to pirazabol (2.6ppmin C_6D_6) (Varian 128.3 MHz) in solutions in CD_3CN [62]. Salt with $n = 1$ has been obtained as a waxy solid, whereas salts with average n of 2, 3 and 7.5 were viscous liquids at room temperature.

4.3 Preparation and characterization of polymer electrolytes

Polymer electrolytes were prepared by casting from solution. After weighing each of the above-mentioned components on the electronic balance the weighted amounts of lithium borate salts and high molecular weight PEO (Aldrich, $M_w = 5 \times 10^6$ g/mol) were mixed in 20 ml of anhydrous acetonitrile (Aldrich). Upon heating to 50 °C on a hot plate and with the speed of the magnetic stirrer set to 500 rev/min, a clear liquid was obtained, which was later poured on flat glass dishes, 6 cm diameter each. This solution was subjected to a two-stage drying process. The first stage involved drying under a low vacuum, which allowed the formation of a thin foil. In the second step, which lasted at least two weeks, the remaining solvent was removed under a high vacuum.

The weight proportions of polymer and oligomeric salts were chosen so that they represented certain molar proportions of EO units (coming both from anion and from polymer) to lithium: 50:1, 32:1, 16:1 and 10:1 (Table 4.2). As the number of EO units contained within the anion varied with the length of the oligomeric groups, for some of the salts the “intrinsic” molar ratio did not allow the preparation of specific electrolyte composition. The value of this intrinsic ratio EO:Li is calculated as the length n multiplied by 3, and therefore for $n=7.5$ it reaches 22.5:1. Therefore, for this salt preparation of electrolytes with EO:Li of 16:1 and 10:1 was not possible.

Table 4.2. Weight proportions (PEO to salt) and molar proportions EO:Li of electrolytes comprising oligomeric borate salts with various length of and PEO. The last row presents intrinsic EO:Li molar proportions of borate salts.

EO:Li	Weight proportions (PEO to salt)			
	$n=1$	$n=2$	$n=3$	$n=7.5$
50:1	6.90	4.48	3.20	1.05
32:1	4.26	2.65	1.79	0.36
16:1	1.91	1.02	0.55	-
10:1	1.03	0.41	0.08	-
Intrinsic EO:Li of salt	3:1	6:1	9:1	22.5:1

All preparations of measurement cell were carried out in an argon-filled glove box. The dry glove box (Fig. 4.1) was also used to keep the reagents as well as the final products. A magnetic stirring plate was used to mix the solution. Stirring allowed to speed up the dissolution process as well as to homogenize the solution. The samples used for DSC measurement were weighted on analytical balance.



Fig. 4.1. Glovebox system.

4.4 Impedance spectroscopy measurements

The measurement method along with the method of analyzing the results obtained has already been described in Section 3.2. In the case of materials tested as part of the work, one of the essential elements of the study was the appropriate preparation of samples. Preparation of polymeric electrolytes for measurement first consisted of placing a small amount of material in the measuring holder, the construction scheme of which is shown in Fig. 4.2, and the picture of the actual device in Fig. 4.3. The measuring holder after cleaning and degreasing the electrodes was introduced into the glove box filled with argon, in which all the samples were stored. Then, in order to obtain an even distribution of material between the electrodes, pre-compression was made by maximum lowering of the upper electrode, covering the handle with a gas-tight lid (Fig. 4.3, No. 1).

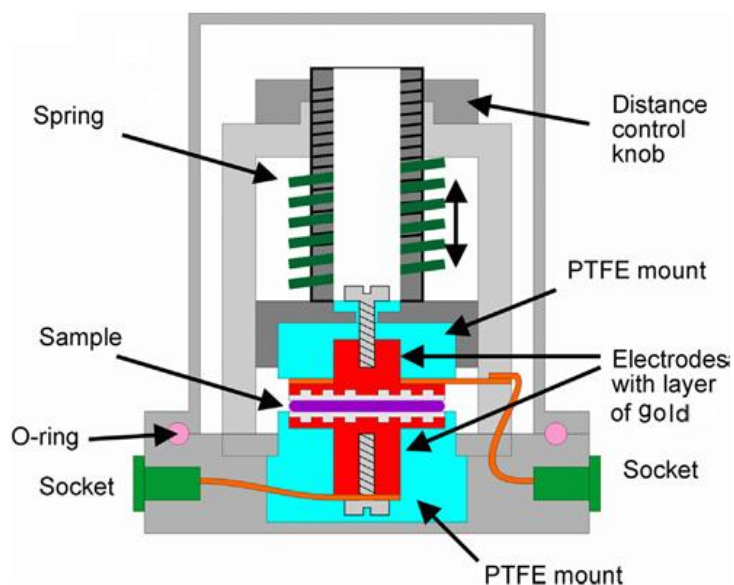


Fig. 4.2. Schematic presentation of cross-section of gas-tight sample holder with adjustable spring loading of upper electrode [69].



Fig. 4.3. Measuring holder (No.2) with gas-tight screwed lid (No.1) and electrode in Teflon cover (No.3).

Blocking electrodes of stainless steel covered with a gold layer were used in the holder. An important element in the construction of the measuring holder is the knob to change the height of the upper electrode, the diagram of which is shown in Fig. 4.4.

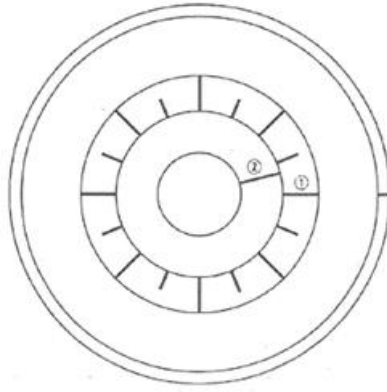


Fig. 4.4. Diagram of the knob for adjusting the distance (top view).

Characteristic grooves on the surface of the knob made it possible to measure the thickness of the tested samples placed between the electrodes before and after the measurement. The mechanism used allowed to keep the spring pressing the electrodes to the sample, while preventing complete squeezing of samples from between the electrodes.

A total of 20 grooves (including 10 deeper ones - shown in Fig. 4.4) are located on the surface of the knob. With a thread pitch of 1 mm, the distance between the two closest grooves corresponds to a change in the distance between the electrodes equal to 50 μm . The distance of the upper electrode relative to the bottom one was set by changing the position of the external groove (line marked with No.1) against the fixed internal groove (line marked with No.2). The thickness measurement required recording the position of the above-mentioned grooves in relation to each other when the two electrodes were in contact (without the sample) and subsequently with the sample inserted between the electrodes. Thanks to the scaling of the clamping mechanism, after the test, the actual thickness of the material can be read and then used to re-scale electrical conductivity values. The use of spring clamping can change the distance by pre-set limit of movement (usually about 50 micrometers), so it is necessary to measure the thickness both before and after the series of measurements.

The measuring stand used for impedance measurements shown in Fig. 4.5 consisted of the Alpha-N frequency response analyzer (Novocontrol) and the temperature stabilization system of the measuring holder. The temperature stabilization system included a thermostat based on the Peltier-type heating and cooling plates, an adjustable thermostat power supply, a Eurotherm 2416 temperature programmer, and the Advantech 4013 temperature sensor.

One of the intentions of this work was to study the behavior of polymeric electrolytes near the glass transition temperature. The detailed objectives included confirmation of the expected transition from the temperature dependence of the Arrhenius type to the VTF-type dependence, and an explanation of an unusual relationship between the glass transition temperature values obtained by calorimetric methods and the ideal glass transition temperature obtained from impedance measurements. In the latter case, the ideal glass transition temperature can be obtained both from the analysis of the temperature dependence of the ionic conductivity (representing the total contribution of all charge carriers and all transport modes) and from the temperature dependence analysis of relaxation times of segmental and local movements of polymer chains (representing only specific transport mechanisms).

Conducting the intended tests required impedance measurements in the vicinity of the glass transition temperature, thus reaching a sufficiently low temperature (around $-60\text{ }^{\circ}\text{C}$). Because the thermostat initially did not provide sufficiently efficient cooling, for this work modifications to its construction had to be made. The walls along with the bottom and the thermostat's cage have been made of aluminum plates, which have been lined with air gel and profiled rubber foam on the inside, for maximum insulation of the measuring holder from the external environment.



Fig. 4.5. The measuring system for impedance spectroscopy.

4.5 Differential scanning calorimetry measurements

The procedure for preparing samples for measurement took place, similarly as in the case of impedance tests, in a glove box under an inert argon atmosphere.

After weighing small fragments of individual materials, each of the samples was placed in a hermetically sealed, aluminum measuring container Fig. 4.6 B. The tests were carried out using the Thermal Analysis Q2000 calorimeter shown in Fig. 4.6 A. All temperature ramps followed the same scheme. First, each sample was cooled to $-120\text{ }^{\circ}\text{C}$, then heated at a constant speed of $20\text{ }^{\circ}\text{C} / \text{min}$. up to $140\text{ }^{\circ}\text{C}$, followed by rapid cooling to $-120\text{ }^{\circ}\text{C}$ at $100\text{ }^{\circ}\text{C} / \text{min}$ and the last heating run to $150\text{ }^{\circ}\text{C}$ at $20\text{ }^{\circ}\text{C} / \text{min}$.



Fig. 4.6. Differential Scanning Calorimeter (DSC) Q2000 series of TA Instruments

4.6 Measurements of lithium transference number

The content of the following subchapter is based on the work of Karol Pożyczka [69], who performed measurements of lithium transference numbers of the studied family of electrolytes as part of his PhD thesis, conducted in the same research team. These results serve as complementary to the present study, which focuses on other properties of the system.

The measurements were conducted in a symmetrical Li|Li cell. The holder used for measurements was similar to the one described previously. Lithium discs of diameter identical to the diameter of the stainless steel electrodes were pressed onto a grooved surface of stainless steel electrodes. During the pressing process, the exposed surface of the lithium electrode was protected by thin Teflon foil. The passivation layer was removed from the lithium surface by peeling off this foil, leaving a shiny active surface. After assembly in the glove box, the measurement holder was closed hermetically.

The measurements of the transference number were performed by recently developed symmetric polarization procedure [69] using a Potentiostat/Galvanostat Autolab PGSTAT 30 in a temperature range from 40 °C to 110 °C with a step of 10 degrees.

Cells were assembled with fresh electrolyte samples and allowed to equilibrate at 90 °C for around 8 hours before their initial measurement. The impedance spectra were initially measured from 50 kHz to 10 mHz with an ac signal of 10 mV or 30 mV rms (the amplitude was 10 mV for samples with low "bulk" resistance and 30 mV for samples with high "bulk"

resistance). A method known as symmetric polarization technique, or SPP for short, was utilized in order to arrive at the transference number results. The applied procedure introduces a modification of the Bruce-Vincent method [74] by application of two potentiostatic polarization segments with opposite sign of d.c. bias ($+\Delta V$ and $-\Delta V$) instead of only one segment, as in the original approach. The main reasons for application of such a procedure are:

- i. Lithium might be in a different condition at the two electrodes. This could be because of surface passivation or other factors.
- ii. There may be differences in how electrolyte sticks to the lithium surface of each electrode.
- iii. Possible difference in temperature or concentration between the lower and upper electrodes in the volume of electrolyte between them.

5. Results and discussion

Chapter presents results obtained for pure oligomeric borate salts (Lithium alkyltrialkoxoborates), as well as electrolytes formed by the addition of those salts to high molecular weight PEO (Aldrich, $M_w = 5 \times 10^6$ g/mol). In this work, two main experimental methods were applied:

- Differential scanning calorimetry for studies of crystallization/melting and glass transition,
- Impedance spectroscopy and subsequent equivalent circuit analysis for studies of ionic conductivity and other electrical properties,

As stated above, this work also cites the results obtained by Symmetrical Polarization electrochemical method used for calculation of lithium transference numbers [69].

5.1 Thermal properties of the studied system

For all studied samples of pure oligomeric salts (Lithium alkyltrialkoxoborates) the glass transition was observed on heating as an endothermic step that occurred in the low temperature range (Fig. 5.1). We can see that the glass transition temperature (T_g) event is present for all salts, although it is most distinctive for the oligomeric chain length of ($n=2$) and ($n=3$). This can be explained by the amount of amorphous phase in the sample, the glass transition is mainly a property of the amorphous phase, and therefore the related signal will be proportionally weaker in the semicrystalline sample.

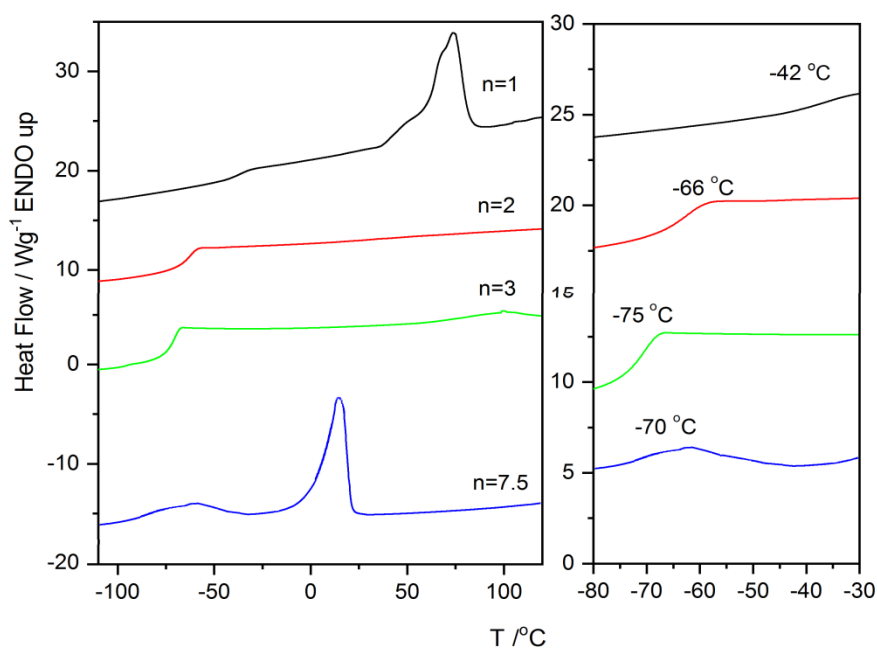


Fig. 5.1. DSC traces recorded during first heating at a rate of 20 °C /min, for pure borate salts with different length of oligomeric chains.

As can be noticed, the salt with substituent $R = -\text{CH}_2\text{CH}_2\text{OCH}_3$ ($n=1$), characterized by a considerably high glass transition temperature ($T_g = -42$ °C), is semicrystalline and melts at 73 °C. The melting peak is asymmetrical and shows a wide pre-melting event. Salts with ($n=2$ and 3) have low T_g of the order of -66 °C to -75 °C. Their thermograms do not exhibit any events related to melting or crystallization, confirming their amorphous state. For salt with ($n=7.5$) the melting peak is observed at ca. 5 °C. In comparison to the results obtained for salt with the shortest oligomeric chains salt with ($n=1$) this event is more narrow on the temperature scale. It may be suspected that in case of this oligomeric salt the side oxyethylene substituents are long enough to form substances of a regular structure. The glass transition event occurs at -70 °C.

The values of heat of fusion obtained by integration of melting peaks from DSC traces of borate salts (Lithium alkyltrialkoxaborates) are presented in Table 5.1. As can be observed for salts with ($n=1$) and ($n=7.5$) the heat of fusion increases with increasing the length of oligomeric segments of crystalline borate salts system.

Table 5.1. The values of T_g , T_o , T_m and Q_f for Lithium alkyltrialkoxypolyborates system with different length of oligomeric groups

Type of polymer electrolytes	$T_g / ^\circ\text{C}$	$T_m / ^\circ\text{C}$	Heat of fusion J/g
1	-42	73	16.7
2	-66°C	—	—
3	-75	—	—
7.5	-70	5	35.9

Figs. 5.2-5.5 show DSC traces of electrolytes with molar ratio EO:Li of 10:1, 16:1, 32:1 and 50:1 comprising borate salt with ($n=1, 2, 3$ and 7.5) respectively. Two features can be distinguished on the plots of electrolytes comprising borate salt with ($n=1, 2$ and 3): endothermic step related to glass transition below room temperature and a melting peak above room temperature. For electrolyte comprising PEO and oligomeric salt with ($n=1$), representing molar ratio EO:Li of 10:1, the DSC traces reveal a distinctive glass transition situated at -51°C as well as a melting peak at 72°C . The thermogram of electrolyte with molar ratio EO:Li of 16:1 prepared using salt with ($n=1$), a glass transition situated at -48°C as well as melting peak at 71°C . The glass transition temperatures for electrolytes with molar ratio EO:Li of 10:1 and 16:1 are lower by about 9 degrees for 10:1 and 6 degrees for 16:1 than that of pure oligomeric salt with ($n=1$), and higher by about 3 degrees for 10:1 and 6 degrees for 16:1 than T_g of pure PEO (-54°C).

The DSC curves of electrolytes with an EO:Li ratio of 10:1 and electrolytes with an EO:Li ratio of 16:1 feature a double melting peak, which may be explained by the fact that the two fractions (PEO and lithium alkyltrialkoxypolyborates salt) melt at slightly different temperature. Such an effect is therefore evidence of segregation of the two compounds. The thermogram of electrolyte with molar ratio EO:Li of 32:1 prepared using salt with ($n=1$) contains one event which can be ascribed to the glass transition situated at -43°C , as well as a distinctive melting peak at 67°C . The thermograms obtained for electrolyte prepared using the same salt, but different molar ratio EO:Li of 50:1 contain one event which can be ascribed to the glass transition at -51°C , as well as a distinctive melting peak at 76°C . The glass transition temperature for electrolytes with molar ratio EO:Li of 32:1 is not much lower than

that of pure oligomeric salt with ($n=1$) and 9 degrees lower than the glass transition of system with EO:Li of 50:1.

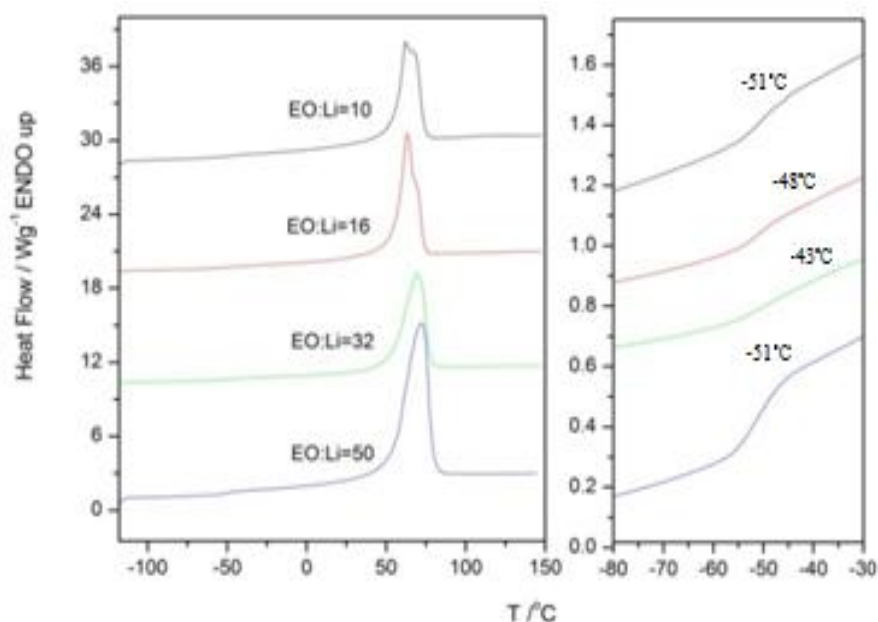


Fig. 5.2. DSC traces of polymer electrolytes composed of high M_w PEO and $[(RO)_3BBu]Li$ ($n=1$) with different EO:Li. All data collected during second heating cycle.

In the case of electrolytes formed by mixing linear PEO with oligomeric chain length ($n=2$) the glass transition event is situated at -63 °C and -66 °C in the case of electrolytes with molar ratio EO:Li 10:1 and 16:1 respectively and at the same temperature of -53 °C for electrolytes with molar ratio EO:Li of 32:1 and 50:1. All electrolytes exhibit a melting peak, situated at 65 , 60 , 72 and 68 °C respectively, as can be seen in Table 5.2.

The values for the heat of fusion were determined by integrating the melting peaks from the DSC traces. As can be seen in Table 5.2, for all electrolyte samples the heat of fusion is reduced with increasing the length of oligomeric groups ($n=1,2,3,7,5$). The electrolyte made using oligomeric salt with ($n=3$) and a molar ratio EO:Li of 32:1 and 50:1 is an exception to this general trend.

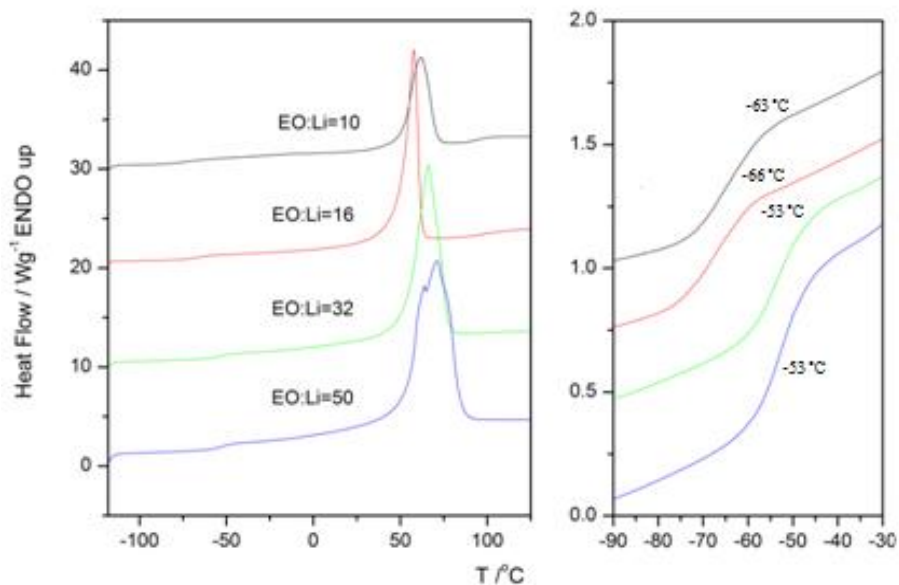


Fig. 5.3. DSC traces of polymer electrolytes composed of linear PEO and borate salts, length of oligomeric arms ($n=2$), measured during second heating. The samples vary by molar ratio EO:Li.

For the electrolyte comprising PEO and oligomeric salt with ($n=3$), representing molar ratio EO:Li of 10:1,16:132:1 and 50, the DSC traces of electrolytes with EO:Li 10:1 and 16:1 reveal a distinctive glass transition located at (-80, -77) °C respectively as well as melting peaks located at (59, 59) °C respectively. Electrolytes with EO:Li 32:1 and 50:1, have an indistinctive glass transition located at (-58, -64) °C and melting peaks located at (73, 61) °C.

In this case, only the glass transition temperature of with molar ratio EO:Li of 10:1 is lower than that of pure oligomeric salt with ($n=3$).

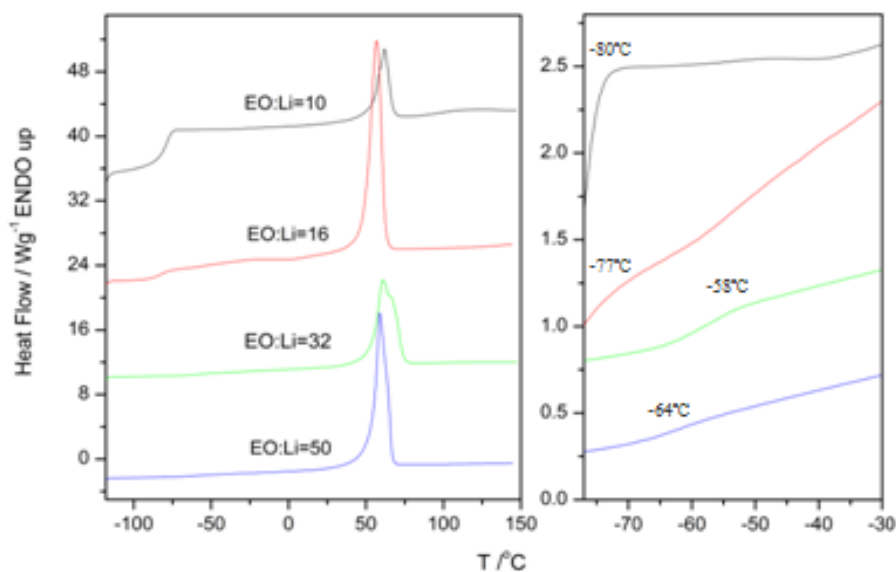


Fig. 5.4. DSC traces of polymer electrolytes composed of linear PEO and borate salts, length of oligomeric arms ($n=3$), measured during second heating. The samples vary by molar ratio EO:Li.

The thermogram of electrolyte with molar ratio EO:Li of 32:1 prepared using salt with ($n=7.5$) contains one event which can be ascribed to the glass transition, as well as three melting peaks. The glass transition, observed in the lower limit of the investigated range, can be possibly attributed to domains of lithium borate salt. The value of $T_g = -74$ °C is lower than that of pure salt, which can be possibly explained by the confinement of the salt by chains of the polymer host [77]. The origin of the next endothermic event, starting at about -30 °C is unclear. The shape of the DSC curve in this temperature region can be interpreted either in terms of second glass transition, or pre-melting of salt. Subsequent sharp peak situated at around 9 °C is most likely related to melting of lithium borate salt. The temperature at which this event occurs is slightly higher than the melting temperature $T_m=5$ °C of pure lithium borate salt with ($n=7.5$). The melting peak of PEO is situated at 56 °C. Between these major events, another minor endothermic peak is found at around 23 °C. A similar minor endothermic event with a maximum at 19 °C has been observed also in the DSC traces of pure lithium borate salt. This may mean that the salt characterized by the average length of oligomeric units ($n=7.5$) is actually composed of two fractions, each with different length of the oligomeric units.

The thermograms obtained for electrolyte prepared using the same salt, but different molar ratio EO:Li of 50:1 contain only three major events: a relatively weak endothermic event related to glass transition at -83 °C, a broad melting peak with a maximum at -14 °C,

and a sharp melting peak at 56 °C. The first melting events can be attributed to the oligomeric salt, whereas the latter to the high molecular weight polymer. A number of possible explanations can be found for the faintly marked glass transition event. Probably, the glass transition of salt is “smeared out” by nearby glass transition of amorphous fraction of PEO (situated around -56 °C for pure polymer [78]). As high temperature limit of this event would overlay with shoulder of the neighboring broad melting peak, these three phenomena may be difficult to separate. It is remarkable, that the glass transition temperature and the melting peak of salt are situated at much lower temperature than that for the pure lithium borate salt.

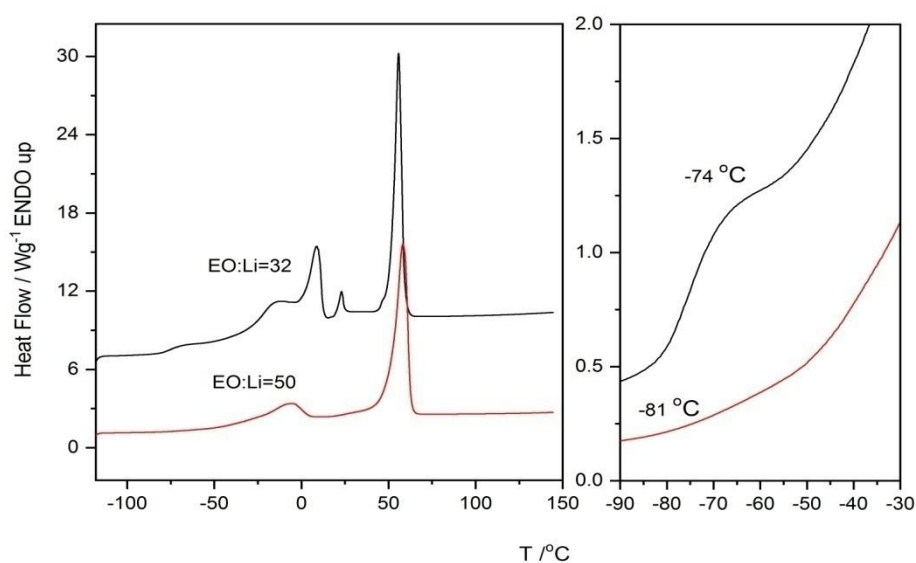


Fig. 5.5. DSC traces of polymer electrolytes composed of linear PEO and borate salts, length of oligomeric arms ($n=7.5$), measured during second heating. The samples vary by molar ratio EO:Li.

As we can see from the DSC traces above, three electrolytes represent both low crystallinity and low T_g , which makes them the best candidates for practical applications taking into account the studied compositions, one is the electrolyte with a molar ratio EO:Li of 10:1 comprising borate salt with ($n=3$), and two electrolytes prepared using salt with ($n=7.5$) with molar ratio EO:Li of 50:1 and 32:1.

Table 5.2. Melting point and heat of fusion, obtained from analysis of DSC data for electrolytes comprising oligomeric borate salts (Lithium alkyltrialkoxo borates) with various length of oligomeric groups and PEO.

EO:Li	Melting point °C / Heat of fusion Jg ⁻¹							
	<i>n</i> =1		<i>n</i> =2		<i>n</i> =3		<i>n</i> =7.5	
	<i>T_m</i> /°C	<i>Q_F</i> /Jg ⁻¹	<i>T_m</i> /°C	<i>Q_F</i> /Jg ⁻¹	<i>T_m</i> /°C	<i>Q_F</i> /Jg ⁻¹	<i>T_m</i> /°C	<i>Q_F</i> /Jg ⁻¹
50:1	76	125	68	114	61	127	-108	27
32:1	67	116	72	80	73	93	-132	58
16:1	71	102	60	90	59	72	-	-
10:1	72	81	65	68	59	13	-	-

PEO $M_w=5 \times 10^6$ g/mol : $T_m = 71$ °C; $Q_F = 145$ Jg⁻¹

Table 5.3. Values of the glass transition temperature T_g (midpoint) obtained for electrolytes comprising oligomeric borate salts (Lithium alkyltrialkoxo borates) with various length of oligomeric unit and PEO.

EO:Li	Glass transition temperature T_g / °C			
	<i>n</i> =1	<i>n</i> =2	<i>n</i> =3	<i>n</i> =7.5
50:1	-51	-53	-64	-81
32:1	-43	-53	-58	-74
16:1	-48	-66	-77	-
10:1	-51	-63	-80	-

PEO $M_w=5 \times 10^6$ g/mol: $T_g = -54$ °C

The comparison between the values of the melting point of investigated electrolytes is plotted in Fig. 5.6. The melting point of pure borate salt with ($n=1$) is slightly higher than that of the pure PEO. The values of the melting point of electrolytes prepared using salt with ($n=1$) are situated between 76 °C and 67 °C. A shallow minimum is observed for EO:Li of 32:1. Borate salts with ($n=2,3$) are amorphous and their thermograms do not exhibit any events related to melting or crystallization. However, the melting point of electrolytes obtained by adding borate salts to linear PEO does not seem to decrease with increasing amount of salt, which could be expected. For all those electrolytes, the melting point is above 60 °C. This is

an indication that the melting event observed in DSC traces is related to the crystalline phase of pure PEO, and that the studied system can be regarded rather as a mixture of domains of borate salt and domains of pure PEO, rather than a typical polymer-salt complex. A similar observation is made for electrolytes comprising borate salt with ($n=7.5$), for which the melting point is lower than that of pure PEO, but does not depend on the molar ratio of the electrolyte.

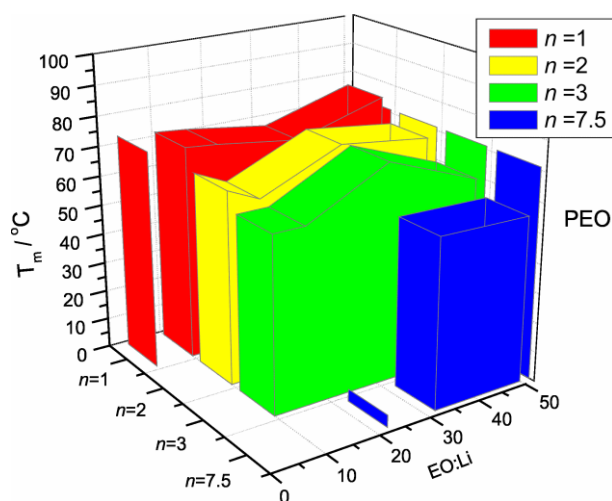


Fig. 5.6. Values of the melting point of studied polymer electrolytes. Melting points of pure borate salts and pure PEO were plotted as references.

The comparison between the values of heat of fusion obtained by integration of melting peaks from DSC traces are presented in Fig. 5.7. As can be observed in the plot, the heat of fusion decreases with increasing amount of borate salts in the system. An exception from this general trend is electrolyte synthesized using oligomeric salt with ($n=2$) and with molar ratio EO:Li of 16:1. For this electrolyte, the heat of fusion is greater than that of electrolyte formed using the same salt, but with molar ratio EO:Li of 32:1. A noticeable effect is that the electrolytes comprising borate salt with longest oligomeric groups ($n=7.5$) are characterized by lowest heat of fusion, despite the fact that this salt crystallizes within studied temperature range, and its heat of fusion is greater than that of salt with ($n=1$).

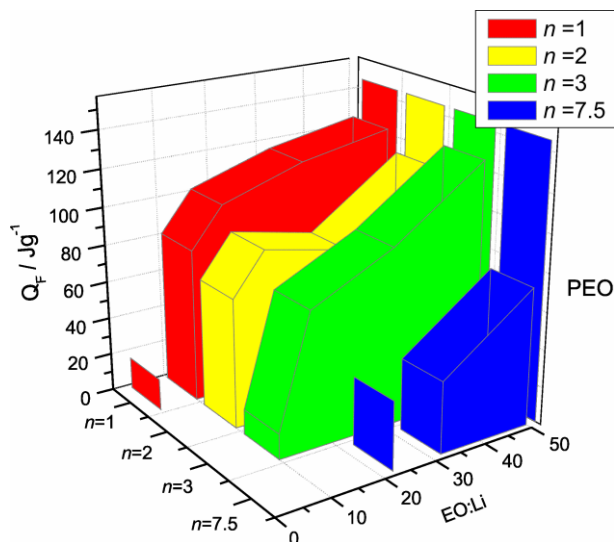


Fig. 5.7. Integrated heat of fusion of studied electrolytes.

The comparison between the values of glass transition temperatures (T_g) of the studied electrolytes are plotted in Fig. 5.8 The values of T_g for lithium borate salts show a strong variation with the length of oligomeric groups: salt with ($n=1$) exhibits an elevated T_g of $-42\text{ }^\circ\text{C}$, whereas for salt with ($n=3$) much lower value of $-75\text{ }^\circ\text{C}$ is obtained. This is much lower than T_g of pure PEO ($-54\text{ }^\circ\text{C}$). Also the glass transition temperatures of salts with ($n=2$) ($T_g = -66\text{ }^\circ\text{C}$) and ($n=7.5$) ($T_g = -70\text{ }^\circ\text{C}$) are lower than that of pure PEO. Even more interesting trend is observed for electrolytes comprising borate salts and PEO: for some of these systems, it is possible to obtain T_g lower than that of parent compounds. Such effect is observed for electrolytes with ($n=3$) and EO:Li of 10:1 ($T_g = -80\text{ }^\circ\text{C}$) and 16:1 ($T_g = -77\text{ }^\circ\text{C}$). Low values of T_g have been obtained also for electrolyte synthesized using salt with ($n=7.5$) with molar ratio EO:Li of 50:1 ($T_g = -81\text{ }^\circ\text{C}$) and EO:Li of 32:1 ($T_g = -74\text{ }^\circ\text{C}$).

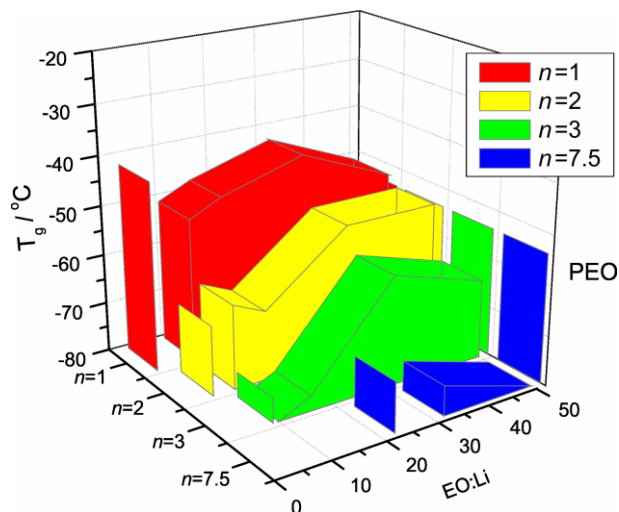


Fig. 5.8. Values of glass transition temperature T_g of studied electrolytes.

5.2 Electrical properties of the studied system

In the impedance measurements, all studied samples have been subjected to a similar thermal cycle, involving initial heating up to 90 °C, subsequent cooling to -50 °C, second heating up to 90 °C, rapid cooling of molten sample to -50 °C, followed by heating to 90 °C and final cooling to ambient temperature. An inspection of the cells after the impedance measurement revealed, that during reference measurements of borate oligomeric salts, the appearance of the salt with ($n=2$) changed from transparent to opaque. The same problem has been observed for salt-rich electrolyte (molar ratio EO: Li of 10:1) prepared using that salt. A minor change of appearance has been observed also for borate salt with ($n=3$). Such an effect may indicate that these two salts may exhibit problems with stability when subjected to prolonged heating and cooling treatment.

5.2.1. Ionic conductivity

Complex plane plots of impedance spectra measured between blocking gold-plated electrodes generally consisted of a semicircle corresponding to the bulk electrolyte, and a low frequency spur which can be related to electrode/electrolyte interface. For measurements performed on samples in a semicrystalline state, a noticeable distortion of the semicircle has been observed, which is caused by inhomogeneity of these samples and following dispersion of conductivity [78]. For all samples, ionic conductivity was calculated according to the total “bulk” resistance.

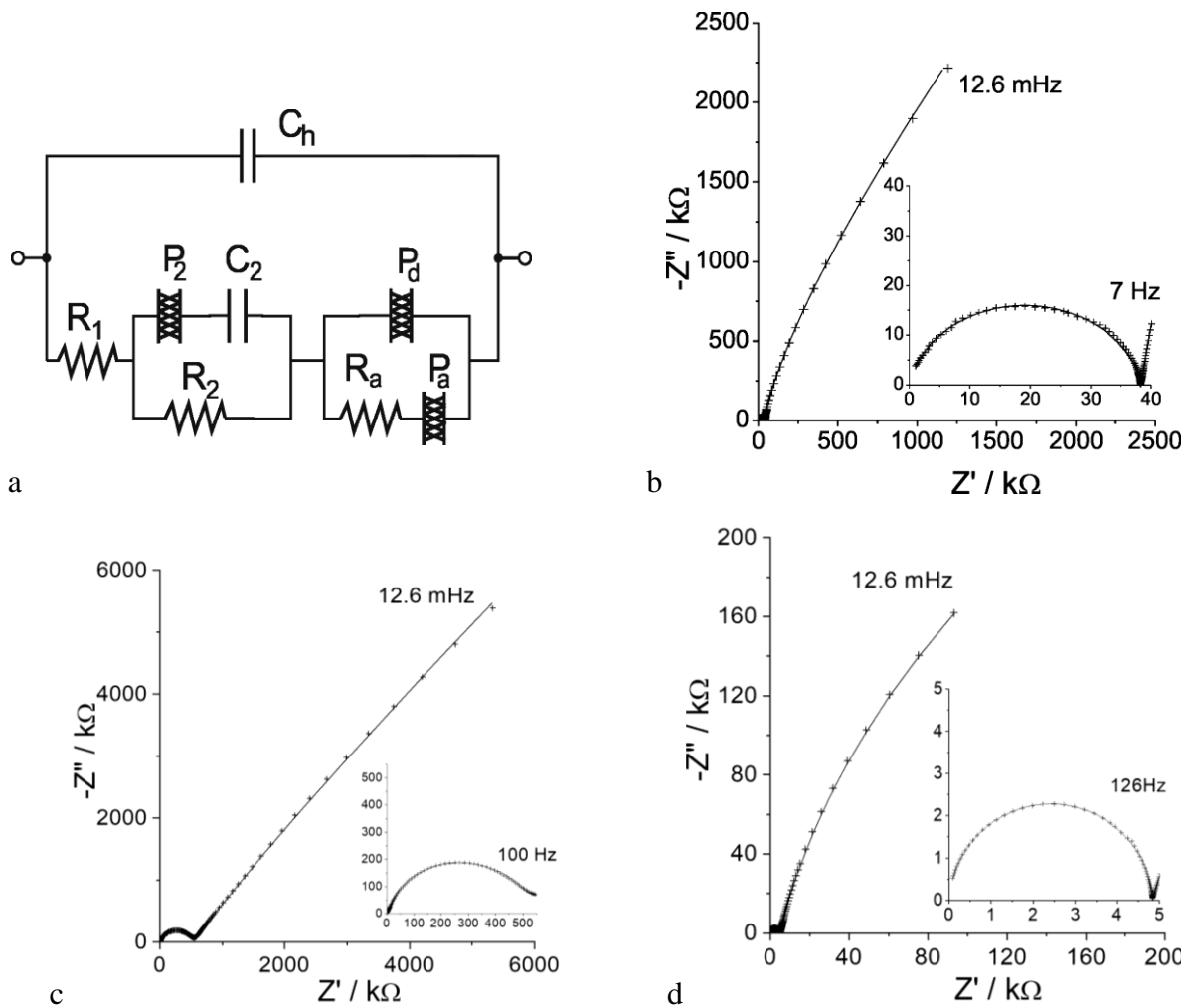


Fig. 5.9. Equivalent circuit used for fitting of impedance spectra (a) and complex plane plots of impedance spectra of selected samples: amorphous lithium borate salt with ($n=7.5$) measured at 25 °C (b), semicrystalline electrolyte EO:Li molar ratio of 32:1 comprising salt with ($n=7.5$) and linear PEO measured at 25 °C (c) and the same electrolyte measured in amorphous state at 70 °C (d). Solid lines represent impedance of the fitted equivalent circuit model.

5.2.1.1 Conductivity of borate salts with different length n of oligomeric groups:

Fig. 5.10 shows the temperature dependence of ionic conductivity during the first cooling run, plotted for salts with different length n of oligomeric groups. For all investigated samples, at first the samples were initially heated up to the temperature of 90 °C, in order to melt and homogenize the material, and to provide good contact between electrodes and electrolyte. The subsequent slow cooling run extended down to about -50 °C .

Upon cooling from an amorphous state to a pure borate salt with ($n=1$), which is characterized by high crystallinity and a high melting temperature, the existence of a crystalline phase limits the conductivity of the material. The variations in ionic conductivity that occur throughout the process of crystallization suggest that the crystalline phase of samples possesses a conductivity that is significantly lower than that of the amorphous phase.

Pure borate salts with ($n=2,3$) are amorphous, salt with ($n=2$) exhibit problems with stability and has the lowest conductivity in comparison to the other salts. In borate salt with ($n=3$) the drop of conductivity upon cooling from an amorphous state is moderate above -20 °C compared to the other salts because as we can see from DSC measurements this salt remains amorphous and has the lowest glass transition temperature (-75 °C). Below -20 °C the conductivity decreases due to stiffening of the sample. Pure borate salt with ($n=7.5$) is characterized by low crystallinity and low melting point and therefore contains more of the well-conductive amorphous phase. At room temperature, this becomes the main advantage of this system. The borate salt remains amorphous. The decrease of conductivity of salts that contain longer oxyethylene segments results probably from the low mobility of this anion caused by the high molecular mass and the possibility of tangling of the substituents with the polymer matrix.

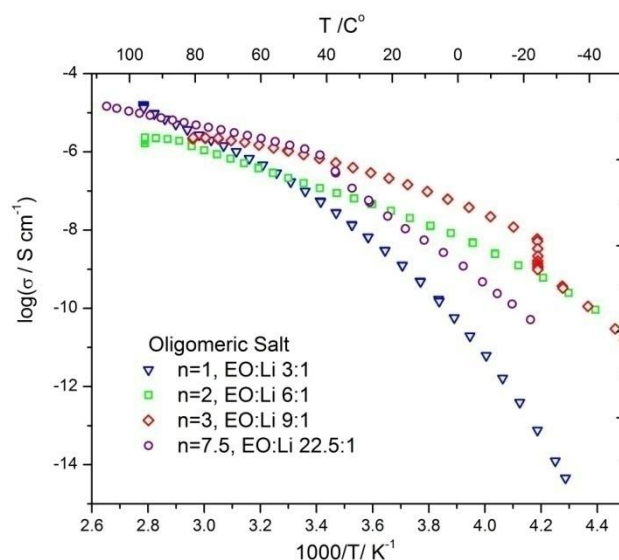


Fig. 5.10. Temperature dependence of ionic conductivity during first cooling run, plotted for salt with different length n of oligomeric groups.

5.2.1.2 Conductivity of electrolytes representing the same molar ratio EO:Li and different length n of oligomeric groups:

The plots of temperature dependence of ionic conductivity, made for electrolytes representing the same molar ratio EO:Li, but different oligomeric groups length in the salt molecules are presented in Figs. 5.11 to 5.14 .

Fig. 5.11 shows a plot of the temperature dependence of ionic conductivity for electrolytes with the same molar ratio EO:Li of 10:1 but different lengths of oligomeric groups. We can see that the electrolyte obtained using borate salt with longer oligomeric chains ($n=3$) has higher conductivity compared with the electrolytes obtained using borate salt with shorter oligomeric chains ($n=1,2$) over a wide range of temperature, since salt with longer oligomeric chains ($n=3$) has low crystallinity and low T_g . Upon cooling from an amorphous state only a moderate decrease of conductivity related to crystallization is observed (at about $-20\text{ }^\circ\text{C}$). For other electrolytes ($n=1$ and $n=2$) the crystallization is observed above room temperature. The plot of conductivity for electrolyte obtained using borate salt with ($n=2$) reveals problems with stability. As stated earlier, the inspection of the cells that took place after the impedance measurement revealed, that during reference measurements of electrolyte (molar ratio EO:Li of 10:1) prepared using salt with ($n=2$), the appearance changed from transparent to opaque, which can be a sign of sample degradation.

For electrolytes with the common molar ratio EO:Li of 16:1 and different oligomeric groups length (Fig. 5.12), we can see that the electrolyte obtained using borate salt with ($n=2$) has higher conductivity compared with the electrolyte obtained using borate salt with ($n=1$) and slightly higher conductivity in comparison with oligomeric chains ($n=1,3$) over a wide range of temperature. Upon cooling from an amorphous state a steep decrease of conductivity is observed for the electrolyte containing borate salt with ($n=2$) at about 36 °C, which can be related to crystallization. For the electrolyte comprising borate salt with oligomeric chain length ($n=3$) a similar event (steep decrease of conductivity) is observed at about 28 °C.

The plot of temperature dependence of ionic conductivity for electrolytes representing the same molar ratio EO:Li of 32:1, but different length of oligomeric groups is presented in Fig. 5.13. These results indicate that the transport of ions is strongly dependent on the heat of fusion and glass transition temperature T_g , with crystallinity being the most important factor, and glass transition temperature a secondary factor. Electrolyte composed of PEO and salt with ($n=7.5$) has the lowest glass transition temperature in this comparison, and also the lowest heat of fusion of the crystalline phase. Therefore, upon cooling from an amorphous state only a moderate decrease of conductivity related to crystallization is observed (at about 40 °C). On further cooling, the conductivity decreases due to the stiffening of polymer chains, but the magnitude of this decrease is again moderate in comparison to that for other electrolytes. During the cooling run, electrolyte with EO:Li of 32:1 exhibited one major decrease of conductivity related to crystallization (starting at about 45 °C, and extending down to room temperature). As a result, in the amorphous state, the relative difference of ionic conductivity between the electrolytes based on salt with ($n=7.5$) and ($n=1$) is about two times higher, whereas at -20 °C the conductivity of electrolyte with ($n=7.5$) is more than 1000 times higher. For electrolyte with molar ratio EO:Li of 32:1, the values of conductivity measured below 0 °C were comparable to the values obtained for oligomeric borate salt: for this composition, lower T_g compensates higher crystallinity.

A comparison of ionic conductivity vs temperature for electrolytes with a common molar ratio EO:Li of 50:1, differing by the length of oligomeric groups is depicted in Fig. 5.14. Upon cooling from an amorphous state all electrolytes exhibit a steep decrease of conductivity that can be related to crystallization. For electrolytes that contain oligomeric borate salts with shorter arms ($n=1,2$ and 3) such an event takes place below 50 °C, whereas for the electrolyte with ($n=7.5$) it occurs between 30 and 20 °C. Above 50 °C the electrolyte based on salt with shorter oligomeric groups ($n=1$) has higher conductivity compared with the electrolytes based on salts with other lengths of oligomeric groups ($n=2,3,7.5$). Below 50 °C electrolyte obtained

based on salt with longer oligomeric groups ($n=7.5$) has higher conductivity than the others. This electrolyte has the lowest glass transition temperature in this comparison, and also the lowest heat of fusion of the crystalline phase.

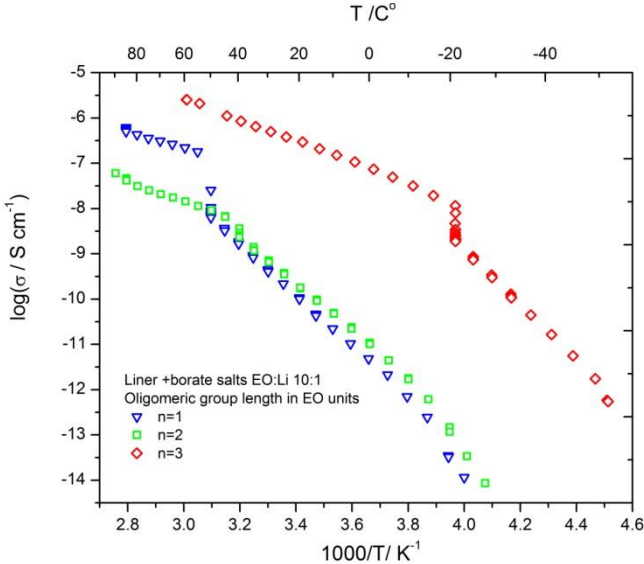


Fig. 5.11. Temperature dependence of ionic conductivity during first cooling run, plotted for electrolytes with the same EO:Li ratio of 10:1, and different length n of oligomeric groups.

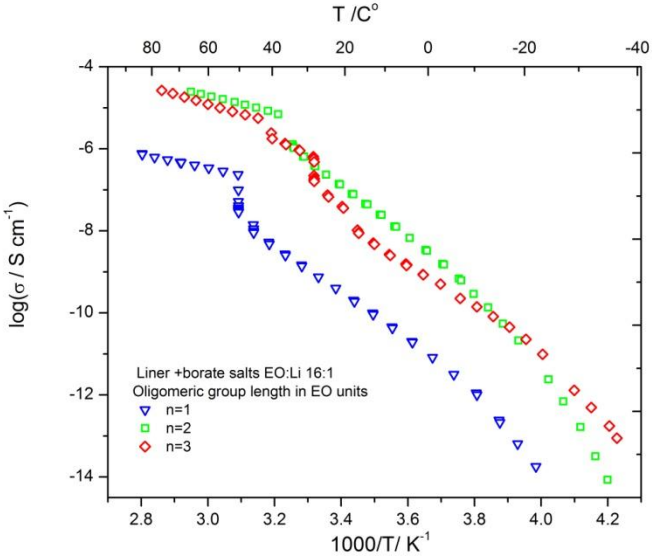


Fig. 5.12. Temperature dependence of ionic conductivity during first cooling run, plotted for electrolytes with the same EO:Li ratio of 16:1, and different length n of oligomeric groups.

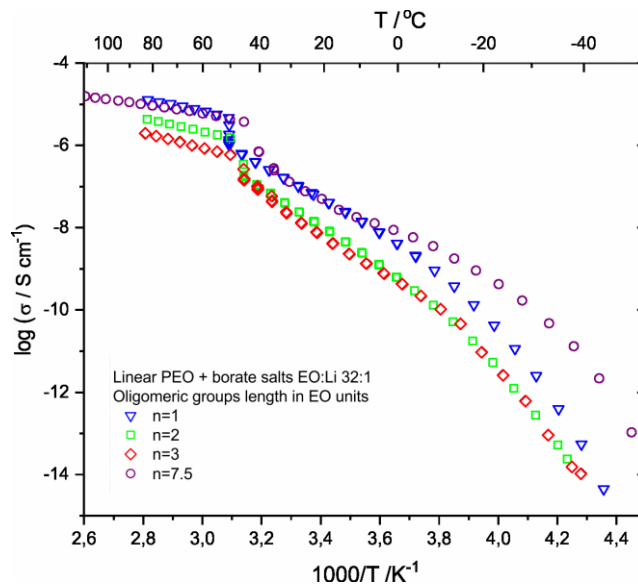


Fig. 5.13. Temperature dependence of ionic conductivity during first cooling run, plotted for electrolytes with the same EO:Li ratio of 32:1, and different length n of oligomeric groups.

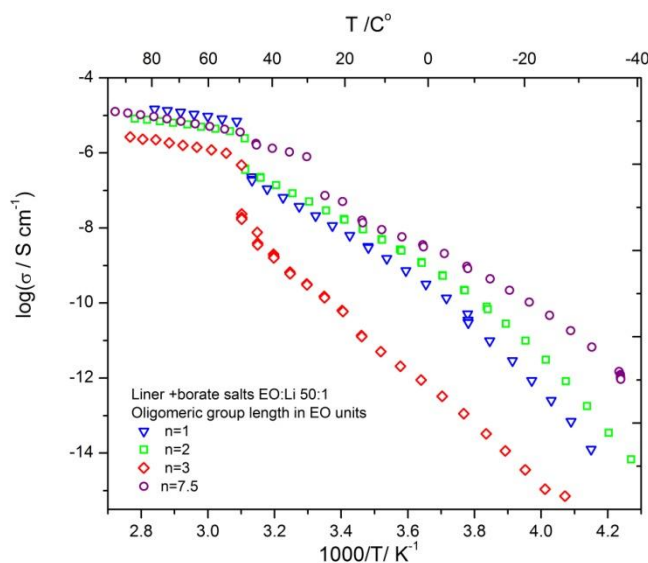


Fig. 5.14. Temperature dependence of ionic conductivity during first cooling run, plotted for electrolytes with the same EO:Li ratio of 50:1, and different length n of oligomeric groups.

For some electrolytes, the conductivity measured during first heating was lower, than in subsequent cycles. Such an effect is caused mainly by the stiffness and rough surface of the foils, which initially had only partial contact with the electrodes, and therefore is more pronounced in samples with higher crystallinity. During the first heating, the surface gradually softened, and the electrolytes gained better contact with electrodes. Moreover, for

all samples the displacement of the spring-loaded upper electrode caused an initial decrease of thickness by the preset limit of 50 μm . For soft samples, this process took place directly after placing in the cell, whereas for stiffer sample it proceeded upon fusion of the crystalline phase. Therefore, for comparison of values of ionic conductivity (Fig. 5.15) values obtained during the first cooling of previously molten samples were taken.

In some cases, a gradual decrease of ionic conductivity in subsequent heating and cooling cycles, or even slow changes taking place at a single temperature has been noted. Such an effect was noticeable especially for pure borate salt with ($n=2$), and for electrolytes based on that salt, for which instabilities of electrical properties were pronounced above 60 $^{\circ}\text{C}$. A slight decrease of conductivity has been also observed for electrolyte prepared using salt with ($n=3$).

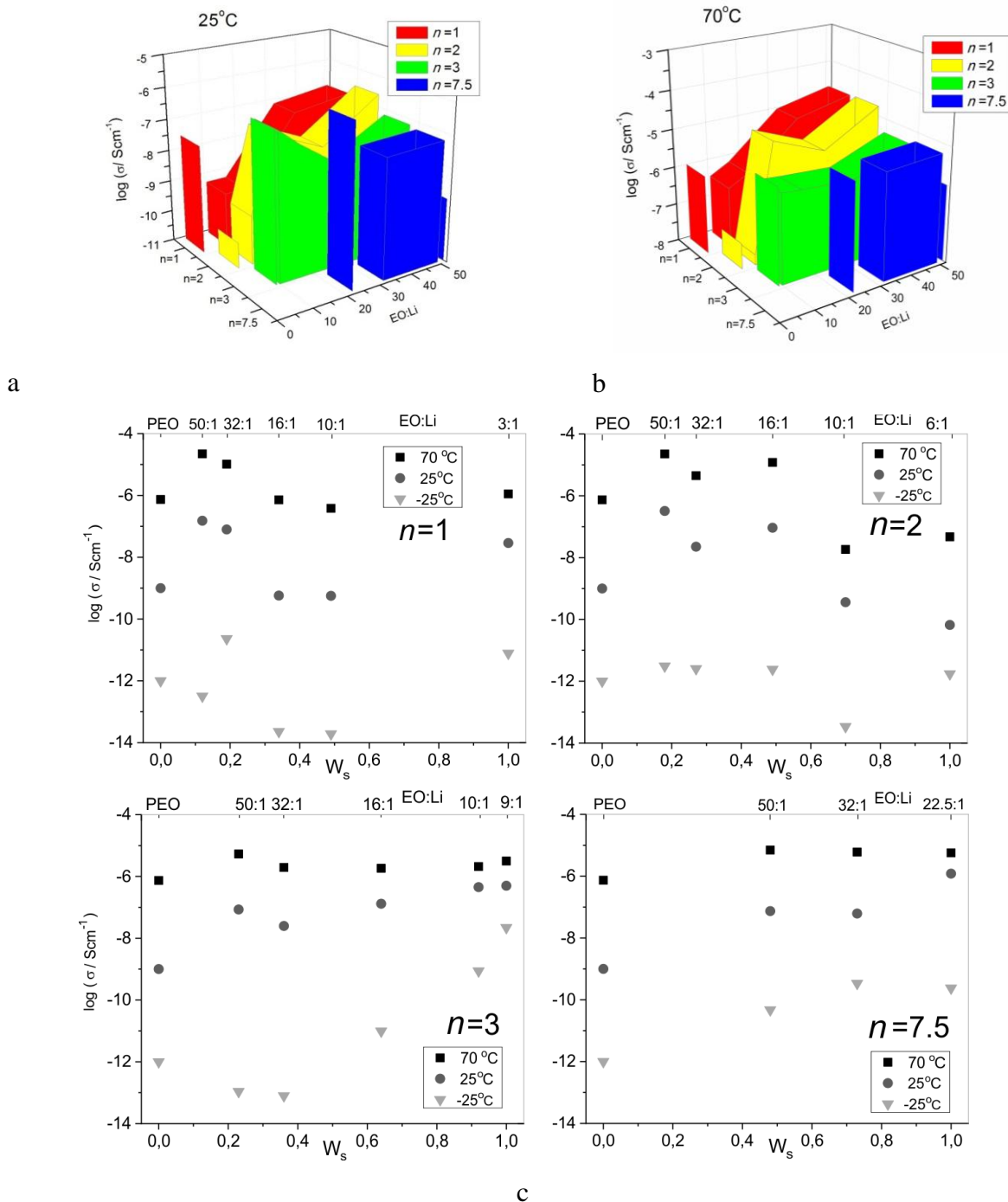


Fig. 5.15. Ionic conductivity of studied electrolytes at 25 °C (a) and at 70 °C (b) as a function of EO:Li. Figure (c) shows conductivity at selected temperatures as a function of borate salt weight fraction in the electrolyte W_s . The conductivity of pure PEO and borate salts are shown as references.

Graphs (a) and (b) compare conductivities at two temperatures: 25 °C, at which some of the studied samples were semicrystalline and at 70 °C, at which all electrolytes and salts were amorphous. The graphs were plotted as a function on EO:Li. In Fig. 5.15 the ionic

conductivities were presented as a function of the weight fraction of each of the oligomeric borate salts in the system, with neat PEO and neat borate salts as references.

At 25 °C, the highest value of conductivity of 1.2×10^{-6} S/cm was obtained for lithium borate salt with ($n=7.5$). A comparison of values of conductivity of pure oligomeric borate salts shows, that it reaches a minimum around ($n=2$). This is in contradiction to the earlier report on the properties of these salts [62], which showed a completely different trend: a gradual increase of conductivity with increasing oligomeric chain length, a maximum of conductivity situated around ($n=3$), followed by a decrease of conductivity for salt with ($n=7.5$). The difference may result from the different experimental procedures: communication with authors of [62] revealed, that their measurement cell involved an inert membrane that was soaked with a liquid sample, whereas in our case the measurement was performed in a holder designed for measurement of semi-liquid samples.

The discrepancy between the present work and earlier report may be also related to the ageing effect and thermal instability of properties of borate salt with ($n=2$) and ($n=3$), already described above. In the previous report, the measurement cycle, performed on freshly synthesized samples, was much shorter and the salts were heated only up to 70 °C. In the present case, at least 6 months passed between the synthesis of borate salts and the measurement of electrical properties. The impedance measurements lasted longer and involved more data points, with a maximum temperature of 90 °C. Therefore, the values of conductivities obtained for salts with ($n=2$) and ($n=3$) and electrolytes synthesized using these salts may be lower than those obtained for electrolytes prepared using salts with ($n=1$) and ($n=7.5$), which we have found to be stable even after prolonged measurement cycles.

For all studied systems, at 70 °C (at which all systems are amorphous and therefore easily comparable) mixing borate salt with PEO allows for achieving higher values of ionic conductivity, than the values of conductivity of neat borate salt. For systems with ($n=1$) and ($n=2$), the maximum conductivity is observed for systems that represent a relatively small addition of oligomeric salt to the high molecular weight PEO (Fig. 5.15c). For systems based on salt with ($n=3$) and ($n=7.5$) the increase of conductivity of mixed system in respect to the neat salt is less evident, but still present. At 70 °C highest values of ionic conductivity approaching 1×10^{-5} S/cm were obtained for borate salt with ($n=7.5$), and electrolyte composed of that salt, with molar ratio EO:Li of 32:1. Conductivity of all electrolytes, which included borate salt with ($n=3$) exceeded 1×10^{-6} S/cm, and the maximum value of 5×10^{-6} S/cm was obtained for electrolyte with EO:Li of 50:1. A more complex behavior has been observed for electrolytes prepared using salt with ($n=2$). For electrolytes of molar ratio between 50:1 and

16:1 the ionic conductivity reached values of about 10^{-5} S/cm. The conductivity of pure borate salt, and electrolyte with a molar ratio EO:Li of 10:1 is much lower. Such an effect can again be attributed to the poor stability of this salt in subsequent thermal cycles. It is probable that, in electrolytes with a low amount of salt, the linear PEO polymer matrix stabilizes the system, whereas in concentrated electrolytes the aging effect decreases conductivity considerably. For amorphous electrolytes synthesized using salt with ($n=1$), the conductivity measured at 70 °C generally decreases with increasing borate salt content, but the trend is less pronounced than in semicrystalline electrolytes measured at 25 °C. The highest value of ionic conductivity equal 2×10^{-5} S/cm has been obtained for the electrolyte with a molar ratio EO:Li of 50:1. Such a trend may support a model already discussed above, in which for electrolytes obtained using borate salt with short oligomeric chains the dissolution process is limiting the conductivity. In electrolyte with a molar ratio of 50:1 EO:Li, each salt molecule is surrounded by numerous EO segments available for lithium coordination. With increasing amount of salt, the number of free EO segments which are not involved in ion transport process is decreasing.

At room temperature (25 °C) a comparison of values of ionic conductivity becomes more complex, as most of the electrolytes are semicrystalline. In the plot of conductivity vs weight fraction of salt (Fig. 5.15c) for mixed PEO-oligomeric salt systems maximum values are obtained at the salt content of around 20 wt.%. Generally, all electrolytes representing a “dilute” regime with EO:Li of 50:1 allow obtaining similar values of ionic conductivity of around 10^{-7} S/cm. A slightly higher value was obtained for a system with oligomeric segment length ($n=2$). For mixed systems with ($n=3$) and ($n=7.5$), the conductivity measured at room temperature is lower than the conductivity of neat salt, which can however be attributed partially to the different states of the measured samples. At room temperature, neat oligomeric salts were amorphous, and mixed electrolyte were semicrystalline (and therefore suffered from both lower bulk conductivity and worse electrode contact).

Another interesting observation is that at room temperature for electrolytes obtained using salt with ($n=1$), the conductivity decreases considerably with increasing content of salt, dropping from the maximum of slightly above 1×10^{-7} S/cm for EO:Li of 50:1, to merely 3×10^{-10} S/cm for EO:Li of 10:1, which is almost two orders of magnitude less than the value obtained for the pure borate salt. Such unexpected behavior does not correspond to DSC results, in which the heat of fusion generally decreases with increasing content of salt. The samples with higher content of salt are less crystalline, which should increase the number of amorphous conduction paths favorable for ion transport. It may be suspected, that the problem is related either to aggregation and separation of salt from PEO, or directly to the mechanism

of ion transport within the system. In the first case, the ions may travel through salt-rich domains or along the PEO chains, but transfer between these regions may impose a problem. A similar problem may occur if we assume that a considerable fraction of the charge transport is not related to Li^+ , but to anions and possibly larger ionic aggregates. In the second approach, the decrease of ionic conductivity with increasing amount of salt may be related to the decrease of free EO units from PEO chains available for the solvation process. The weaker dissolution process may in this case result in the trapping of Li^+ ion by the anion, thus creating a molecule, which does not move along the external electric field.

The conductivity measured at around $-25\text{ }^\circ\text{C}$ depends strongly on the state of the samples. For electrolytes prepared using oligomeric salt with ($n=7.5$), the conductivity of mixed electrolyte with EO:Li of 32:1, or the weight fraction of about 70%, is slightly higher than that of the neat oligomeric salt (Fig. 5.15c). Both are semicrystalline and have similar heat of fusion (see also Fig. 5.6 and 5.7). At that temperature, the conductivity of electrolyte with less amount of oligomeric salt is lower, which can be attributed mainly to higher crystallinity. For electrolytes prepared using salt with ($n=3$), the conductivity calculated at around $-25\text{ }^\circ\text{C}$ clearly decreases with the increasing amount of PEO in the system, which again can be attributed mainly to crystallinity (neat salt is amorphous even at that temperature). Interestingly, it does fall below the conductivity of neat PEO, which however may be caused also by the electrode contact of semicrystalline samples. For electrolytes with ($n=2$), the low-temperature conductivity exhibits a slight increase in mixed systems with respect to neat the oligomeric salt. For systems prepared using the shortest oligomeric salts, a maximum of low-temperature conductivity is observed at around 20% weight of salt in the system, or EO:Li of 50:1.

Table 5.4. Ionic conductivity of electrolytes samples in case of cooling run at 25 °C and 70 °C

EO:Li	Ionic conductivity at 25 °C and 70 °C							
	<i>n</i> =1		<i>n</i> =2		<i>n</i> =3		<i>n</i> =7.5	
	σ at 25 °C	σ at 70 °C	σ at 25 °C	σ at 70 °C	σ at 25 °C	σ at 70 °C	σ at 25 °C	σ at 70 °C
50:1	-6.82	-4.65	-6.5	-4.64	-7.07	-5.27	-7.13	-5.15
32:1	-7.10	-4.98	-7.8	-5.48	-8.11	-5.84	-7.21	-5.23
16:1	-9.24	-6.14	-7.03	-4.92	-6.88	-5.73	-	-
10:1	-9.25	-6.41	-9.44	-7.73	-6.35	-5.68	-	-
Intrinsic EO:Li of salt	3:1		6:1		9:1		22.5:1	
	σ at 25 °C	σ at 70 °C	σ at 25 °C	σ at 70 °C	σ at 25 °C	σ at 70 °C	σ at 25 °C	σ at 70 °C
	-7.54	-5.95	-10.18	-7.32	-6.3	-5.5	-5.92	-5.24

PEO $M_w = 5 \times 10^6$ g/mol : σ at 25 °C = -9 S/cm⁻¹; σ at 70 °C = -6 S/cm⁻¹

5.2.2 Ideal Glass Transition Temperature T_0

As mentioned in Chapter Two, by incorporating salt into the polymer matrix, a polymer electrolyte is produced. As cations are coordinated by the polymer chain, the polymer matrix functions as a solid solvent [27]. Large-scale segmental motions of the polymer chain, which assist in breaking and replacing coordination bonds required for cation transport on the one hand and supply the free space required for anion transport on the other, are thought to enhance ion transport in such a system. The free volume available in an amorphous electrolyte therefore determines its conductivity. The Vogel–Tammann–Fulcher formula (2.6) expresses its temperature dependency above the glass transition point [79-80].

By fitting Eq. (2.6) to the obtained conductivity values, the ideal glass transition temperature T_0 , was determined. An example of the fitted curves is presented in Fig.5.16. This figure shows the temperature dependence of conductivity for the electrolyte prepared using salt with ($n=7.5$) and a molar ratio EO:Li of 50:1 in several heating and cooling cycles. This electrolyte represents as we mentioned earlier both low crystallinity and low T_g . Since the VTF dependence is characteristic for an amorphous material above the glass transition temperature, it seems that flexibility of polymer chains, characteristic for amorphous regions of semicrystalline polymer, determines the ionic conductivity. VTF-type dependence was

observed for all heating and cooling cycles – both for electrolyte rapidly cooled from amorphous melt and for slowly cooled electrolyte which is regarded as semicrystalline.

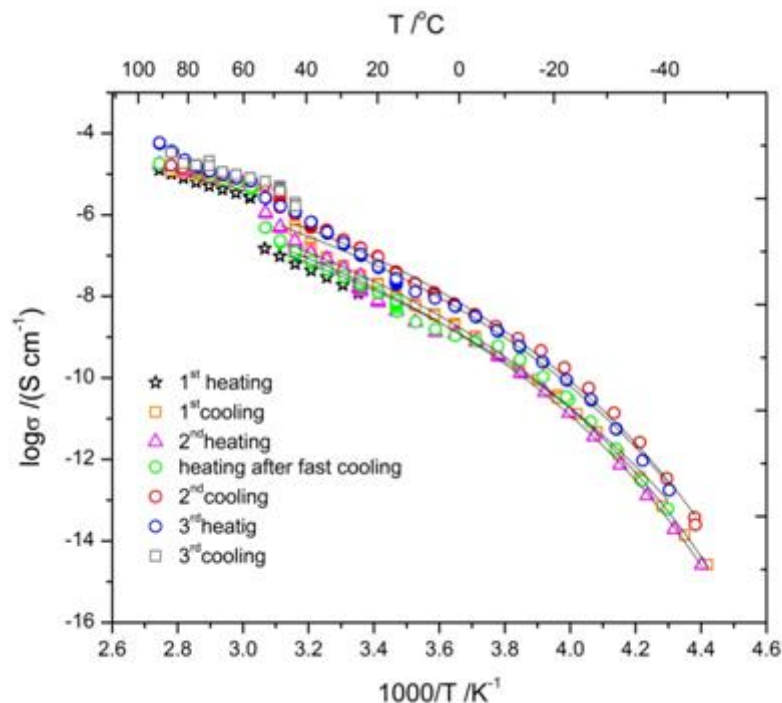


Fig. 5.16. Temperature dependence of ionic conductivity plotted for electrolyte with EO:Li of 50:1, and length of oligomeric arms ($n=7.5$). Solid lines represent fit with VTF function.

In comparison to the T_g determined by DSC, the ideal glass transition temperature, T_0 , predicted for the temperature dependence of the ionic conductivity is much lower. Table 5.5 also includes the variation between T_g and T_0 . All uncertainties (Standard deviation) are given in parentheses following a value for each parameter estimated by fitting the VTF function, acceptable uncertainty was lower than 10% of the determined value. The value of $T_g - T_0$ ranges from 22 °C for electrolytes with a molar ratio of 50:1 EO:Li comprising oligomeric borate salt with ($n=3$) to 69 °C for electrolytes with a molar ratio of 32:1 EO:Li comprising oligomeric borate salt with ($n=1$). The significant discrepancy supports the idea that segmental mobility, which encourages ion movements by providing free space, is not the only factor affecting the conductivity. Another important factor is the degree of coupling between the motions of the polymer matrix and the charge transport.

Table 5.5. Values of the ideal glass transition temperature T_0 obtained from fit of VTF function to conductivity data for electrolytes comprising oligomeric borate salts with various length of oligomeric and PEO, and $(T_g - T_0)$.

EO:Li	Ideal glass transition temperature $T_0 / ^\circ\text{C}$; $(T_g - T_0) / ^\circ\text{C}$							
	$n=1$		$n=2$		$n=3$		$n=7.5$	
	T_0	$(T_g - T_0)$	T_0	$(T_g - T_0)$	T_0	$(T_g - T_0)$	T_0	$(T_g - T_0)$
50:1	-100(5)	49	-102(5)	49	-86(1)	22	-108(6)	27
32:1	-112(5)	69	-87(2)	34	-105(5)	47	-132(8)	58
16:1	-92(3)	44	-95(3)	29	-111(6)	34	-	-
10:1	-101(5)	50	-101(5)	38	-126(8)	46	-	-
Intrinsic	3:1		6:1		9:1		22.5:1	
EO:Li of salt	T_0	$(T_g - T_0)$	T_0	$(T_g - T_0)$	T_0	$(T_g - T_0)$	T_0	$(T_g - T_0)$
	-100(5)	58	-131(8)	65	-	-	-111(6)	41

PEO $M_w = 5 \times 10^6$ g/mol: $T_0 = -96$ °C ; $T_g - T_0 = 42$ °C

The values of T_0 for lithium borate salts show a strong variation with the length of oligomeric groups: salt with ($n=1$) exhibits an elevated T_0 of -100 °C, whereas for salt with ($n=2$) much lower value of -131 °C is obtained. This is lower than T_0 of pure PEO (-96 °C). Also the ideal glass transition temperatures of salts ($n=7.5$) ($T_0 = -111$ °C) are lower than that of pure PEO.

Even more interesting trend is observed for electrolytes comprising borate salts and PEO: for some of these systems, it is possible to obtain T_0 lower than that of parent compounds. Such effect is observed for electrolytes with ($n=1$) and EO:Li of 32:1 ($T_0 = -112$ °C) and electrolytes with ($n=7.5$) and EO:Li 32:1 ($T_0 = -132$ °C).

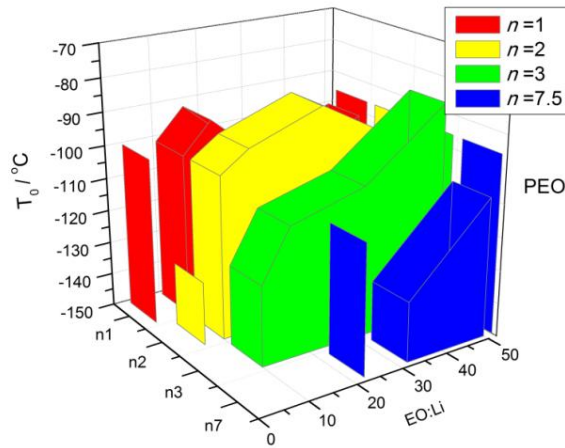


Fig. 5.17. Values of ideal glass transition temperature T_0 of studied electrolytes.

Another quantity that can be calculated for the studied systems is the decoupling index. The decoupling index, or R_τ , can be used to quantify the extent to which ion motion is coupled to matrix motion. It is defined as follows:

$$R_\tau = \tau_s / \tau_\sigma \quad (5.1),$$

whereas τ_s represents the structural relaxation time and τ_σ denotes conductivity relaxation time. The ions ought to travel separately from the frozen structure in a decoupled system below T_g . Large ionic clusters may undergo cooperative bond exchanges or void-to-void leaping as part of the transport process. In accordance with the latter mechanism, an ion (such as Li^+) enters the conducting path at one end of the cluster and exits at the other.

In many cases, the decoupling index is estimated at the glass transition temperature T_g as [86]:

$$\log(R_\tau) = 14.3 + \log(\sigma_{T_g}) \quad (5.2),$$

where σ_{T_g} is expressed in Scm^{-1} . For all samples the logarithm of the decoupling index, $\log(R_\tau)$ values were extracted based on Eq.(5.2), based on the values of conductivity measured at the glass transition temperature T_g . The conductivity was calculated according to extrapolation of the fit of VTF function to the glass transition temperature. The function was fitted to the temperature dependence of conductivity, restricting the fit the part of the data that was not influenced by crystallization or melting events. The fitted function had three parameters $\log\sigma_0, B$ and T_0 , where:

- $\log\sigma_0$: Logarithm of the pre-exponential factor σ_0 setting the baseline for the electrical conductivity in the high-temperature limit.
- B : Material-specific constant, indicating the rate at which the conductivity changes with temperature, related to the activation energy.
- T_0 : Ideal glass transition temperature, indicating a critical temperature below which the conductivity behavior changes dramatically.

For the glass transition temperature T_g the value measured by DSC was used.

Fixing B parameter in this work can help achieve better stability and convergence during the fitting process. Allowing many parameters to vary can make the fitting algorithm less stable, leading to poor or non-convergent fits.

Figures (5.18-5.19) Included two plots that illustrate the fitting process with marked T_g , and the extrapolated VTF, for the two limiting cases (lowest and highest value of $\log(R\tau)$) the values of $\log(R\tau)$ values are situated between -11.1 for electrolyte with molar ratio EO:Li of 50:1 prepared using salt with ($n=7.5$) and 3.8 for electrolyte with molar ratio EO:Li of 50:1 prepared using salt with ($n=1$).

As can be seen from Table 5.6, the values of the decoupling index are decreasing with increasing the length of with molar ratio for electrolytes comprising oligomeric borate salts with various length of oligomeric and PEO. An exception from this general trend are electrolytes synthesized using oligomeric salt with $n=3$ and with a molar ratio EO:Li of 10:1,EO:Li of 16:1 and electrolytes synthesized using oligomeric salt with $n=7.5$ with a molar ratio EO:Li of 32:1.

The low values indicate a very strong coupling between ion transport and movements of the matrix. In contrast, the high values of the decoupling index calculated for some electrolytes, like electrolytes with a molar ratio EO:Li of 32:1 prepared using salt with ($n=1,7.5$) and EO:Li of 50:1 prepared using salt with ($n=1,2$), for which it is assumed that the lithium cation motion is highly decoupled from the structural.

It should be noted that the fitted values of the decoupling index may be treated only as a rough approximation. The model of temperature dependence of conductivity was based only VTF function and did not include any hopping (Arrhenius) conductivity mechanism. A full model with two mechanisms would have two more parameters, which, together with possibly weak separation between the two processes in the temperature range of interest, could strongly decrease the reliability of the fit. It can be expected, that at low temperatures the input of the second mechanism to the total conductivity may be comparable to or greater than that of “frozen” segmental chain motion. Unfortunately, the temperature range near the glass

transition was not available for the equipment used in the electrical measurements. Extending it would validate the preliminary results.

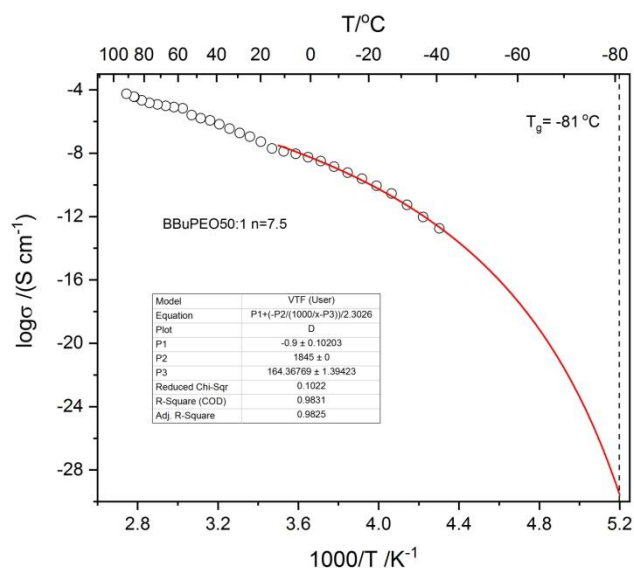


Fig. 5.18. Temperature dependence of ionic conductivity plotted for electrolyte with EO:Li of 50:1, and length of oligomeric arms ($n=7.5$). Solid lines represent fit with VTF function.

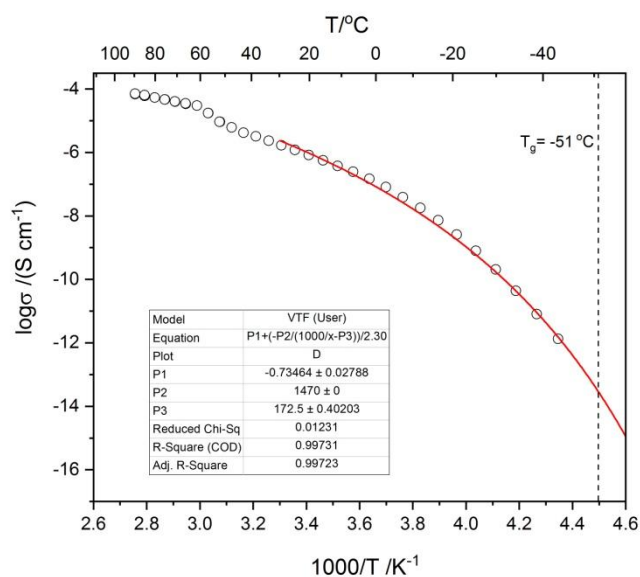


Fig. 5.19. Temperature dependence of ionic conductivity plotted for electrolyte with EO:Li of 50:1, and length of oligomeric arms ($n=1$). Solid lines represent fit with VTF function.

Table 5.6. Logarithm of Decoupling Indexes ($\text{Log}R\tau$) of electrolytes comprising oligomeric borate salts with various length of and PEO

EO:Li	$\text{Log}R\tau$			
	$n=1$	$n=2$	$n=3$	$n=7.5$
50:1	3.1	1.1	-3.8	-11.1
32:1	2	-2.3	-3.1	1.1
16:1	-3.1	-10.6	-10.2	-
10:1	-1.9	-7.6	-1.1	-

5.2.3 Dielectric properties

Ionic conductivity discussed above is the most important quantity from the point of view of practical applications. However, to understand the origin of observed trends, and in order to link electrical properties to thermal properties, a deeper discussion of other effects observed in impedance spectra is needed. These processes include:

- (i) dielectric relaxations related to polar groups within the polymer chain,
- (ii) polarization on phase boundaries resulting from structural inhomogeneity
- (iii) interfacial polarization and charge transport at the electrode/electrolyte interface.

The effects observed in the impedance spectra can be described and quantified by fitting an appropriate equivalent circuit model. The model we use to fit impedance spectra (see Fig. 5.9a) is comprehensive enough to allow for modelling of all the phenomena mentioned. However, not all of these phenomena can be undoubtedly deconvoluted from an impedance spectrum measured at a single temperature. Therefore, a more accurate and reliable result can only be obtained by analyzing measurements made over a wide temperature range.

At the lowest temperatures, the interfacial polarization time constant is too high to be observed in the selected frequency range (it should be visible at frequencies lower than 10 mHz). Therefore, during the fitting process a part of the model related to that phenomenon in those temperatures was kept fixed. Conversely, the effects of dielectric relaxations are clearly visible because the dielectric-loss peak is not buried under the much stronger ionic conductivity signal.

At the high temperature end of investigated range (70 °C and above), the interfacial polarization phenomena can be precisely quantified, while the dielectric relaxations caused by the oscillation of polar groups (dipoles) are masked by stronger influence of the ionic conductivity or exceed the experimentally obtainable frequency range.

The discussion of parameters obtained using the refined fit procedure is restricted to those collected for samples comprising oligomeric salt with an average number of ethylene oxide units ($n=7.5$). As already presented, electrolytes comprising salt with ($n=7.5$) exhibit promising properties when conductivity, stability, and glass transition temperature are considered. As we intend to show how the presence of oligomeric salt influences the properties of composite electrolytes, focusing on one oligomeric species introduces more clarity to the discussion. All data regarding composite electrolytes are presented together with reference measurements of pure PEO and oligomeric salt.

Dielectric loss spectra measured at the lower end of the studied temperature range (around -45 °C) which can be described as close to glass transition temperature reveal the presence of two loss peaks (Fig. 5.20). The one situated near the high-frequency limit of the studied frequency range will be denoted as β . As already discussed in our previous publications on PEO-based systems [81-82], this peak can be related to local conformational displacements of atoms within the polymer chain. Such a local relaxation may change the local energy landscape for ion travel but is not effective in providing the transport of lithium ions along the polymer chain. In the equivalent circuit, this relaxation is modeled by the Cole-Cole symmetrical relaxation peak. The loss peak is rather broad, with the shape parameter of the peak a around 0.6 for electrolytes composed of oligomeric salt and PEO, 0.64 for pure PEO, and 0.58 for pure oligomeric salt. A broader peak for neat PEO may result from its relatively higher crystallinity because the response of tightly packed molecules in lamellae greatly differs from those in a disordered amorphous state.

The difference between neat PEO and oligomeric systems is however most evident in the β loss peak frequency. The frequency is lower for neat PEO. This means that either the presence of oligomeric salt has a dominant role in improving local molecular dynamics of the whole system, or it gives a stronger loss response due to higher content of amorphous phase than neat PEO. In electrolytes with oligomeric salt the relaxation strength ($\Delta\varepsilon$) was about 1.5 times greater than for neat PEO.

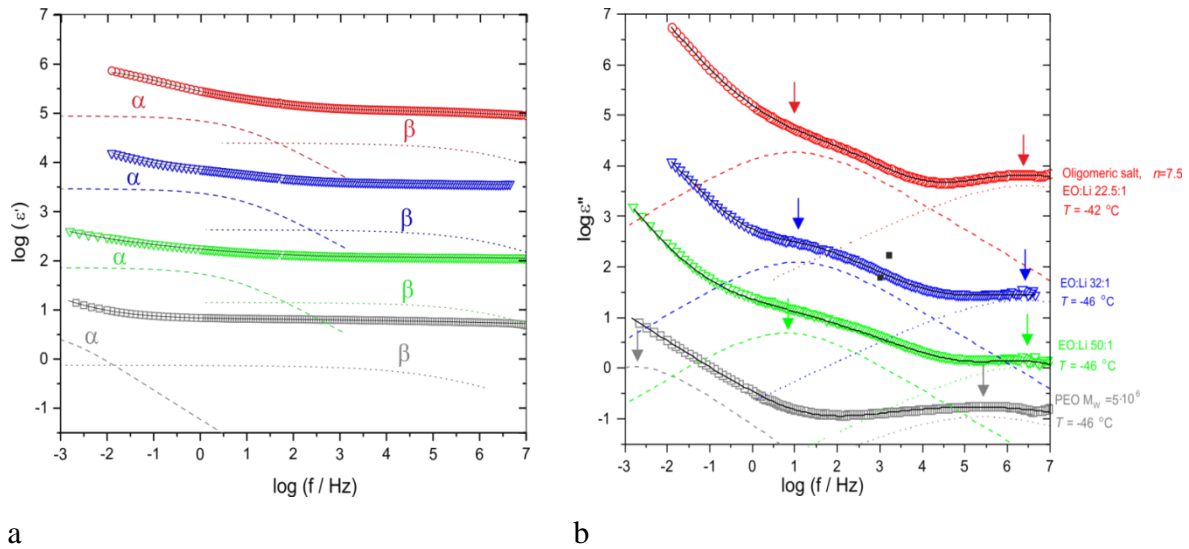


Fig. 5.20. Real (a) and imaginary (b) part of dielectric function ϵ for electrolytes prepared using oligomeric salt with ($n=7.5$) at the low temperature limit of investigated range. Data for pure PEO and oligomeric salt are presented as reference. Solid lines represent equivalent circuit fit. Dotted and dashed lines represent dielectric relaxations. Plot for pure PEO is plotted according to Y scale, other plots were shifted by 1.5 in respect to each other.

Another dielectric relaxation peak is situated around 10 Hz and will be denoted as α . Despite temperatures around -45 °C, all samples exhibited measurable ionic conductivity. Therefore, in the fitting procedure the loss peak had to be subtracted from a low-frequency conductivity “slope” (Fig. 5.20b). The peak was fitted by Cole-Cole function using the shape of the peak α set to 0.49. The α peak corresponds to segmental relaxations of polymer chains. In PEO-based electrolytes, such relaxations promote the conductivity of both Li^+ cations and anions and tend to exhibit similar temperature dependence as ionic conductivity [81-82]. Therefore, they provide also a probe of the glass transition temperature of the system.

For electrolytes that contain oligomeric salts the frequency which corresponds to the maximum of the loss peak is distinctly higher than for the case of neat PEO. It should be noted that the neat oligomeric salt was measured at a slightly higher temperature than the rest of the samples which can account for a shift towards higher frequencies. Nevertheless, the frequency of the α relaxation process for the electrolyte representing molecular ratio EO:Li 32:1 is slightly higher, and for the electrolyte with EO:Li of 50:1 is similar. According to these observations, it can be concluded that a eutectic-type behavior is observed. For electrolytes comprising oligomeric salt and PEO the segmental motions are much faster, than

for pure PEO, but also slightly faster, than for pure oligomeric salt. This finding corresponds well with the trend observed in the glass transition temperature (Fig. 5.8) and indicates that oligomeric molecules enhance conductivity by both bringing more structural disorder to the system and directly improving the mechanism of ion transport.

Another point of comparison was chosen around $-25\text{ }^{\circ}\text{C}$, which is also the lowest limit of the practical application range for Li-ion batteries. At this temperature, all systems included in the comparison are semicrystalline. Dielectric relaxations still provide a significant contribution to the impedance spectra. However, in the dielectric loss spectrum, the ionic conductivity contribution becomes the dominant factor. The temperature around $-25\text{ }^{\circ}\text{C}$ also allows for a detailed study of conductivity dispersion between DC value (responsible for charge transport between electrodes) and high-frequency value, related to faster charge transport on a local scale. The spectral plot of real and imaginary parts of the dielectric function, as well as the real part of conductivity (normalized to electrolyte area and thickness), are shown in Fig. 5.21.

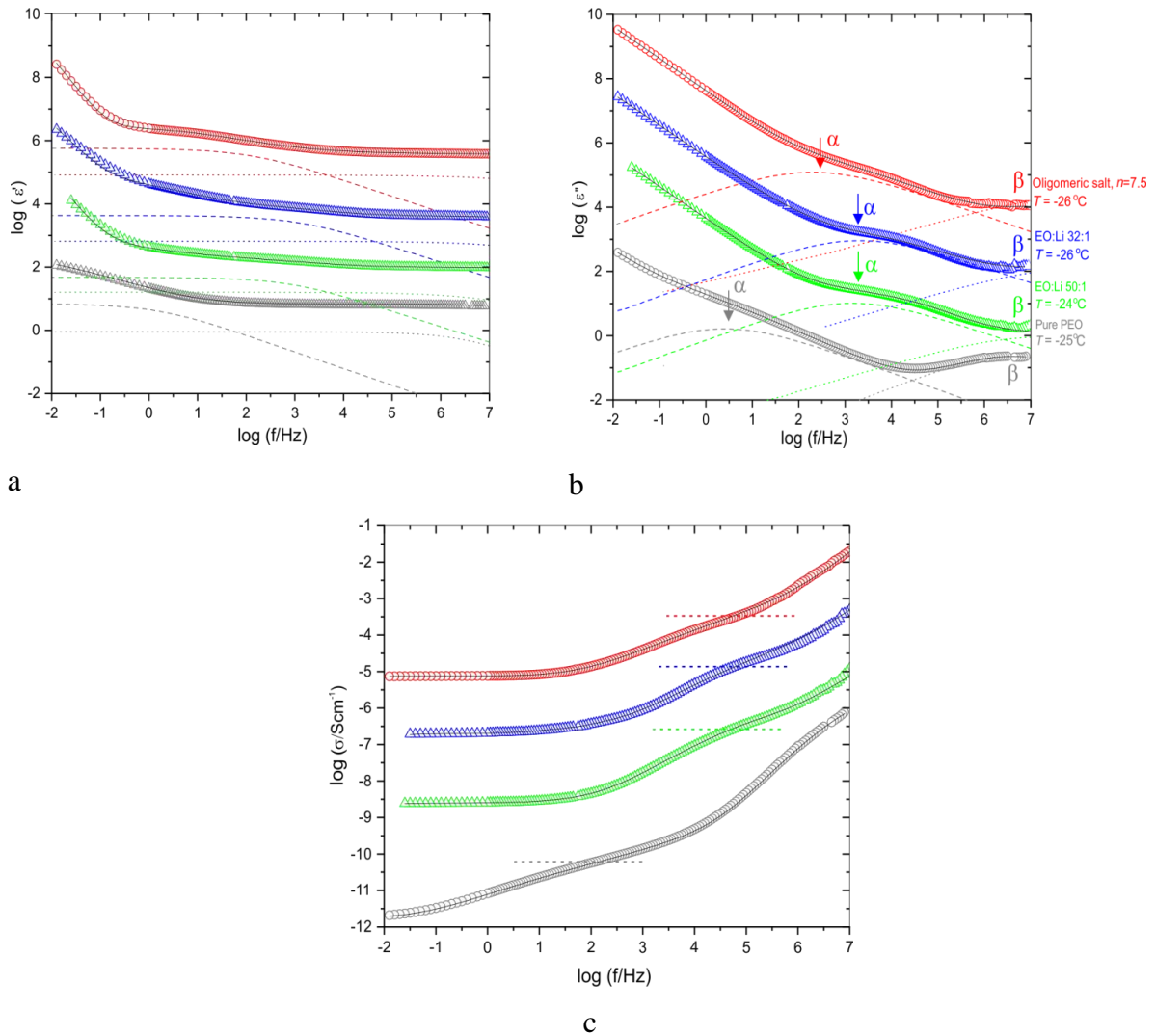


Fig. 5.21. Real (a) and imaginary (b) part of dielectric function ϵ and real part of conductivity σ (c) for electrolytes prepared using oligomeric salt with ($n=7.5$). Data for pure PEO and oligomeric salt are presented as reference. Solid lines represent equivalent circuit fit. Dotted and dashed lines in (a) and (b) represent dielectric relaxations, and dashed lines in (c) represent local conductivity. Plot for pure PEO is plotted according to Y scale, other plots were shifted by 1.5 in respect to each other.

The dielectric response related to β relaxation partially exceeds the measured frequency range, which strongly limits the accuracy of fit for this relaxation. However, the α relaxation peak is situated well within the experimental frequency window, which allows for fitting characteristic relaxation frequency. For electrolytes comprising oligomeric molecules and PEO the frequency which corresponds to the maximum of the loss peak is much higher than that of pure PEO, but also higher than the frequency observed for the neat oligomeric salt (Fig. 5.21b). This indicates that the segmental motion of polymer chains in the systems comprising PEO and oligomeric anions is faster, which is favorable for ionic conductivity. The real part of conductivity shows a clear DC plateau at low frequencies (Fig. 5.21c). With

increasing frequency, two regions described by power-law type dependence are observed, separated by a less inclined part. Such type of plot can be fitted by a model which includes a separate resistor R_1 (Fig. 5.9a), intended to describe the local charge transfer process. The position of the less inclined region in the plot is assigned to this local conductivity. In the model, resistor R_2 corresponds to the bulk (DC) conductivity, and the power law dependence is fitted by a constant phase element CPE P_2 . Fig. 5.21c shows that all electrolytes that contain oligomeric salt have similar local conductivity as well as similar characteristic time constant which corresponds to this fast charge transfer process, while for neat PEO this process is observed at a lower frequency.

At room temperature, the dielectric relaxations are masked by other phenomena such as ionic conductivity, polarization on phase boundaries, and polarization at the electrode/electrolyte interface which have a greater impact on the impedance spectrum. The complex plane impedance plots of electrolytes composed of PEO and oligomeric salts feature a heavily distorted arc at high and medium frequencies, followed by a spur caused by a blocking-type electrode at low frequencies (Fig. 5.22a-d). The distortion of the arc is related to conductivity dispersion between faster local process and slower “DC” ionic conductivity. These processes give two partially overlaying semicircles. The capacitance C_2 was incorporated into the equivalent circuit to better fit the shape of the impedance spectrum plot. It models polarization on phase boundaries and fits a bump in the kHz frequency range on the plot of the real part of permittivity (Fig. 5.22e). In neat PEO the relative increase of dielectric permittivity related to this effect is around 200 with respect to the geometrical capacitance of the sample. For semicrystalline electrolytes composed of PEO and oligomeric salts the relative increase of dielectric function related to this element is lower, about 20 for both electrolytes with EO:Li of 32:1 and 50:1. This value is higher than the values of dielectric constant ϵ_h of the electrolyte, calculated according to the capacitance C_h . The dielectric constant calculated at room temperature ranged from 7.5 (pure PEO in semicrystalline state and semicrystalline electrolytes comprising PEO and oligomeric salts) to 9 (oligomeric salt). Taking into account that, for fitting performed at room temperature, this value depends also on the contribution of dielectric relaxations (which could no longer be fitted separately with reasonable accuracy), it is in agreement with our previous reports on dielectric properties of polymer electrolytes. We have reported the high-frequency dielectric constant (without the contribution of dielectric relaxations) to be about 4 in the amorphous state and 3 in the semicrystalline state, and the strength of the α dielectric relaxation of the order of 10 in the amorphous electrolyte, and about 5 in semicrystalline electrolyte [78][81].

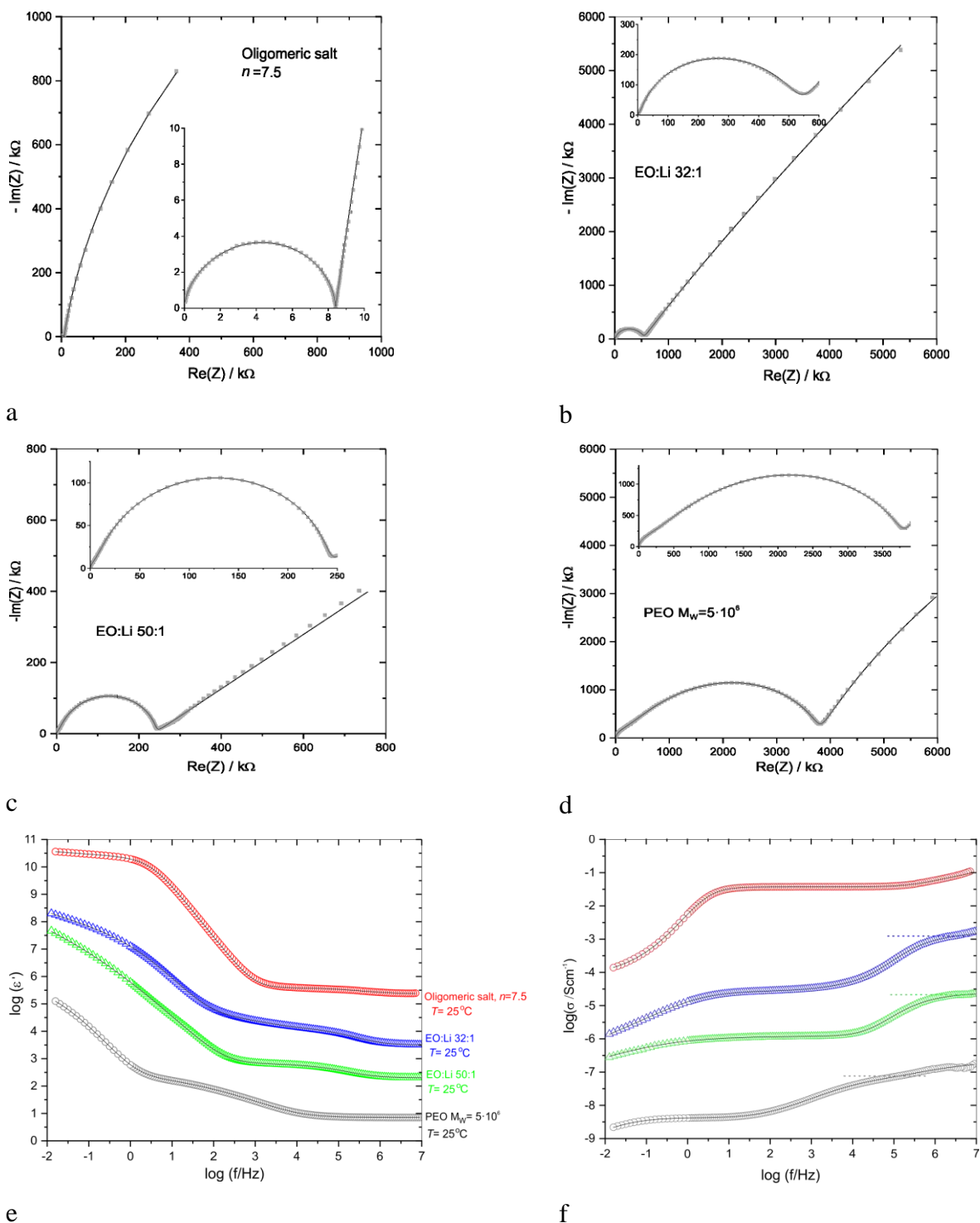


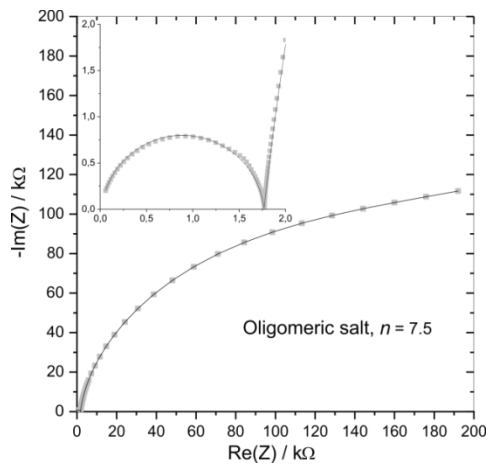
Fig. 5.22 a-d: Complex plane plots of plots of impedance spectra measured at room temperature: oligomeric salt with ($n=7.5$) (a), electrolyte comprising oligomeric salt, ($n=7.5$) and PEO, EO:Li molar ratio of 32:1 (b), electrolyte comprising oligomeric salt, ($n=7.5$) and PEO, EO:Li of 50:1 (c), pure PEO (d). e-f: Spectral plots of real part of dielectric permittivity (e) and real part of conductivity (f). Solid lines represent equivalent circuit fit. Dashed lines in (f) represent local conductivity. Data for pure PEO are plotted according to Y scale, other plots are shifted by 1.5 in respect to each other.

Dispersion of conductivity between lower DC and higher “local” values can be also observed on the plots of the real part of electrolyte conductivity measured at 25 °C (Fig. 5.22 f). For oligomeric salt, only one plateau of conductivity is present, as the system is in an amorphous state. For electrolytes composed of PEO and oligomeric salts, the DC conductivity plateau is situated at much lower values, than the conductivity of the short-ranged conduction process. For the electrolyte with EO:Li of 32:1, the DC conductivity is about 40 times lower, whereas for the electrolyte with the molar ratio of 50:1 it is about 20 times lower than the local conductivity. Interesting conclusions can be drawn if the conductivity of oligomeric salt is compared to the local conductivity of electrolytes. First of all, the values are much closer to each other than the values of DC conductivity. The local conductivity of the electrolyte with EO:Li 32:1 is 1.5 times lower than the conductivity of oligomeric salt. For the electrolyte with EO:Li 50:1 the local conductivity is about 2 times lower than the DC conductivity of oligomeric salt. Therefore, the local value of conductivity may reflect the conductivity of amorphous domains that exist in the semicrystalline structure. Electrolyte representing a molar ratio EO:Li of 50:1 is characterized by a higher heat of fusion, and therefore also contains less amorphous phase. Therefore, the conductivity multipliers mentioned above can be interpreted as the difference in the volume of the amorphous phase.

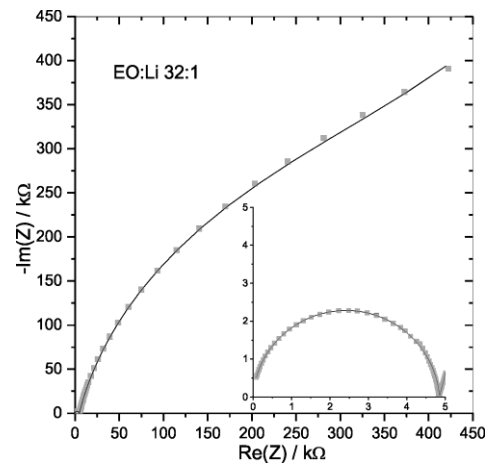
Spectra measured at room temperature exhibit also differences in polarization at the electrode/electrolyte interface. These differences can already be spotted in complex plane plots: the electrode spur of amorphous oligomeric salt is well separated from the bulk electrolyte semicircle, and steep inclination indicates nearly capacitive behavior. Such a shape of electrode spur has its reflection in the parameters of the fitted equivalent circuit model: the exponent n of a “leading” CPE element P_d used for the description of electrode polarization was close to 0.9. For semicrystalline electrolytes, the electrode spur is less inclined, and instead of a sharp turn of the impedance curve, the separation between the bulk electrolyte arc and the electrode spur is rather observed as a “saddle”. This is due to a proportionally lower capacitance related to the electrode polarization process. The exponent n of element P_d was fitted as 0.6 for electrolyte with EO:Li of 32:1, 0.4 for electrolyte with EO:Li of 50:1, and 0.7 for the neat PEO. As observed in Fig. 5.21e, the increase of the low-frequency permittivity (and the capacitance) related to interfacial polarization is significantly lower for the electrolyte with EO:Li of 32:1, than for the electrolyte with EO:Li of 50:1. As the properties of the interface of semicrystalline electrolyte rely on many factors including sample history [27], this may not necessarily be a permanent property of the studied systems. The lower interfacial capacitance of the 32:1 EO:Li electrolyte may also mean, that higher values of bulk DC ionic

conductivity of this sample could possibly be obtained by improving the surface layer properties. This effect may also account for different ratios of local conductivity to DC conductivity in 32:1 and 50:1 EO:Li samples, described above.

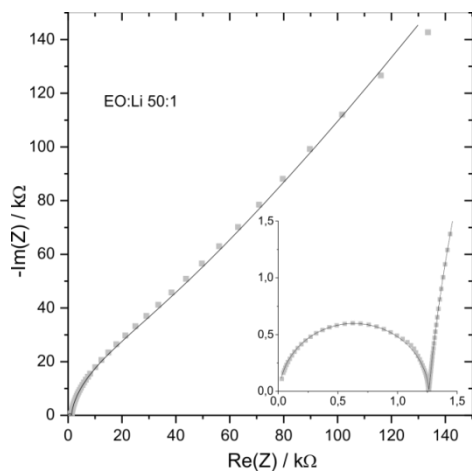
Ionic conductivity and interfacial properties are most appropriately compared when all chosen electrolytes are above their melting points. Herein such conditions are certainly met at a temperature of 70 °C. In Fig. 5.23, complex plane plots (a-d) as well as spectral plots of the real part of permittivity (e) and conductivity (f) are presented. In the complex plane plots, a similar shape of the plot is observed for all samples: a single semicircle followed by an electrode spur. Only one plateau is visible for each sample on the spectral plot of conductivity (Fig. 5.23f), as expected for an amorphous system. In the plots of the real part of permittivity, the low-frequency part is dominated by the influence of the electrode polarization process. The pseudo-capacitances related to the constant phase elements P_d and P_a , which are obtained from fits of the model (Fig. 5.9a), are similar for the neat oligomeric salt and the electrolytes composed of the oligomeric salt and the PEO, which corresponds to the similar increase of capacitance at low frequencies (Fig. 5.23e). However, there were substantial differences in values of exponent n of element P_d between the studied samples. For oligomeric borate salt, the fitted exponent n was equal 0.38, for the electrolyte with molar ratio EO:Li 32:1 the value equaled 0.84, and for the electrolyte with molar ratio EO:Li of 50:1 $n=0.94$, which is close to the value obtained for the neat PEO. This gradual shift from “resistive” to “capacitive” behavior is also observed in the shape of electrode polarization spur (Fig. 5.23 a-d). Such result may suggest that the presence of high molecular weight polymer chains at the electrolyte influences the mechanism of ionic double-layer formation with respect to a system composed of shorter (and probably more mobile) oligomeric chains. In this case, the comparison to the neat PEO has limited relevance because, in neat PEO, electrode polarization is probably caused by other ionic species.



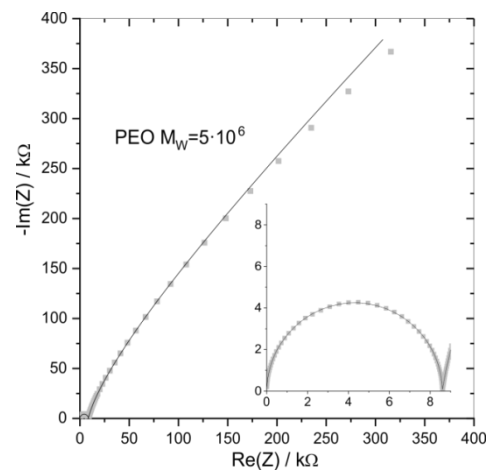
a



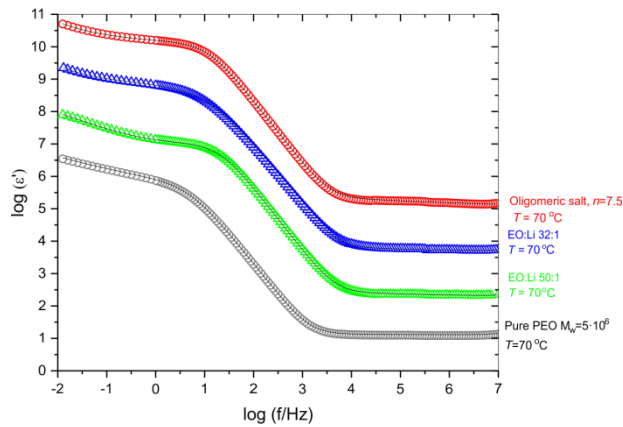
b



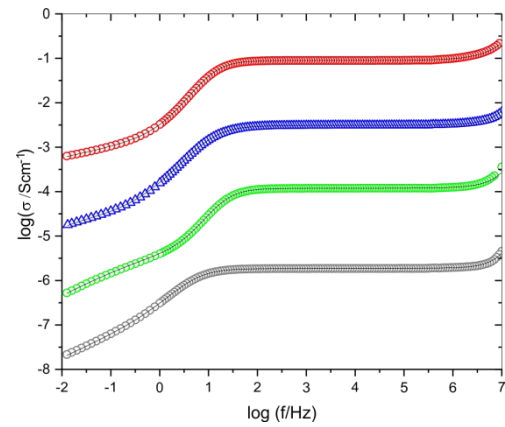
c



d



e



f

Fig. 5.23 a-d: Complex plane plots of impedance spectra measured at 70°C: oligomeric salt with $n=7.5$ (a), electrolyte comprising oligomeric salt, ($n=7.5$) and PEO, EO:Li molar ratio of 32:1 (b), electrolyte comprising oligomeric salt, ($n=7.5$) and PEO, EO:Li of 50:1 (c), pure PEO (d). e-f: Spectral plots of real part of dielectric permittivity (e) and the real part of conductivity (f). Solid lines represent equivalent circuit fit. Dashed lines in (f) represent local conductivity. Data for pure PEO are plotted according to the Y scale, other plots are shifted by 1.5 in respect to each other.

5.3 Transference numbers

As mentioned earlier, this section cites results measured during doctoral studies of Karol Pożyczka, which were presented in this work to show a possibly complete set of electrical properties of the studied system. Electrolytes containing borate salt with oligomeric arms of length ($n=7.5$) were studied using the Symmetrical Polarization Procedure (SPP) [83]. The temperature of the samples during the measurement was maintained at 80 °C, which is low enough to secure a stable interface with lithium metal. Additionally, all samples are amorphous at this temperature, thus providing proper conditions for comparison. The results of the measurements are presented in Fig. 5.24.

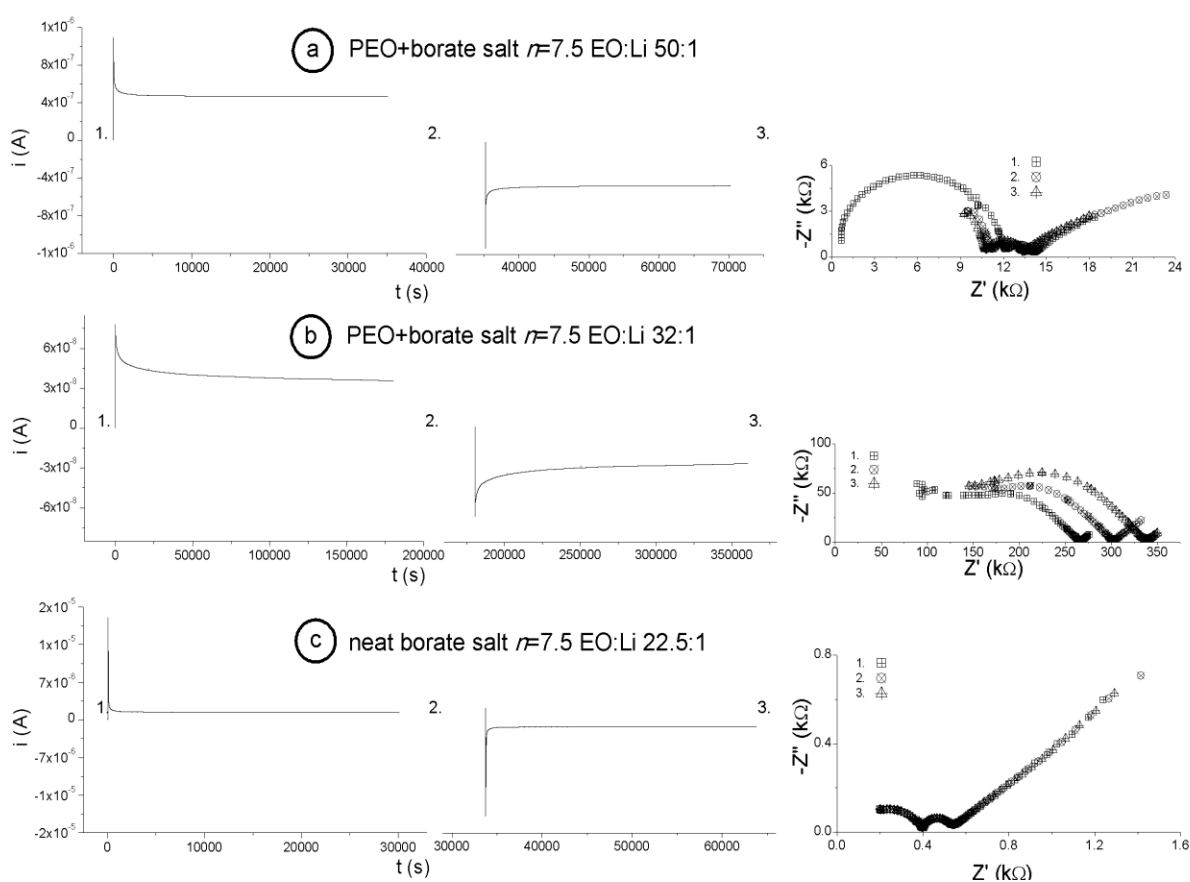


Fig. 5.24. The chronoamperometric and the impedance data, used for calculation of the apparent lithium transference numbers (t^+) of electrolytes based on the borate salt with oligomeric arm length of ($n=7.5$): the electrolyte with a ratio of ethylene monomer to lithium (EO:Li) of 50:1 comprising the salt and PEO (a), the electrolyte EO:Li=32:1 comprising salt and PEO (b), the neat salt EO:Li=22.5:1 (c). All measurement were performed at 80 °C [69].

Table 5.7 contains the values of the apparent transference number (t^+) calculated using two methods: the Bruce-Vincent and the Watanabe. Both methods yield similar results. The

highest value of $t^+=0.39$ was obtained for the “salt in polymer” sample, which has a molar ratio of EO:Li=50:1 and contains more than 50% by weight of linear PEO chains. For the “polymer in salt” system with a ratio of ethylene monomer to lithium of 32 (EO:Li=32:1), a slightly lower value ($t^+=0.38$) was obtained. The small difference in t^+ between these samples suggests that above a certain concentration of the linear polymer, its effect on lithium transport becomes minor.

The cited work of Karol Pożyczka revealed that the neat oligomeric salt had the lowest apparent lithium transference number, with only around 5% of the charge transported by cations between the electrodes. Such a surprisingly low t^+ value may be due to the weak dissociation of lithium ions, resulting in the charge being preferably transported by anions or ion complexes in this ionic liquid. To some extent, this effect can also be explained by the supposed presence of other variations of oligomeric anions, such as those that consist of two butyl groups and two oligomeric arms (Fig. 4.1). As already stated above, this variant of the salt could constitute a significant portion (26%) of all salt molecules. Preliminary studies on salts where the two-butyl-group variant dominated showed that these anions had much higher mobility compared to anions with three or four oligomeric arms. These observations align well with the substantial improvement of t^+ in electrolytes with poly (ethylene oxide) matrix. The presence of a sufficiently dense PEO matrix creates a restrictive effect on the movement of bulky ionic species by forming a network of very weakly mobile chains.

It should be noted that for the electrolyte with a molar ratio of EO:Li of 32:1, the resistance of the interphase significantly increased over time (Fig. 5.24b), preventing the system from reaching a steady state during the chronoamperometric polarization. Despite a very long potentiostatic polarization time of over 100 hours, a true steady state was not reached, and a minor decrease in current was persistently observed. This may be due to stability issues with the electrode/electrolyte interface. In contrast, the electrolyte with a molar ratio of EO:Li of 50:1 showed a much smaller, if any, increase in interphase resistance, suggesting that a higher concentration of linear PEO may stabilize the electrode/electrolyte interface.

Table 5.7. The apparent transference numbers (t^+) of electrolytes based on the borate salt with oligomeric arm length of ($n=7.5$) (neat salt or with PEO) measured at 80 °C.

Composition	t^+ (Bruce-Vincent)	t^+ (Watanabe)
PEO:salt 1.05:1 wt. EO:Li 50:1 $n=7.5$	0.39 ±0.01	0.39 ±0.02
PEO:salt 0.36:1 wt. EO:Li 32:1 $n=7.5$	0.38 ±0.05	0.38 ±0.06
Neat salt, $n=7.5$	0.05 ±0.01	0.05 ±0.01

6. Conclusions

(i) Analysis of results obtained by electrical methods shows that by addition of high molecular weight PEO to oligomeric borate lithium salts, it is possible to obtain electrolytes that exhibit ionic conductivity comparable to that of the pure borate salts.

(ii) The addition of high molecular weight polymer allows for obtaining free-standing membranes, which seem to be more appropriate as an electrode separator than the pure borate salts, which are usually obtained as waxes or viscous liquids. In the temperature range below room temperature, the decrease of conductivity caused by the presence of crystalline phase in mixed PEO-borate systems can be partially compensated by their low glass transition temperature.

(iii) For some of the studied electrolyte compositions, the value of T_g measured by calorimetric methods and T_0 calculated from the fit of VTF formula, were lower than that of the parent compounds. The lowest value of $T_g = -81$ °C and $T_0 = -132$ °C were obtained for the electrolyte with a molar ratio EO:Li of 50:1, and EO:Li of 32:1, comprising PEO and oligomeric salt with ($n=7.5$) respectively. These values are nearly 30 °C lower, than the glass transition temperature and 36 °C lower than the ideal glass transition temperature of pure PEO, and much lower than that of electrolytes composed of PEO and lithium imide or triflate salts with similar molar ratio EO:Li. This shift of glass transition temperature was also reflected in frequencies of dielectric relaxations, studied in detail for electrolytes formed using borate salt with average oligomeric segment length ($n=7.5$).

(iv) In electrolytes composed of borate salts and linear PEO the frequencies of segmental relaxation, which promotes ion transport were shifted to higher frequencies in respect to the parent compounds. At room temperature, the mixed borate salt-linear PEO systems are semicrystalline, which is reflected in their impedance spectra. A dispersion of conductivity and the presence of high and low-frequency plateaus is observed in spectral plots of conductivity. The low-frequency plateau depends rather on sample crystallinity (related to sample structure and history), while the high-frequency plateau reflects the conductivity of amorphous domains, and may be interpreted as a limit of conductivity possible to achieve if crystallization could be suppressed. In the impedance spectra measured at 70 °C, for which all studied samples were in the molten state, differences in electrode polarization were observed between the pure oligomeric salt and mixed systems.

(v) The capacitance related to electrode polarization is of a similar order for all studied systems, but a transition from more “resistive” to more “capacitive” behavior was observed with the increase of the fraction of linear PEO.

(vi) A short study of apparent lithium transference numbers for the system based on oligomeric salt with oligomeric segment length ($n=7.5$) showed, that the addition of linear PEO chains to the system increases the values of t_+ with respect to the neat salt. Probably, the presence of PEO chains promotes salt dissociation, and subsequent transport of lithium cations across the electrolyte.

(vii) PEO may also improve the selectivity of the electrolyte by obstructing the movement of branched anions. The electrolyte with a molar ratio EO:Li of 50:1 has similar conductivity to the electrolyte with molar ratio of 32:1 EO:Li and is characterized by a similar lithium transference number, but exhibits better stability of electrolyte/electrode interface.

References:

- [1] L. Ji, Z. Lin, M. Alcoutlabi, X. Zhang, *Energy & Environment Science*, 4 (2011) 2682.
- [2] J. B. Goodenough, Y. Kim, *Chemistry of Materials*, 22 (2010) 587.
- [3] P. G. Bruce, B. Scrosati, J. Tarason, *Angewandte Chemie*, 47 (2008) 2930.
- [4] N. Choi, Y. Yao, Y. Cui, J. Cho, *Journal of Materials Chemistry*, 21 (2011) 9825.
- [5] S. Chung, Y. Kim, S. Choi, *Advanced Functional Materials*, 20 (2010) 4219.
- [6] A. Yamada, J. B. Goodenough, *J. Electrochem. Soc.*, 145 (1998) 737.
- [7] K. W. Park, H. J. Ahn, Y. E. Sung, *J. Power Sources*, 109 (2002) 500.
- [8] F.M. Gray, *Solid Polymer Electrolytes*, Wiley-VCH, (1991).
- [9] A. Ghosh, P. Kofinas, *Journal of The Electrochemical Society* (2008) 131.
- [10] D. Linden, T. Reddy, *Handbook of Batteries*, 3rd Edition McGraw Hill Professional (2002).
- [11] J. Tarascon, M. Armand, *Nature* (2001) 359.
- [12] C. Daniels, J. Besenhard, *Handbook of Battery Materials*, J., John Wiley and Sons (2011).
- [13] M.B. Armand, *Solid State Ionics*, (1983) 745.
- [14] K. Xu, *Chem. Rev.*, 104, (2004) 4303.
- [15] B. Scrosati, J. Garche, *J. Power Sources*, 195, (2010) 2419.
- [16] M. Galinski, A. Lewandowski, I. Stepniak, *Electrochim. Acta*, 51 (2006) 5567.
- [17] K. Murata, S. Izuchi, Y. Yoshihisa, *Electrochim. Acta*, 45, (2000) 1501.
- [18] M. B. Armand, *Ann. Rev. Mater. Sci.*, 16, 245 (1986) 245.
- [19] G. K. Shenoy, J. N. Mundy, P. Vashishta, *Elsevier North Holland*, (1979) 774.
- [20] P. V. Wright, *British Polymer Journal*, (1975) 319.
- [21] C. Berthier, W. Gorecki, M. Minier, M. B. Armand, J. M Chabagno, P. Rigaud, *Solid State Ionics*, 11(1) (1983) 91.
- [22] S. K. F. Shirey, PhD thesis, *The Pennsylvania State University*, (2009).
- [23] W. H. Meyer, *Advanced Materials*, (1998) 439.
- [24] F. Mullerplathe, W. F. Vangunsteren, *Journal of Chemical Physics*, 103(11), (1995) 4745.

- [25] Q. Li, E. Wood, H. Ardebili, *Applied Physics Letters*, 102(24), (2013) 243903.
- [26] M. Yoshio, R. J. Brodd, A. Kozawa, *Lithium-Ion Batteries*, Springer, (2009).
- [27] F. M. Gray, *Polymer Electrolytes*, Ed. J.A. Connor, *Royal Society of Chemistry*, (1997).
- [28] F. Croce, G. B. Appetecchi, L. Persi, B. Scrosati, *Nature*, 394 (6692) (1998) 456.
- [29] J.-L. Souquet, M. Lévy, M. Duclot, *Solid State Ionics*, 70&71 (1994) 355.
- [30] H. Vogel, *Physics Z*, 22 (1921) 645.
- [31] J.-L. Souquet, M. Duclot, M. Lévy, *Solid State Ionics*, 85 (1996) 245.
- [32] G. Nazri, and G. Pistoia, *Science and Technology*, Springer (2009).
- [33] S.-E. Cheon, K.-S. Ko, J.-H. Cho, S.-W. Kim, E.-Y. Chin, H.-T. Kim, *Journal of the Electrochemical Society*; 150(2003) A800.
- [34] Liang X, Wen Z, Liu Y, Wu M, Jin J, Zhang H, Wu X, *Journal of Power Sources*, 196 (2011) 9839.
- [35] J.-W. Choi, J.-K. Kim, G. Cheruvally, J.-H. Ahn, K.-W. Kim, *Electrochimica Acta*, 52 (2007) 2075.
- [36] D. R. Chang, S. H. Lee, S. W. Kim and H. T. Kim, *Journal of Power Sources*, 112 (2002) 452.
- [37] S. Kim, Y. Jung, S.-J. Park, *Journal of Power Sources*, 152 (2005) 272.
- [38] J.-W. Choi, G. Cheruvally, D.-S. Kim, J.-H. Ahn, K.-W. Kim, H.-J. Ahn, *Journal of Power Sources*, 183 (2008) 441.
- [39] J.Y. Song, Y.Y. Wang, C.C. Wan, *Journal of Power Sources*, 77 (1999) 183.
- [40] H.V. Venkatesetty, *Lithium battery technology*, Ed. H.V. Venkatesetty, *John Wiley and Sons*, New York, (1984).
- [41] D.P. Wilkinson, J.R. Dahn, *US patent*, (1992) 5130211.
- [42] C. Nanjundiah, J.L. Goldman, L.A. Dominey, V.R. Koch, *Journal of Electrochemical Society*, 135 (1988) 2914.
- [43] Ogata, N., *Ion-Conducting Polymers*. In *Functional Monomers and Polymers*, k. Takemoto, R. M. Ottenbrite, Eds. M. Kamachi, *CRC Press*, (1997).
- [44] T. Osaka, S. Komaba, X. Liu, *Ionic conducting polymers for applications in batteries and capacitors*. In *Nonaqueous Electrochemistry*, Ed. A. Doron, *Dekker: New York*, (1999).
- [45] G. Feuillade, Ph. Perche, *J Appl. Electrochem.*, 5 (1975) 63.

- [46] D.E. Fenton, J.M. Parker, P.V. Wright, *Polymer* 14, (1973) 589.
- [47] L. C. Hardy, D. F. Shriver, *Macromolecules*, 17(1984) 975.
- [48] G. B Appetecchi, G. Dautzenberg, B. Scrosati, *Journal of the Electrochemical Society*, 143 (1996) 6.
- [49] H. Cheradame, J. F. LeNest, , Polymer Electrolyte Reviews , Eds. J. R. MacCallum, C. A. Vincent, *Elsevier Applied Science* , New York, (1987).
- [50] L.Lestel, S.Boileau , H.Cheradame, In Proc. 2nd International Symposium on Polymer Electrolytes , Ed. B. Scrosati, *Elsevier Applied Science* , New York, (1990).
- [51] M. Kono, K. Furuta, S. Mori, M. Watanabe, N. Ogata, *Polym. Adv. Technol.* 4, (1993) 85.
- [52] N. Kubota, H. Watanabe, G. Konaka, Y. Eguchi, *J. Appl. Polym. Sci.*, 76, (2000) 12.
- [53] N. Kubota, F. Shigetada, N. Tatsumoto, T. Sano, *J. Appl. Polym. Sci.*, 83, (2002) 2655.
- [54] W. H. Meyer, *Adv. Mater.*, 10, (1998) 439.
- [55] J. Guo, PhD thesis, *The University of Akron*, (2010).
- [56] R. O. Ebewele, Polymer science and technology , *CRC press*, (2000).
- [57] I. Osada, H. de Vries, B. Scrosati, S. Passerini, *Angew. Chem. Int. Ed.*, 55 (2), (2016) 500.
- [58] C. Sun, J. Liu, Y. Gong, D. P. Wilkinson, J. Zhang, *Nano Energy*, 33, (2017) 363.
- [59] Y. Takahashi and H. Tadokoro, *Macromolecules*, 6, (1973) 672.
- [60] J.R. MacCallum and C.A. Vincent, eds. Polymer Electrolyte Reviews , *Elsevier Applied Science*, London, (1987).
- [61] M. Grünebaum, M.M. Hiller, S. Jankowsky, S. Jeschke, B. Pohl, T. Schürmann, P. Vettikuzha, A.- C. Gentschev, R. Stolina, R. Müller, H.-D. Wiemhöfer, *Prog. Solid State Chem.*, (2014) 1.
- [62] E. Zygadło-Monikowska, Z. Florjańczyk, K. Służewska, J. Ostrowska, N. Langwald, A. Tomaszewska, *Journal of Power Sources*, 195 (2010) 6055.
- [63] J.O.M. Bockris, A.K.N. Reddy, *Modern Electrochemistry 1*, Second Edition: Ionics ,*Kluwer Academic publishers*,(1998).

- [64] M.M. Hiller, M. Joost, H.J. Gores, S. Passerini, H.-D. Wiemhöfer, *Electrochimica Acta*, 114 (2013) 21.
- [65] S. Zugmann, M. Fleischmann, M. Amereller, R.M. Gschwind, H.D. Wiemhöfer, H.J. Gores, *Electrochimica Acta*, 56 (2011) 3926.
- [66] M. Amereller, T. Schedlbauer, D. Moosbauer, C. Schreiner, C. Stock, F. Wudy, S. Zugmann, H. Hammer, A. Maurer, R.M. Gschwind, H.-D. Wiemhöfer, M. Winter, H.J. Gores, *Solid State Chem.*, (2014) 1.
- [67] P.M. Richardson, A.M. Voice, I.M. Ward, *Electrochimica Acta*, 130 (2014) 606.
- [68] P.R. Sørensen, T. Jacobsen, *Electrochimica Acta*, (1982) 1671.
- [69] K. Pożyczka, M. Marzantowicz, J.R. Dygas, F. Krok, *Electrochim. Acta*, 227 (2017) 127.
- [70] M.C. Wintersgill, J.J. Fontanella, ed. J. R. MacCullum, C.A. Vincent. *Elsevier Applied Science*, (1989) 45.
- [71] G. Hougham, G. Tesoro, A. Viehbeck, J. D. Chapple-Sokol, *Macromolecules*, 27 (1994) 5964.
- [72] P. Debye, Polar molecules, *Chemical Catalog Company, reprinted in New York by Dover Publications*, (1929).
- [73] R. J. Young, Introduction to Polymers, *Chapman & Hall Ltd*, (1989).
- [74] J. Evans, C.A. Vincent, P.G. Bruce, *Polymer*, 28 (1987) 2324.
- [75] M. Watanabe, S. Nagano, K. Sanui, N. Ogata, *Solid State Ionics*, 28–30 (1988) 911.
- [76] Y. Kato, K. Hasumi, S. Yokoyama, T. Yabe, H. Ikuta, Y. Uchimoto, M. Wakihara, *Solid State Ionics*, 150 (2002) 355.
- [77] J. A. Forrest, K. Dalnoki-Veress, J. R. Dutcher, *Phys Rev E*, 56 (1997) 5705.
- [78] J.R. Dygas, B. Misztal-Faraj, Z. Florjańczyk, F. Krok, M. Marzantowicz, E. Zygadło-Monikowska, *Solid State Ionics*, 157 (2003) 249.
- [79] C. Labrèche, I. Lévesque, J. Prud'homme, *Macromolecules*, 29 (1996) 7795.
- [80] G. S. Fulcher, *Journal of American Chemical Society*, 8, (1025) 339.
- [81] M. Marzantowicz, J.R. Dygas, F. Krok, Z. Florjańczyk, E. Zygadło-Monikowska, *Journal of Non-Crystalline Solids*, 353 (2007) 4467.
- [82] M. Marzantowicz, J.R. Dygas, F. Krok, Z. Florjańczyk, E. Zygadło-Monikowska, *Journal of Non-Crystalline Solids*, 352 (2006) 5216.
- [83] K M. Pożyczka, *Electrochimica Acta*, 424 (2022) 140683.

- [84] M. Marzantowicz, PhD thesis, *Warsaw University of Technology, Faculty of Physics*,(2005).
- [85] H.K.D.H. Bhadeshia , *Differential Scanning Analysis* ,University of Cambridge, *Material Science & Metallurgy*, (2002).
- [86] C.A. Angell, *Annu.Rev. Phys. Chem.*, 43 (1992) 693.
- [87] S. Lascaud, M. Perrier, A. V., S. Besner, J. Prud'homme, M.Armand, *Macromolecules*, 27 (1994)7469.
- [88] L. Edman, M. M. Doeff,A. Ferry, J. Kerr, L.D. De Jonghe, *J. Phys. Chem. B*, 104 (2000) 3476.
- [89] Z. Xue, D. He, X. Xie, *Journal of Materials Chemistry A*, 3(38) (2015) 19218.
- [90] X.Wang , R. Kerr , H.Chen, P. G. Bruce, *Nature Materials* , 7(2), (2008) 138.
- [91] M. Marzantowicz , F. Krok , J.R. Dygas , Z. Florjańczyk , E. Zygadło-Monikowska, *Solid StateIonics*, 179 (2008) 1670.
- [92] G. Höhne, W. Hemminger, H.-J. Flammersheim, *Differential Scanning Calorimetry Springer-Verlag*,(1996).